2017

Geothermal Deep Foundations: Bridge Anti-icing and Thermo-Mechanical Response

Suguang Xiao
Lehigh University

Geothermal Deep Foundations: Bridge Anti-icing and Thermo-Mechanical Response

By

Suguang Xiao

A Dissertation

Presented to the Graduate and Research Committee

Of Lehigh University

In Candidacy for the Degree of

Doctor of Philosophy

In

Civil Engineering

Lehigh University

May, 2017

Suguang Xiao

Geothermal Deep Foundations: Bridge Anti-icing and Thermo-Mechanical Response

Approved and recommended for acceptance as a dissertation in partial fulfillment of the requirements for the degree of Doctor of Philosophy in Civil Engineering on this date of _____.

_____

Clay J. Naito, Ph.D.
Dissertation Committee Chair
Department of Civil and Environmental Engineering
Lehigh University

_____

Muhannad T. Suleiman, Ph.D
Dissertation Supervisor and Advisor
Department of Civil and Environmental Engineering
Lehigh University

_____

Sibel Pamukcu, Ph.D.
Internal Committee Member
Department of Civil and Environmental Engineering
Lehigh University

_____

Sudhakar Neti, Ph.D.
External Committee Member
Department of Mechanical Engineering and Mechanics
Lehigh University

_____

Mesut Pervizpour, Ph.D.
Internal Committee Member
Department of Civil and Environmental Engineering
Lehigh University

Date Accepted: _____

DEDICATION

I dedicate my dissertation to my father, Yutang, and my mother, Lanying, whose encouragement and support were my main source of energy and patience; to my wife, Huihua (Alice), who gives me great love and support, and brought me a lovely daughter -- Olivia Xiao -- the biggest surprise at the end of the doctoral period; to my father-in-law, Zhengyi, and mother-in-law, Jihua, whose great support makes me focus my research; to my sister, Suling, who always provides great help to the large family.

ACKNOWLEDGEMENT

I would first like to thank and express my cordial gratitude to my academic advisor Dr. Muhannad Suleiman. His “fighter” spirit, positive energy, great personality, strong technical skills, and dedication to helping his students enabled me to grow incredibly during my Ph.D. journey. Special thanks to Dr. Sudhakar Neti for the opportunity to work with him and his advice on numerical simulations.

I would like to thank all other members of my committee for their insightful and valuable advice and encouragement: Dr. Clay Naito, Dr. Sibel Pamukcu, and Dr. Mesut Pervizpour.

I would also like to thank the technicians at Lehigh University ATLSS Center for their great help during the development of my experimental device: Edward Tomlinson, Darrick J. Fritchman, Carl Bowman, Peter Bryan, Todd Anthony, and Roger Moyer.

I feel grateful to my friends at Lehigh University for their continuous support throughout the time in grad school, including, but not limited to: Lusu Ni, Hai Lin, Michael German, Yi Dong, Rehab Elzeiny, Hang Dong, Jialan Zhu, You Dong, Jie Liu, Hanna Moussa Jabbour, Kewei Gao, and Jianbo Gu; also, many undergraduate students, including: Allison Stevens, Huan Xie, Chris Guilcapi, Juan Tzoc, Kawsar Hooda. Ben Cohen, and Mallory Elliott.

I also am deeply appreciative for the financial support from the Qatar National Research Fund during my Ph.D.

Table of Contents

DEDICATION iv

ACKNOWLEDGEMENT v

LIST OF TABLES xi

LIST OF FIGURES xii

ABSTRACT 1

1. INTRODUCTION 2

1.1 OVERVIEW 2

1.2 MOTIVATION AND IMPORTANCE 3

1.3 SCOPE AND ORGANIZATION 5

2. LITERATURE REVIEW 7

2.1 BACKGROUND 7

2.2 Bridge or Pavement Deicing Using Geothermal Energy 8

2.3 Heat Transfer Mechanisms of Bridge with Geothermal Deicing Systems 10

2.4 Thermo-Mechanical Behavior of Energy Pile 11

2.5 Load Transfer Analysis of Vertically-loaded Piles 17

2.6 Direct Measurement of Soil-pile Interaction 18

2.7 Temperature Effects on Volume Change and Shear Strength of Soils 20

3. A NEW MODELLING APPROACH OF HEAT TRANSFER OF BRIDGES CONSIDERING VEHICLE-INDUCED THERMAL EFFECTS 22

3.1 INTRODUCTION 22

3.2 BACKGROUND 25
3.2.1 Natural Factors 25
3.2.2 Vehicle Effects 25
3.3 NUMERICAL MODEL 28
3.3.1 Governing Equations 28
3.3.2 Natural Boundaries 28
3.3.3 Vehicle Boundaries 33
3.4 MODEL VALIDATION 36
3.4.1 Description of the Bridge 36
3.4.2 Finite Element Model 37
3.4.3 Material Properties 38
3.4.4 Input Weather Data 39
3.4.5 Results and Discussion 40
3.5 VEHICLE EFFECTS 45
3.5.1 Results with Local/Light Traffic 47
3.5.2 Effects of Heavy Traffic 49
3.6 SUMMARY AND CONCLUSIONS 52
4. INVESTIGATION OF EFFECTS OF TEMPERATURE CYCLES ON SOIL-CONCRETE INTERFACE BEHAVIOR USING DIRECT SHEAR TESTSINTRODUCTION 54
4.1 BACKGROUND 55
4.1.1 Temperature Effects on Volume Change and Shear Strength of Soils 55
4.1.2 Temperature Effects on Water Migration in Soils 56

4.1.3 Temperature Effects on Soil-structure Interface 57
4.2 TESTING APPARATUS 58
4.3 MATERIALS AND PREPARATION 60
4.4 TEST PROCEDURES 60
4.5 RESULTS AND DISCUSSION 62
4.5.1 Smooth Interface Analysis 62
4.5.2 Rough Interface Analysis 63
4.5.3 Vertical Deformation 67
4.5.4 Moisture Contents after Temperature Cycles 69
4.5.5 Effects of Moisture Contents 70
4.6 SUMMARY AND CONCLUSIONS 74
5. MODIFIED-THERMAL BOREHOLE SHEAR TEST DEVICE AND TESTING PROCEDURE TO INVESTIGATE THE SOIL-STRUCTURE INTERACTION OF ENERGY PILES 76
5.1 INTRODUCTION 76
5.2 BACKGROUND 77
5.2.1 Operation of Energy Piles 77
5.2.2 Soil-structure Interaction of Axially Loaded Energy Piles 79
5.2.3 Borehole Shear Test Devices 81
5.3 DESIGN AND SETUP OF MODIFIED-TBST 83
5.3.1 Overview 83
5.3.2 Design of the Shear Head 85

5.3.3 Loading System 86
5.3.4 Heating and Cooling System 86
5.3.5 Control System 86
5.4 CALIBRATION OF MODIFIED-TBST 88
5.4.1 Effect of Temperature on Displacement Reading 88
5.4.2 Temperature Effects on Horizontal Force 89
5.5 MATERIALS AND PREPARATION 90
5.5.1 Soil Properties 90
5.5.2 Soil Preparation 91
5.6 TESTING PROCEDURE 91
5.6.1 Consolidation Stage 92
5.6.2 Applying Temperature Change and Cycles 94
5.6.3 Applying Radial Displacement Change and Cycles 95
5.6.4 Shearing Stage 96
5.7 PRELIMINARY RESULTS AND ANALYSIS 97
5.7.1 PID vs. LCDT Control 97
5.7.2 Effect of Radial Consolidation Time Interval 98
5.7.3 Load Control vs. Displacement Control during Shearing Stage 100
5.7.4 Preliminary Test Results 101
5.8 SUMMARY AND CONCLUSIONS 103

6. EFFECTS OF TEMPERATURE AND RADIAL DISPLACEMENT CYCLES ON SOIL-CONCRETE INTERFACE PROPERTIES USING MODIFIED THERMAL BOREHOLE SHEAR TEST 105

6.1 INTRODUCTION 105

6.2 BACKGROUND 106

6.2.1 Temperature Effects on Volume Change and Shear Strength of Soils 106

6.2.2 Temperature Effects on Water Migration in Soils 107

6.2.3 Temperature Effects on Soil-Pile Interaction and Interface 108

6.3 EXPERIMENTAL SETUP 109

6.4 TEST SOIL AND TESTING PROCEDURE 111

6.5 TESTING PLAN 113

6.6 RESULTS AND ANALYSIS 115

6.6.1 Effects of Temperature Change and Cycles (Tests No. 2 to 7) 115

6.6.2 Effects of Radial Displacement Cycles (Tests No. 8 to 15) 122

6.6.3 Combined Effects of Temperature and Radial Displacement Cycles 126

6.7 SUMMARY AND CONCLUSIONS 129

7. CONCLUSIONS AND FUTURE RESEARCH 132

7.1 CONTRIBUTIONS 132

7.2 FUTURE RESEARCH 133

REFERENCES 135

VITA 154

LIST OF TABLES

Table 2.1 Summary of Thermo-mechanical Responses of Energy Piles, (a) Pile and Ground Informations-1 14

Table 2.2 Summary of Thermo-mechanical Responses of Energy Piles, (a) Pile and Ground Informations-2 15

Table 2.3 Summary of Thermo-Mechanical Responses of Energy Piles, (b) Thermo-Mechanical Responses 16

Table 3.1 Equations 29

Table 3.2 Weather conditions of 10 specific days 37

Table 3.3. Thermal and physical properties of materials 38

Table 6.1 Testing plan of Modified Thermal-BSTs 114

LIST OF FIGURES

Figure 2.1 Geothermal bridge heating system (a) 3D bridge schematic, and (b) deep foundation.. 9

Figure 2.2 Heat transfer mechanics for conventional and geothermal bridge systems..... 10

Figure 2.3 Details of the t–z model: (a) idealized pile, (b) pile discretization, (c) nonlinear springs with Kshaft representing the shaft resistance at soil–pile interface for element i with normal stress equals to σh , (d) t–z curve for element i, and (e) q–w curve at the pile tip..... 18

Figure 2.4 (a) BST components (modified after Handy (2008), courtesy of Handy Geotechnical Instruments, Inc.), (b) grooved shear plates used in conventional BST, (c) new smooth plates, and (d) sample t–z curve measured using modified device. (modified after AbdelSalam et al., 2012)..... 19

Figure 3.1 Configurations of heat transfer model for bridge deck, (a) Natural factors; and (b) Vehicle factors 27

Figure 3.2 Vehicle-induced wind (after Fujimoto et al., 2008) 34

Figure 3.3 Natural wind and vehicle-induced wind..... 35

Figure 3.4 Finite element mesh for half of the bridge cross section for the Jamestown Verrazzano Bridge 38

Figure 3.5 Comparison of the measured data and computed results from the ASHRAE model and improved model in whole year period (a): top slab, (b): bottom slab. 41

Figure 3.6 Comparison of the measured data and computed results from the ASHRAE model and improved model in 10 days (a): top slab, (b): bottom slab. 42

Figure 3.7 Comparisons of CHTC of different models 44

Figure 3.8 Wind speed, solar radiation, and temperature difference between the air and predicted deck surface temperature 45

Figure 3.9 Hourly traffic rate and vehicle speed at light and heavy traffic conditions..... 47

Figure 3.10 Comparison of the measured data and computed temperature at P1 (top slab) from the improved model with vehicle effects in 10 days..... 48
Figure 3.11 Bridge surface temperature differences (T_{sv} - T_s) predicted by improved model with and without vehicle effects in one year's simulation. 49
Figure 3.12 Surface temperature differences (T_{sv} - T_s) between models with and without vehicle effects..... 50
Figure 3.13 Surface temperature of two days under different weather condition. 51
Figure 3.14 The hourly average heat flux of each component..... 52
Figure 4.1 Profile of modified direct shear test device 59
Figure 4.2 Layouts of the heating/cooling tubes in the concrete plate and thermocouples at soil-concrete interface: (a) profile of top shear box and concrete plate; (b) concrete plate with heat pumps; (c) concrete plate with smooth surface; (d) concrete plate with rough surface 59
Figure 4.3 Average temperature at soil-concrete interface during heating and cooling cycles 61
Figure 4.4 Shear stress vs. displacement and volume change with smooth concrete surface..... 64
Figure 4.5 Shear stress vs. displacement and volume change of rough concrete surface 65
Figure 4.6 Failure envelopes for soil-concrete interface subjected to different temperature cycles, (a) smooth interface; (b) rough interface 67
Figure 4.7 Vertical deformation and voids ratio of the soil specimen during temperature cycles at different normal stresses: (a) vertical deformation; (b) voids ratio..... 69
Figure 4.8 Moisture contents changes during temperature cycles: (a) moisture at interface; (b) average moisture in the soil specimen 71
Figure 4.9 Effects of moisture content and temperature on failure envelope of soil-concrete interface: (a) smooth interface; (b) rough interface)..... 73

Figure 5.1 Pile subjected to vertical loading showing horizontal stresses normal to the soil-pile interface, (a) Conventional pile; (b) radial expansion of energy pile during heating; and (c) radial contraction of energy pile during cooling 80
Figure 5.2. Configuration of the Modified-TBST system 84
Figure 5.3 Configuration of concrete plates and shear head: (a) side view of the shear head; (b) cross section of concrete plate; (c) left plate and heat exchange pipe; (d) right plate and heat exchange pipe; (e) photo of the shear head with concrete plates. 85
Figure 5.4 Block diagram of PID control system 87
Figure 5.5 Calibration of the change of radial displacement sensor readings due to temperature effects on the shear head 89
Figure 5.6 Relationship between the horizontal (normal) force of pneumatic piston and air pressure at different temperatures 90
Figure 5.7 Radial displacement at consolidation pressure of 41.4 and 69.0 kPa during consolidation stage, (a) horizontal pressure vs. radial displacement; (b) change of radial displacement as a function of time 93
Figure 5.8 Temperature and displacement cycles of the test device 95
Figure 5.9 Comparison of PID control and LCDT, (a) horizontal pressure vs. displacement for expansion cycles; (b) horizontal pressure and radial displacement at the beginning of PID control and LCDT 99
Figure 5.10 t-z curves of soil-concrete interface at different consolidation times 100
Figure 5.11 Comparison of t-z curves with load control and displacement control in radial direction during shearing 101
Figure 5.12 t-z curves at initial consolidation pressure of 41.4 kPa 103
Figure 6.1 Schematic diagram of the daily operation of ground source heat pumps and the changes of surrounding soil temperature 106
Figure 6.2 Configuration of the Modified-TBST system 110

Figure 6.3 Grain size distribution curve of the test soil 111
Figure 6.4 Temperature distribution with distance during heating and cooling cycles 116
Figure 6.5 Suction and temperature changes during heating and cooling cycles; (a) TC = 10, (b) TC = -10, and (c) suction change per temperature cycle 118
Figure 6.6 Temperature effects on the measured t-z curves of soil-concrete interface; (a) heating cycles, (b) cooling cycles 120
Figure 6.7 Interface shear stiffness and moisture at different temperature cycles 122
Figure 6.8 Measured horizontal displacements and corresponding pressures during radial expansion and contraction cycles 123
Figure 6.9 Effect of displacement cycles on the measured t-z curves, (a) expansion cycles; and (b) contraction cycles 125
Figure 6.10 Combined effects of ±0.5 displacement and temperature cycles on measured t-z curves 127
Figure 6.11 Measured t-z curves and horizontal pressures with heating cycles; (a) t-z curve, and (b) horizontal pressure 128
Figure 6.12 Measured t-z curves and horizontal pressures with cooling cycles; (a) t-z curve, and (b) horizontal pressure 129

ABSTRACT

Energy piles provide sustainable energy alternative to transfer the heat for bridge anti-icing, which support the structural loads and exchange heat with surrounding soils using closed-loop ground source heat pump (GSHP) systems. However, the application potential of energy piles for bridge anti-icing has not been fully explored for different climate conditions. Moreover, GSHPs connected to energy piles operates in cycles where it functions for a period of time (running time) then stops for another period of time (stoppage time). This intermittent operation subjects the piles and surrounding soil to changes of temperature and temperature cycles. The temperature change and cycles result in cyclic displacement (expansion and contraction) in both axial and radial directions of the pile and alter soil properties. Researches have investigated the effects of pile axial expansion and contraction (considering the end-restraint) on shear stresses at the soil-pile interface and on axial stresses in the pile. However, the effects of thermally-induced radial expansion and contraction and their cyclic effects on the soil-foundation interaction for energy piles have not been fully investigated. Furthermore, there is no laboratory or field method to investigate the cyclic temperature effect on the soil-pile interface response and to simulate the radial expansion and contraction of energy piles.

The goal of the research presented in this dissertation focuses on: (1) investigating application of geothermal potential energy (energy piles) for bridge anti-icing using numerical analysis of bridge heat transfer model; (2) investigating cyclic thermo-mechanical response of soil-concrete interfaces of different roughness subjected to temperature change and cycles using a modified direct shear tests; (3) developing Modified Thermal-Borehole Shear Tests (Modified-TBSTs) in normally-consolidated soil to investigate the effects of temperature cycles and radial expansion/contraction displacement cycles on the soil-energy pile interaction.

1. INTRODUCTION

1.1 OVERVIEW

Deicing chemicals are corrosive and reduce the longevity of bridge infrastructure making it difficult to achieve the national goal of a 100-year or more bridge service life (Koch et al. 2002; Azizinamini et al. 2014), and the pavement or bridge temperature can be lower than the working range of these chemicals in extreme cold weather (Lund 1999; Joerger and Martinez. 2006; Minsk 1999). The annual direct cost of corrosion for highway bridges are in the range of $5.9 to $9.7 billion (Koch et al. 2002) including the cost of replacing structurally deficient bridges and maintenance cost of bridge structures. Shallow geothermal energy, one of the most promising renewable energy sources, takes advantages of the nearly constant and moderate temperature of the ground to heat and cool buildings, which can be also employed to melt the snow on the bridge deck minimizing or eliminating the use of deicing salt (Spitler and Ramamoorthy 2000; Brandl, 2006; Xiao et al., 2013). The application potential of energy piles for bridge deicing has not been fully explored for different climate conditions. In this research, the geothermal potential energy (energy piles) for bridge anti-icing was assessed using numerical analysis of bridge heat transfer model considering different meteorological factors (e.g., air temperature, wind speed/direction, precipitation, solar radiation, and infrared radiation).

Energy piles are used as structural members to support applied loads and to function as heat exchanger with surrounding soil. Borehole heat exchangers (BHE) were traditionally used as ground heat exchangers to exploit geothermal energy. To reduce the drilling cost of BHE, geothermal deep foundations (or energy piles), which incorporate embedded closed-loop primary pipes circulating a liquid (water or antifreeze), function as a heating and cooling system by providing access to the steady temperature of the subsurface soil (Brandl 2006). The shallow ground, 1 to 3 m below the ground surface, maintains a temperature ranging from ~10 to 25°C in

different environments, which is warmer than the air during the winter and cooler in the summer (Suleiman et al. 2007; Coccia et al. 2011; Akrouch et al. 2013).

The heat pump connected to energy pile systems operates intermittently because of the heating and/or cooling demands variation of bridges and buildings. The heating and cooling cycles of the energy pile result in expansion and contraction of concrete and alter the soil-pile interactions (Amatya et al. 2012). The use of energy pile has been documented in several case histories (Brandl 2006; Hamada et al. 2007; Wood et al. 2009; Bourne-Webb et al. 2009; Amis 2011; Abdelaziz et al. 2011; Shang et al. 2011; Akrouch et al. 2013; Murphy and McCartney 2015; Batini et al. 2015； Loveridge et al. 2016). Researches have investigated the effects of pile axial expansion and contraction (considering the end-restraint) on shear stresses at the soil-pile interface and on axial stresses in the pile. However, the effects of thermally-induced radial expansion and contraction and their cyclic effects on the soil-foundation interaction for energy piles have not been fully investigated. Furthermore, there is no laboratory or field method to investigate the cyclic temperature effect on the soil-pile interface response and to simulate the radial expansion and contraction of energy piles.

The research summarized in this dissertation addresses some of these knowledge gaps focusing on investigating the application of geothermal potential energy for bridge anti-icing using a new numerical approach. In addition, soil-structure interaction of energy piles subjected to temperature and radial expansion/contraction cycles was studied using a newly developed laboratory devices.

1.2 MOTIVATION AND IMPORTANCE

The use of geothermal foundations to support buildings and to function as heat exchangers with the surrounding ground for heating and cooling purposes has been pursued in Japan (Ooka et al. 2007) and Europe (Brandl 2006; Laloui et al. 2006; Adam and Markiewicz 2009; Bourne-Webb

et al. 2009; and Wood et al. 2009), with exponential growth to achieve the net zero-carbon building requirements of the code of sustainable buildings by 2019 (Bourne-Webb et al. 2009). These foundations are commonly referred to as thermo-active foundations, geothermal foundations, or energy piles. Based on geothermal foundation applications in Europe, energy piles are commonly constructed with diameters ranging from 0.3 to 1.5 m, lengths of 10 to 30 m and with heat exchangers made of polyethylene pipe (Laloui and Di Donna 2013). The net thermal output of energy piles ranges from 18 to 120 W per meter of the foundation length and the system typically provides 3 to 5 energy units for each unit consumed in operation (Preene and Powrie 2009; Bourne-Webb 2013). Geothermal deep foundations take advantages of the nearly constant and moderate temperature of the ground to heat and cool buildings, which can be also employed to melt the snow on the bridge deck minimizing or eliminating the use of deicing salt (Spitler and Ramamoorthy 2000; Brandl 2006; Xiao et al., 2013). The application potential of energy piles for bridge deicing has not been fully explored for different climate conditions.

The ground source heat pump (GSHP) connected to energy piles operates in cycles where it functions for a period of time (running time) then stops for another period of time (stoppage time). This intermittent operation subjects thermo-active geo-structures and surrounding soil to changes of temperature and temperature cycles (Shang et al. 2011; Xiao et al. 2017a). In practice, the daily running and stoppage times of GSHP ranges from 30 minutes to 24 hours depending on the heating and cooling loads (Hamada et al. 2007; Wood et al. 2009; Montagud et al. 2011; Luo et al. 2015). If the soil temperature during stoppage time does not return to the original ground temperature, the soil will experience a cumulative increase or decrease of temperature with number of cycles (Plum and Esrig 1969). Temperature change and cycles also induce volume changes of soil components and affect their interaction (Campanella and Mitchell 1968; Romero et al. 2001; Uchaipichat and Khalili 2009). The effects of temperature change on soils have been well explored in the literature

using triaxial and oedometer tests; however, limited investigations have been focusing on evaluating the effects of temperature cycles.

Temperature changes and cycles also induce axial and radial expansion and contraction of energy piles altering the interaction along the soil-pile interface (Suleiman and Xiao 2014; Saggu and Chakraborty 2015). Researchers have investigated the effects of pile axial expansion and contraction (considering the end-restraint) on shear stresses at the soil-pile interface and on axial stresses in the pile (e.g., Brandl 2006; Laloui et al. 2006, Bourne-Webb et al. 2009; McCartney and Murphy 2012; Suryatriyastuti et al. 2012, Olgun et al. 2014, Xiao et al. 2015, 2017b). However, the effects of thermally-induced radial expansion and contraction and their cyclic effects on the soil-foundation interaction for energy piles have not been fully investigated.

1.3 SCOPE AND ORGANIZATION

The goal of the research presented in this dissertation is to investigate the feasibility of using geothermal pile for bridge anti-icing, and soil-energy pile interaction using a newly designed fully-automated laboratory device. The outline of this dissertation research activities that focused on achieving this research goal is listed below.

- Chapter Two: This chapter presents a general literature review of heat transfer model of bridge deck and energy piles. The thermo-mechanical interaction of energy pile is also reviewed.
- Chapter Three: A new modelling approach of heat transfer of bridge anti-icing considering different meteorological factor were proposed.
- Chapter Four: Modified-direct shear test (Modified-DST) were utilized to investigate the effect of temperature change and cycles on soil-concrete interface properties of energy piles.

- Chapter Five: Modified-Thermal Borehole Shear Test (Modified-TBST) device was developed to investigate the soil-structure interaction of energy piles. The testing procedure and control system were described in detail.
- Chapter Six: Modified-TBST device was utilized to investigate the soil-structure interaction of energy piles subjected to radial deformation cycles coupled with temperature cycles
- Chapter Seven: This chapter provides general conclusions and offers recommendations for future studies.

2. LITERATURE REVIEW

2.1 BACKGROUND

The use of energy piles to support buildings and also to function as heat exchangers with the surrounding ground for heating and cooling purposes has been pursued in China (Gao et al. 2008), Japan (Ooka et al. 2007; Hamada et al. 2007), and Europe (Brandl 2006; Laloui et al. 2006; Adam and Markiewicz 2009; Bourne-Webb et al. 2009; and Wood et al. 2009), with exponential growth to achieve the net zero-carbon building requirements of the code of sustainable buildings by 2019 (Bourne-Webb et al. 2009). Energy pile, where the heat exchange pipes are embedded in concrete, is a form of closed-loop systems combined with ground source heat pump. These piles are commonly referred to as thermo-active foundations, geothermal foundations, or energy piles.

Energy piles are commonly constructed as drilled shafts or precast piles, with diameters ranging from 0.3 to 1.5 m, lengths of 10 to 30 m and with heat exchangers made of polyethylene pipe (Laloui and Di Donna 2013). The net thermal output of energy piles ranges from 18 to 120 W per meter of the foundation length and the system typically provides 3 to 5 energy units for each unit consumed in operation (Preene and Powrie 2009; Bourne-Webb 2013).

Currently, polyethylene pipes are commonly used as heat exchange loops in the energy piles, however PVC pipes were also utilized in the past (Gao et al 2008; Tarnawski et al. 2009; Morino 1994). Prior to drilling the hole, the heat exchange loops are attached to the steel reinforcement cage. Polyethylene pipe joints are installed using heat fused method to produce a 100% leak proof joints that are as strong, or stronger, than the pipe itself. The pipe diameters range from 20 to 40 mm (0.8 to 1.6 inch) and their length depends on several factors including pile length and performance requirements (ASHRAE 2011). The common shapes of heat exchange loops in energy piles include single, double, and triple U-shaped pipes and W-shaped piles as shown in Figure 2 (Gao et al. 2008; Florides and Kalogirou 2007). Single U-shaped were reported as the most economic choice due to the low initial cost and high workability (Hamada et al. 2007). According to experiments and analytical studies by Gao et al. (2008),

the W-shaped loops had higher efficiency than U-shaped loops, however they also have higher cost. In cooling-dominant regions, where the fluid temperature in the pipe is higher than the freezing temperature, water may be used as a heat exchange fluid. In colder regions, antifreeze solutions are commonly used including saline solutions, water and glycol mixture, brine, and potassium acetate (Brandl 1998; Brandl 2006; Tarnawski et al. 2009; Cane et al. 1998; Ozgener and Hepbasli 2005).

2.2 Bridge or Pavement Deicing Using Geothermal Energy

Energy pile, takes advantages of the nearly constant and moderate temperature of the ground to heat and cool buildings, which can be also employed to melt the snow on the bridge deck minimizing or eliminating the use of deicing salt (Spitler and Ramamoorthy 2000; Brandl 2006; Xiao et al. 2013). The feasibility of energy piles for bridge deicing has not been fully explored for different climate conditions.

The geothermal deicing system circulates heat exchange fluid through a pipe network embedded in the bridge deck or pavement to melt snow and ice on the surface. Figure 2.1 presents the configuration of bridge deicing system using geothermal energy pile. In addition to supporting structural loads, geothermal energy piles, which include embedded closed-loop primary pipes circulating a liquid (water or antifreeze), function as a heat exchange system with the surrounding soil (see Figure 2.1). Heat exchange pipes can be also embedded in the embankments. A secondary pipe system is installed in the bridge deck in order to heat it by exchanging energy with the fluid in the primary pipes connected to a heat pump.

Geothermal bridge/pavement heating system will result in reduction of carbon dioxide emissions compared to conventional electric snow-melting equipment (Miyamoto and Takeuchi 2008). The geothermal energy source can be hot spring water directly used for pavement such as the case at Sapporo in Japan, which services 10,405 m^2 pavement (Sato and Sekioka 1979). In Klamath Falls Project of Oregon, ground water cooperated with heat pump is used for bridge and pavement snow melting system covering 2,044 m^2 (Lund 1999). The bridge embedded with heat exchangers also enable to collect solar radiation and store it in the

ground. In Switzerland, a solar energy pilot project (SERSO) has been installed on a bridge in highway network (Schlup and Schatzmann 1998; Rauber 1995). SERSO was used to collect the solar radiation in the summer and heat the bridge surface during frost periods in winter. The heat sink consists of 91 vertical borehole exchangers reaching a depth of 65 m (Lund 1999). All the energy for bridge deck heating was from geothermal or stored solar energy in the ground. Electricity is only used for circulation pumps. The alternative approach using geothermal energy piles for preventing icing was utilized in a bridge in Fukui, Japan (Miyamoto and Takeuchi 2008). Bridge deck deicing using energy piles has been investigated by Bowers and Olgun (2015) with experimental tests. The results indicated that the energy piles were able to keep a model bridge deck (1.2 m x 3.0 m) snow-free when the air temperature was above -5 °C and the precipitation rate was less than 2 mm/hour (water equivalent); however, the energy piles could not melt the snow in extremely cold weather. In the U.S., there is no practical application of bridge deicing using energy piles.

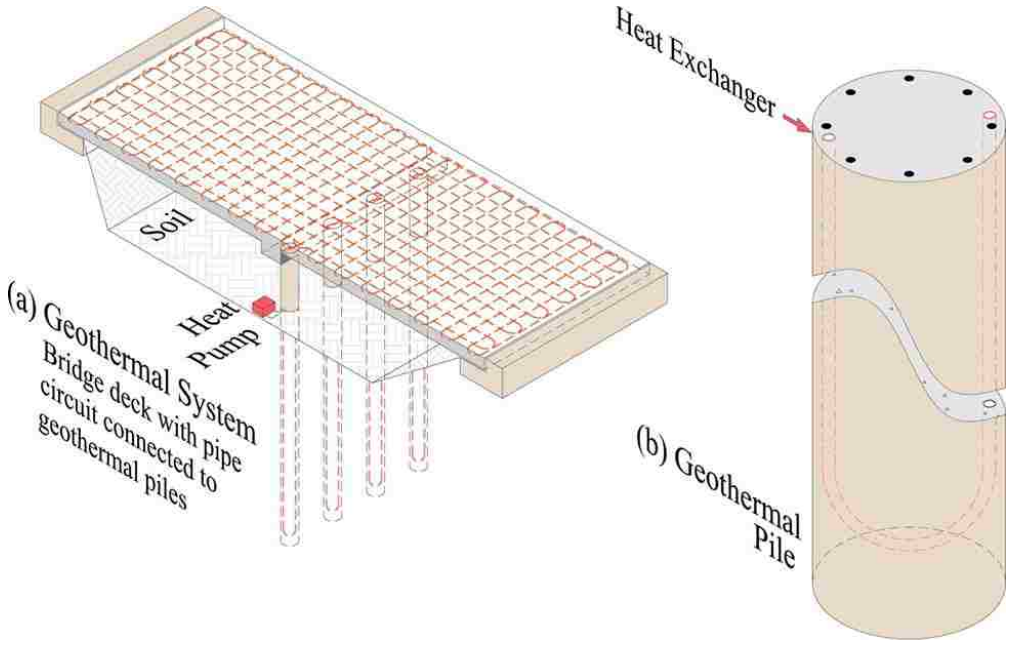

Figure 2.1 Geothermal bridge heating system (a) 3D bridge schematic, and (b) deep foundation

2.3 Heat Transfer Mechanisms of Bridge with Geothermal Deicing Systems

The pavement heat transfer mechanisms have been studied by a number of researchers that contributed to the design guidelines of deicing systems (e.g., Chapman 1952; Leal and Miller 1972; Schnurr and Falk 1973; Ramsey et al. 1999; Chiasson et al. 2000; Rees et al. 2002; Qin and Hiller 2013). Based on these studies, a conventional bridge (i.e., with no geothermal system) subjected to weather changes transfers heat through four major mechanisms, which include: (1) conduction within the bridge slab due to temperature gradients; (2) convection (or sensible heat exchange) between the ambient air and the bridge; (3) radiation to the bridge (i.e., solar or short radiation, and incoming longwave radiation) and from the bridge (i.e., outgoing longwave radiation to ambient air, water, and ground, etc.); and (4) precipitation which includes both sensible (associated with rainfall and snowfall on the bridge deck) and latent heat due to evaporation and melting (heat of fusion).

Figure 2.2 Heat transfer mechanics for conventional and geothermal bridge systems

For the case of a bridge slab with geothermal system (see Figure 2.2), two other heat transfer processes need to be considered: (1) conduction between the heating pipe (i.e., heating source) and the bridge slab; and (2) convection between the heat transfer fluid and the heating

pipe. However, the bridge deicing capacity using energy piles has not been evaluated in the United States or in different climate conditions.

2.4 Thermo-Mechanical Behavior of Energy Pile

The ground source heat pump (GSHP) connected to thermo-active geo-structures (such as energy piles) operates in cycles where it functions for a period of time (running time) then stops for another period of time (stoppage time). This intermittent operation subjects thermo-active geo-structures and surrounding soil to changes of temperature and temperature cycles (Shang et al. 2011; Xiao et al. 2017a). In practice, the daily running and stoppage times of GSHP ranges from 30 minutes to 24 hours depending on the heating and cooling loads (Hamada et al. 2007; Wood et al. 2009; Montagud et al. 2011; Luo et al. 2015).

The temperature of energy piles used at various locations was investigated by researchers using field monitoring and numerical analyses, and the temperature at the pile surface was found to range from 0 to 33°C (Brandl 2006; Hamada et al. 2007; Bourne-Webb et al. 2009; Abdelaziz et al. 2011; Rouissi et al. 2012; Akrouch et al. 2013; Wang et al. 2015; Mimouni and Laloui 2015). The pile temperature can rise over 40°C in cooling-dominated environments, extreme climate condition, or when energy piles function as solar energy storage sinks (Gabrielsson et al. 2000).

The thermo-mechanical response of energy pile brings challenges to the design of the buildings and bridges due to the temperature-induced soil-pile interaction. Temperature change and cycles lead to expansion and contraction of the pile in the axial and radial directions, both of which affect the soil-pile interaction of axially loaded energy piles. When an energy pile is heated, it expands in both axial and radial directions, and the pile contracts when it is cooled affecting the shear resistance at the soil-pile interface. The thermal-induced expansion and contraction (or deformation) depends on the load and restraint on the top, toe resistance, and surrounding soil properties.

The research on the thermo-mechanical behavior of energy pile is summarized in Table 2.1-Table 2.3. Researchers have been focusing on temperature induced expansion/contraction,

axial stress, shaft resistance, and end-restraint effects (Brandl 2006; Laloui et al. 2006, Bourne-Webb et al. 2009; McCartney and Murphy 2012; Suryatriyastuti et al. 2012, etc.). The monitored results of temperature and strain in the energy pile for a pilot research project in Austria, reported by Brandl (2006) with full operation system for two years, indicate that temperature changes alter the stress distribution along the pile shaft. The decrease of temperature generated tension stress at the upper part of the energy pile and compressive stress increased at the lower part. Field tests were also performed in London, UK (Amis et al., 2008; Bourne-Webb et al., 2009), Lausanne, Switzerland (Laloui et al. 2006; Mimouni and Laloui 2015), Denver, US (McCartney and Murphy, 2012), Melbourne, Australia (Wang et al. 2015) to investigate the thermo-mechanical response of full-scale energy piles.

When an energy pile is heated, it expands in both axial and radial directions. The axial deformation (axial expansion) is opposed by a shear resistance at the soil-pile interface. When the pile is cooled, the pile contracts and the thermally-induced shear resistance at the soil-pile interface is reversed. The axial deformation effects were well described by Bourne-Webb et al. (2009) and Amatya et al. (2012) for thermal and mechanical loading conditions. Wang et al. (2011) conducted laboratory scale tests of energy piles in silica sand and the shaft resistance of model energy pile showed a significant reduction (20%-50%) in the maximum value when the pile was tested after subjected to heating followed by cooling. Field test results of London and Lausanne cases demonstrate that the absolute change of thermal-induced shaft friction (restraint) increased approximately linearly with temperature (Amatya 2012).

The restraints provided at the soil-pile interface and pile tips produce thermally-induced axial stress, which is compressive when the pile is heated. The thermal axial stresses of two full-scale energy piles (end bearing boundary) were estimated by McCartney and Murphy (2012) using the measured temperature along the shafts. The results showed that thermal induced tensile stresses ranged from 500 to 1100 kPa as the average temperature of pile decreased by 5°C. When the temperature increased by 3°C, compressive stresses of 200-1000 kPa were estimated.

Thermal axial displacements of energy piles also strongly depend on thermal loading and the restraint from the surrounding soil and superstructures. In the field test in London, the loading frame at the surface ensures that the pile head can move freely, but with a constant load being maintained (Bourne-Webb et al., 2009). The pile head moved downward 2.4 mm after the imposed cooling of 19°C (from ~20 to 1°C) of the pile. When the thermal loading was switched to heating, the pile head moved upward by 2 mm (Amis et al. 2008). However, only 0.003 mm upward movement of pile head was observed for maximum change in temperature of 3 °C due to the strong restraint from the slab in the Denver case (McCartney and Murphy, 2012). The research discussed above mainly focus on temperature induced axial expansion/contraction, axial stress, shaft resistance, and end-restraint effects. However, radial expansion and contraction of geothermal foundations alter the normal (horizontal) pressure at the soil-pile interface and affect the axial thermo-mechanical responses of the piles (Suleiman and Xiao 2014; Minouni and Laloui 2015). Those effects on the soil-pile interaction have not been fully investigated or directly measured.

Table 2.1 Summary of Thermo-mechanical Responses of Energy Piles, (a) Pile and Ground Informations-1

Reference	Test types/loads	Soil types	Pile information	No. of tested piles	Pile temperature range during the test (°C)	Ground or lab temperature (°C)	Temperature cycles
Laloui et al. 2006	Field test /~1300 kN	0-12 m: soft clay; 12-21.6 m: soft sandy gravelly clay; 21.6 - 25.8 m: stiff sandy gravelly clay; Bottom: week sandstone	Drilled shaft, length: 25.8 m, Diameter: 0.88 m	1	10-31	10	7
Brandl, 2006	Field test	0-5 m: loam; 5 -10 m: silty sand to clayed silt; 10-15 m: clayey to sandy silt	Drilled shaft, length: 9 m, diameter: 1.2 m	1	~2-20	~15	NA
Amis 2008; Bourne-Webb et al. 2009	Field test /1200 kN	0-4 m: granular fill and sand and gravel; 4-23 m: stiff, fissured silty clay	Drilled shaft, length: 23 m, diameter: 0.55 m (main shaft)	1	0.3-27	18-20	2
Wang et al. 2011	Laboratory model test/40, 50, 90 N	Fine sand and flour	Steel model pile, diameter: 25.4 mm	1	23-32	~22	NA

Table 2.2 Summary of Thermo-mechanical Responses of Energy Piles, (a) Pile and Ground Informations-2

Reference	Test types/loads	Soil types	Pile information	No. of tested piles	Pile temperature range during the test (°C)	Ground or lab temperature (°C)	Temperature cycles
McCartney and Murphy 2012	Field test	0- 3 m: fill; 3-7.6 m: sand and gravel; 7.6-14.9 m: Claystone	Drilled shaft (end bearing), length: 14.8 m and 13.4 m, diameter: 0.91 m	2	10-20	~15	NA
Tang et al. 2013	Laboratory model test	Sand	Aluminum model pile, length: 0.8 m, diameter:0.14 m	1	25-55	NA	2
Stewart and McCartney 2013	Centrifuge model / (24 g), 443 kN	Bonny silt	Drilled shaft, length: 553.4 mm, diameter: 50.8 mm	1	21-40	~21	4
Wang et al. 2015	Field test, O-cell testing	0-1.5 m: fill; 1.5-2.5 m: sand clay; 2.5-18.6 m: very dense sand	Drilled shaft, length: 16.1 m diameter: 0.6 m	1	17-40	17-18	2
Mimouni and Laloui (2015)	Field test/ 0, 800, 2200, and 2100 kN	0-7.7 m: very soft alluvial clay; 7.7-15.7 m: Loose sandy gravelly moraine; 15.7-19.2 m: Stiff bottom moraine; 19.2-28 m: Sandstone	Drilled shaft, length: 28 m diameter: 0.9 m	4	15-25	~15	1

Table 2.3 Summary of Thermo-Mechanical Responses of Energy Piles, (b) Thermo-Mechanical Responses

Reference	Testing duration	Thermal axial displacements*	Additional thermal-induced load or stress	Shaft resistance
Wang et al. 2011	22 hrs	NA	NA	20-50% reduction
Tang et al. 2013	~190 hrs	0.5 mm settlement after two heating cycles	NA	Shaft resistance inverted in some parts of the pile
McCartney and Murphy 2012	Over 100 days	-0.003 mm at 3 °C change	Cooling: 5 °C decrease causes a tensile force of 500-1100 kPa Heating: 3 °C increase causes a compressive force of 200-1000 kPa (calculated results)	NA
Laloui et al. 2006	28 days	~ - 4 mm	1.3-2.1 MPa	Decrease ~50 kPa in the top soft clay (0-12 m), little change in the rest
Brandl 2006	More than 10 years	NA	Cooling: upper part generated tension stress, compressive stress increased at lower part	NA
Amis et al., 2008; Bourne-Webb et al. 2009	NA	~ 2.8 mm at the end of cooling ~ -2 mm during heating	Cooling: 200-500 kN tensile force or 2 MPa stress Heating with 10 C increase: ~700 kN compressive force	The mobilized shaft resistances increase about 60 kPa in the upper shaft and reduce or reverse in the lower shaft during cooling. Reverse effect occurs during heating.
Stewart and McCartney 2013	24000 s	-1.4 mm at first temperature cycle, -1.26 mm after four temperature cycles	Heating:1200 kN compressive force (Prototype-scale)	NA
Wang et al. 2015	130 days	0.05-0.08 mm of radial expansion	NA	Pile shaft resistance increase at least 14%
Mimouni and Laloui 2015	6 and 24 days	-0.36 to -0.84 mm	Heating: 100-1500 kN compressive force	NA

* Negative: uplift; positive: settlement

2.5 Load Transfer Analysis of Vertically-loaded Piles

For conventional piles, a simplified load-transfer analysis (also called t-z method) is commonly used to analyze the soil-pile interaction for vertically loaded deep foundations. The one-dimensional t-z method models the soil-pile interaction using nonlinear springs simulating the soil-pile interface along the shaft (t-z curves) and one spring modeling the end bearing at the pile tip (q-w curve) (Misra and Chen 2004; and Alawneh 2006). As shown in Figure 2.3a, the t-z curves represent the relationship between shear stress and displacement of the soil-pile interface at a specific depth along the shaft, while the q-w curve defines a relationship between the normal stress and displacement at the pile tip. The pile can be divided into small elements as illustrated in Figure 2.3b. Examples of the nonlinear spring relationships of the t-z and q-w curves are shown in Figure 2.3d and e. As shown in Figure 2.3c, the t-z curve for an element i depend on the horizontal (or normal) stress (σ_h) at the soil-pile interface. This normal stress (σ_h) changes with installation method, depth below ground surface, and soil properties. The normal stress and soil properties are also altered by temperature change and cycles and due to pile expansion and contraction in the case of energy piles (Tang et al. 2013; Suryatriyastuti et al. 2012). However, limited direct measurements of the heat exchange effect on soil-pile interface properties were conducted, and the long-term effects of temperature cycles on soil-pile interface properties have not been investigated. The proposed testing methods (Modified-DST and Modified-TBST) and procedures will address these two knowledge gaps by directly measuring the soil-concrete interface response at different temperatures and after subjected to different temperature cycles.

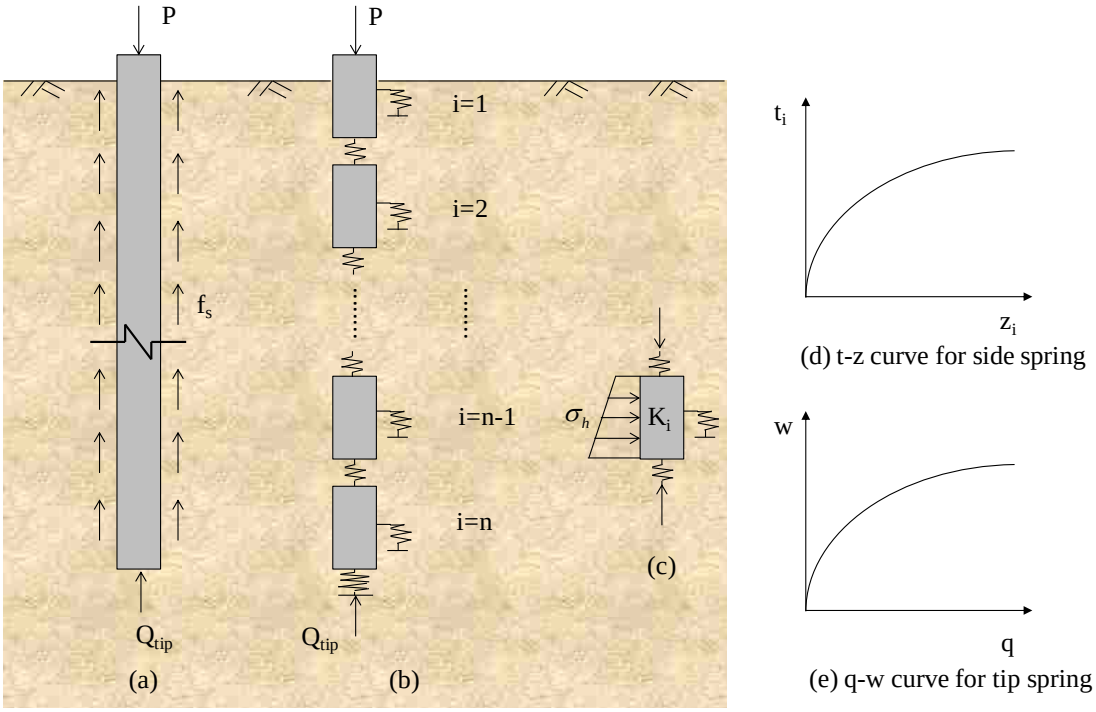

Figure 2.3 Details of the t–z model: (a) idealized pile, (b) pile discretization, (c) nonlinear springs with Kshaft representing the shaft resistance at soil–pile interface for element i with normal stress equals to σh , (d) t–z curve for element i, and (e) q–w curve at the pile tip.

2.6 Direct Measurement of Soil-pile Interaction

To directly measure the shear stress-displacement response (t-z curves) at the soil-pile interface for conventional steel vertically loaded piles, the Borehole Shear Test (BST) equipment and testing procedure were modified by Suleiman et al. (2011) and AbdelSalam et al. (2012) to produce the modified Borehole Shear Test (mBST). The conventional BST was designed by Handy and Fox (1967) to provide a direct field measurement for the drained soil shear strength parameters. The BST equipment consists of the dynamometer and the shear head (Figure 2.4a). Lutenegger et al. (1978) and AbdelSalam et al. (2012) describe the procedure of conducting the BST test using the grooved plates (Figure 2.4b) as follow: (1) the shear head is lowered into an open drilled borehole (or through a hollow stemmed auger) to reach the desired depth, (2) a constant stress normal to the surface of the borehole is applied (P_n in Figure 2.4a), and (3) the soil is sheared by

manually applying an upward pulling force (T in Figure 2.4a). The dynamometer gauge measures the shear stress. When conducting the BST, only the maximum shear stress is recorded AbdelSalam et al. (2012). The BST can be conducted three to six times at approximately the same depth using different P_n values to produce a Mohr-Column envelop (Handy and Fox, 1967; and Handy, 1986).

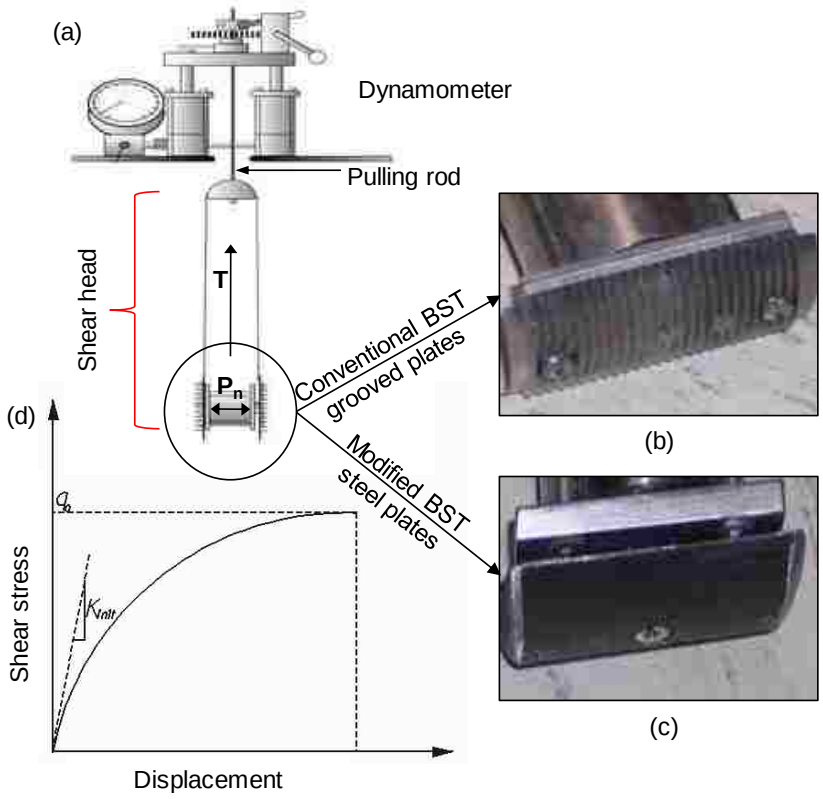

Figure 2.4 (a) BST components (modified after Handy (2008), courtesy of Handy Geotechnical Instruments, Inc.), (b) grooved shear plates used in conventional BST, (c) new smooth plates, and (d) sample t–z curve measured using modified device. (modified after AbdelSalam et al., 2012)

The modification by Suleiman et al. (2011) and AbdelSalam et al. (2012) are as follows: (1) a dial gauge was added to the apparatus base plate to measure the vertical displacement of the shear head during shearing; (2) the grooved shear plates used in the conventional BST (see Figure 2.4b) were replaced with steel plates to better represent the surface of the steel piles (see Figure 2.4c), hence more accurately modeling the soil-pile interface; and (3) the data collection procedures were modified to record the shear stress as a function of the measured vertical displacement, which

essentially yields a measured t-z curve (see Figure 2.4d). The applied shear stress and the displacement were recorded manually, which required more than one operator in the field.

2.7 Temperature Effects on Volume Change and Shear Strength of Soils

The temperature change of the pile also alters the temperature of the surrounding soil and its mechanical properties. Temperature effects on soil properties depend on its thermal history, stress history, and hydraulic conductivity (Graham et al 2001; Burghignoli et al. 2000; Hueckel et al. 2009). Temperature changes induce volumetric strain (volume change) in normally consolidated and overconsolidated saturated soils (Campanella and Mitchell 1968; Demars and Charles 1982; Cekerevac and Laloui 2004; Uchaipichat and Khalili 2009; Tawati 2010). Normally consolidated and slightly overconsolidated saturated clays contract when subjected to drained heating and experience significant irreversible (plastic) volumetric strain when returning to the initial temperature leading to an increased shear strength (e.g., Cekerevac and Laloui 2004). When subjected to undrained heating, expansion of soil components and thermally-induced excess pore water pressure lead to a reduction in shear strength (Campanella and Mitchell 1968; Mitchell and Soga 2005). Highly overconsolidated saturated clays subjected to drained heating; however, experience irreversible volumetric expansion that decreases with overconsolidation ratio (OCR) (Plum and Esrig 1969; Sultan et al. 2002). If heated beyond a threshold temperature, saturated overconsolidated clays may contract (Hueckel and Baldi 1990; Cekerevac and Laloui 2004). Cekerevac and Laloui (2004) and Abuel-Naga, et al. (2007) reported an increase of shear strength for overconsolidated soils when subjected to drained heating. For unsaturated soils, Uchaipichat and Khalili (2009) reported responses similar to those described above for normally and overconsolidated saturated soils. It is worth noting; however, that the critical state shear envelope is independent of temperature change (not cycles) for both saturated and unsaturated soils (Cekerevac and Laloui 2004; Uchaipichat and Khalili 2009; Alsherif and McCartney 2016). When subjected to cycles of heating and/or cooling, soils experience an accumulated permanent

volumetric contraction regardless of stress history due to thermal creep (Campanella and Mitchell 1968; Burghignoli et al. 1992; Vega and McCartney 2015; Xiao et al. 2017a).

3. A NEW MODELLING APPROACH OF HEAT TRANSFER OF BRIDGES CONSIDERING VEHICLE-INDUCED THERMAL EFFECTS

3.1 INTRODUCTION

Road infrastructure systems support safe, rapid, and reliable transportation of people, goods, and services in a wide range of weather conditions including ice and snow conditions. The most common method for pavement deicing utilizes chemical salts that lower the freezing point of water on the pavement or bridge deck surfaces. However, deicing chemicals are corrosive and reduce the longevity of bridge infrastructure making it difficult to achieve the national goal of a 100-year or more bridge service life (Koch et al. 2002; Azizinamini et al. 2014), and the pavement or bridge temperature can be lower than the working range of these chemicals in extreme cold weather (Lund 1999; Joerger and Martinez. 2006; Minsk, L. D. 1999). Alternative approaches to mitigate the corrosion damage caused by the deicing chemicals have been attempted since 1950s. For instance, pavement or bridge deck surface can be heated by electric cables, conductive concrete, or thermal pipes circulating a heated fluid instead of using deicing chemicals for snow melting (Xie, et al. 1996; Zenewitz 1977; Lee et al. 1984; Cress et al. 1995; New Item 1998). However, the designs and applications of the bridge deicing methods require an understanding of heat transfer mechanisms of the bridge and accurate prediction of bridge deck temperature. The electric or thermal energy demand also need to be estimated for different locations and weather conditions to design the bridge heating systems.

The bridge temperature depends on local weathers (i.e. air temperature, wind speed, precipitation, longwave or infrared radiation, and shortwave radiation). One of the important factors that balances the bridge surface temperature is longwave radiation including incoming and outgoing. However, incoming longwave radiation is considered to be the most poorly quantified from observations (Trenberth and Fasullo 2012; Trenberth et al. 2009). There are two common methods of representing incoming longwave radiation from atmosphere based the Stefan–

Boltzmann law. The first method treats the atmosphere as a black body with a uniform temperature T_{sky}. Another method treats the atmosphere as an isothermal grey body at the same temperature of the air, and an effective emissivity is employed (Ramsey et al. 1982). The first method was used in Ramsey et al. (1999), Chiasson (2000), Liu et al. (2007), ASHRAE (2011), and Xiao et al. (2013) for the heat transfer simulation of pavement or bridge, and the calculated T_{sky} is 10 to 40 °C lower than air temperature (Ramsey et al. 1982). However, extensive studies showed that the longwave radiation received by the ground surface corresponds essentially to radiation emitted by the lowest hundred meters of the atmosphere, where the temperature is close to air temperature (Zhao et al. 1994; Brown 1998; Trigo et al. 2010; Moene and van Dam 2014). Therefore, the second method was employed in our model, where the air temperature was considered as the radiant temperature, and the effective emissivity of atmosphere was used. The results from those two methods are compared in this study.

The passage of the vehicle also influences the temperature of the pavement and bridge surfaces (Parmenter and Thornes 1986). The temperature of pavement surface decreases with increasing vehicle speed and increases with vehicle body temperature and traffic volume (Ishikawa et al. 1999). Limited numerical modelling simulated vehicles effects on the bridge surface temperature (Fujimoto et al. 2008). Moreover, there is no model combining the effects of natural wind and vehicle-induced wind on the convection boundary on the bridge deck surface.

The main objective of this study is to propose a new approach to accurately predict the temperature of the bridge deck, and assess the effects of radiation and convection. The vehicle-induced effects were also considered in the analysis.

Main Notation

a	albedo of the bridge surface	θ	natural wind direction (°)
c_p	heat capacity (J kg^{-1}K^{-1})	ρ	density, (kg m^{-3})
h	convective heat transfer coefficient (W m^{-2})	ν	kinematic viscosity (m^2 s^{-1})
I	shortwave incidence (J m^{-2})	Subscripts	
k	thermal conductivity (Wm^{-1}K^{-1})	*a*	air
L_{ch}	characteristic length of the bridge deck (m)	*aviw*	average vehicle-induced wind
L_{hf}	specific latent heat of fusion (J kg^{-1})	*b*	bottom
L_v	length of vehicle (m)	*clw*	corrected longwave radiation
$\dot{p}''$	water equivalent precipitation rate, (m s^{-1})	*cond*	conduction
N_v	hourly traffic volume (vehicle hr^{-1})	*conv*	convection
$\overline{Nu}$	Nusselt number	*csw*	corrected shortwave radiation
OV	occupancy of vehicle	*e*	ambient environment (water or ground)
Pr	Prandtl number	*evap*	evaporation
q''	heat flux (W m^{-2})	*eviw*	equivalent vehicle-induced wind
Re_L	Reynolds number	*ew*	effective wind
t	time (s)	*lw*	longwave radiation
T	temperature (°C)	*mp*	melting point
T_{sky}	temperature of sky or mean radiant temperature (K)	*nw*	natural wind
T_{sv}	bridge surface temperature with vehicle effects	*rad*	radiation
$\vec{V}$	velocity (m s^{-1})	*rf*	rain fall
$\overrightarrow{V_{rd}}$	relative velocity at driving direction (m s^{-1})	*sb*	surface of bottom deck
$\overrightarrow{V_{rec}}$	recorded wind velocity from the weather station (m s^{-1})	*s*	bridge surface
x	x-axis coordinate (m)	*sf*	snow fall
y	y-axis coordinate (m)	*sm*	snow melting
z	height of bridge (m)	*st*	surface of top deck
z_{rec}	height at which the wind speed is measured (m)	*sw*	shortwave radiation
α	thermal diffusivity (m^2 s^{-1});	*t*	top surface
ε	emissivity	*vb*	bottom of vehicle
ε^*	effective emissivity of atmosphere	*w*	water
ε_v	emissivity of vehicle bottom	$\downarrow$	incoming
σ	Stefan-Boltzmann constant (kg s^{-3} K^{-4})	$\uparrow$	outgoing

3.2 BACKGROUND

3.2.1 Natural Factors

The pavement heat transfer mechanisms have been studied by a number of researchers that contributed to the design guidelines of deicing systems (e.g., Chapman 1952; Leal and Miller 1972; Schnurr and Falk 1973; Ramsey et al. 1999; Chiasson et al. 2000; Rees et al. 2002; Qin and Hiller 2013). Based on these studies, the heat fluxes due to natural factors are summarized in Figure 3.1a, which include: (1) conduction within the bridge slab due to temperature gradients; (2) convection (or sensible heat exchange) between the ambient air and the bridge; (3) radiation to the bridge (i.e., solar or short radiation, and incoming longwave radiation) and from the bridge (i.e., outgoing longwave radiation to ambient air, water, and ground, etc.); and (4) precipitation which includes both sensible (associated with rainfall and snowfall on the bridge deck) and latent heat due to evaporation and melting (heat of fusion).

3.2.2 Vehicle Effects

The model shown in Figure 3.1a considers the natural factors in the prediction of the bridge surface temperature. However, the passing vehicle also alters the heat transfer boundary at the pavement surface for different traffic conditions. Using the thermal mapping technique, a heavy traffic flow was found to affect the temperature of the pavement surface by approximately 1.5 °C (Gustavsson and Bogren 1991). Chapman and Thournes (2005) reported 1.5°C temperature difference of the road surface due to different traffic conditions on a multi-lane highway.

Numerical modeling of traffic effects on the road surface temperature (RST) evaluated by limited investigations (Fujimoto et al. 2008). The numerical results of Parmenter and Thornes (1986) indicated that the increased volume of vehicles at low speed produced increased RST of up to 2 °C. Ishikawa et al. (1999) conducted a boundary simulation of road surface with snow cover to evaluate the contribution of infrared radiation from the vehicles under different traffic volumes. The total incoming long-wave radiation of the road surface with traffic increased by 50% in

comparison with no traffic for 30 minutes. Chapman et al. (2001) assumed an increase of 2 m/s of wind speed induced by vehicles in the theoretical simulation to simplify the vehicle effect on the convection. Fujimoto et al. (2008, 2012) conducted numerical simulations considering the vehicle effect in the dry pavement condition and presented the relationship between the vehicle speed and vehicle-induced wind; the simulation showed that the RST at the vehicle-passage area is ~3 °C lower than nonvehicle-passage area during the daytime. However, the work by Fujimoto (2008 and 2012) did not consider the interaction between natural wind and vehicle-induced wind, which is addressed in this paper.

As shown in Figure 3.1b, the effects of vehicles on the heat transfer of bridge deck surface include: (1) longwave radiation from the bottom of the vehicle; (2) convection heat induced by the vehicle; (3) frictional heat from tires; and (4) the effect of the presence of vehicles on the incoming longwave from the atmosphere and incoming shortwave radiation. It is noted that radiative and convective heat can play typically significant roles in the heat exchange between the vehicle and road surface (Prusa 2002; Fujimoto 2006).

To estimate the bridge surface temperature, an improved boundary modelling of the bridge deck surface is utilized. The model is based on models proposed by ASHRAE (2011), Ramsey et al. (1999), Chiasson (2000), and Xiao et al. (2013). Initially, a two-dimensional (2D) simulation was validated using results of measured temperature of Jamestown Verrazzano Bridge in Rhode Island that were reported by Tsiatas et al (2002). Using the 2D model with a series of meteorological data (e.g., air temperature, solar radiation, and hourly average wind speed, etc.) from the local weather station, the bridge temperature was calculated and compared with measured temperatures. Once validated, the model was extended to incorporate the effects of vehicles. The effective wind velocity is introduced using the concept of the effective pollutant advection velocity proposed by Rao et al. (2002) to combine the natural wind and vehicle-induced wind. The daily and seasonal vehicle effects were also investigated. Furthermore, the heat flux contribution of the vehicles on the bridge surface is also presented in clear and snowing weather conditions, separately.

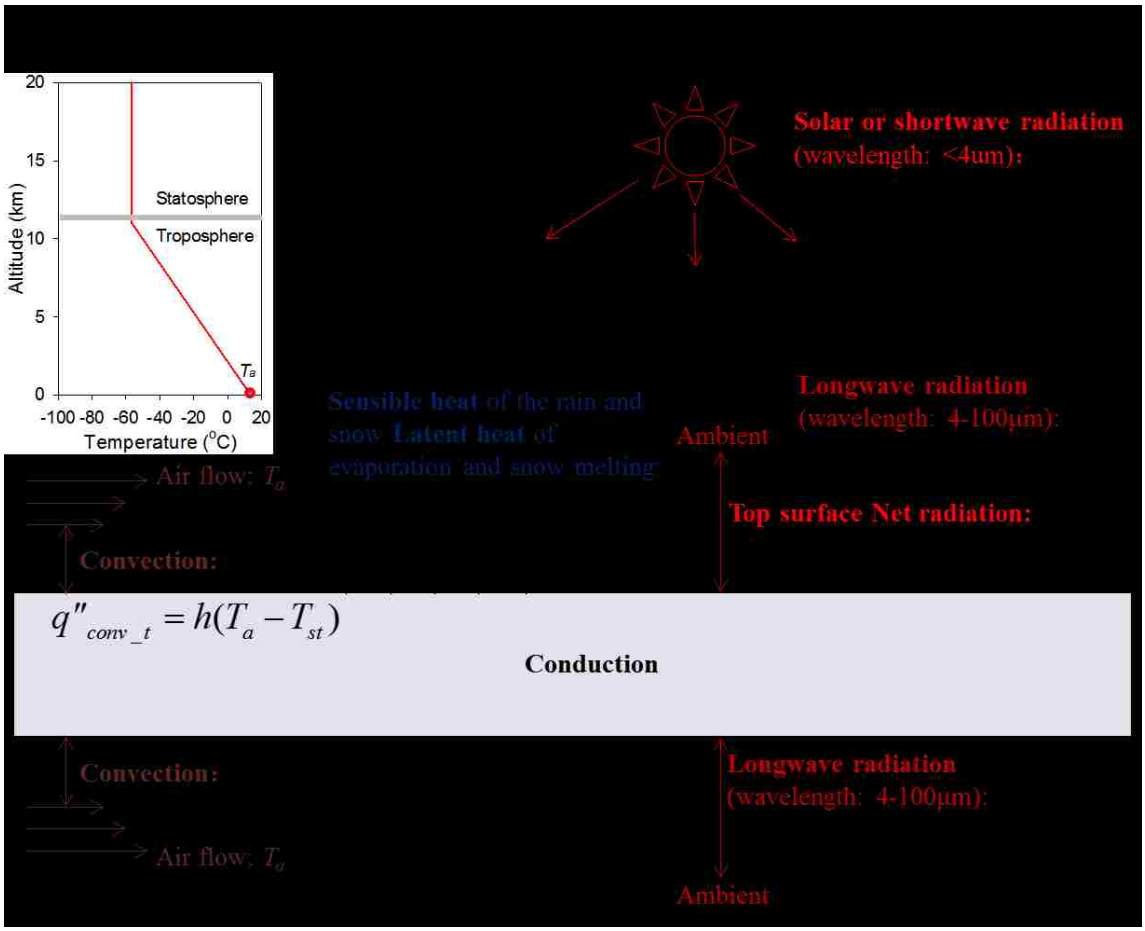

(a)

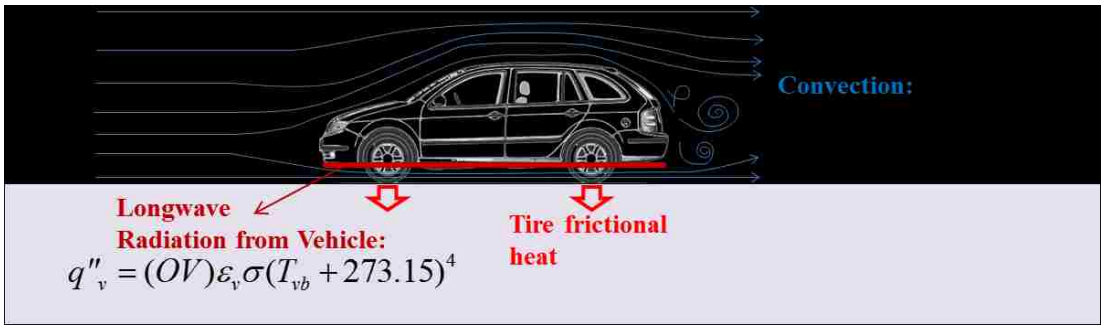

(b)

Figure 3.1 Configurations of heat transfer model for bridge deck, (a) Natural factors; and (b) Vehicle factors

3.3 NUMERICAL MODEL

3.3.1 Governing Equations

In our model, the finite element method has been used to solve the heat conduction equation that describes the temperature distribution of the bridge slab. The governing transient 2D heat conduction equation can be expressed in Eq. 1. α is the thermal diffusivity (m^2/s) of the bridge slab material which is calculated by Eq. 2. All the equations shown in this paper were tabulated in Table 3.1.

3.3.2 Natural Boundaries

The heat fluxes at the top surface of the bridge deck q''_t (W/m^2) due to the natural factors shown in Figure 3.1a can be represented by Eq. 3, which include net radiation (longwave and shortwave radiation, q''_{lw_t} and q''_{sw_t}), convective heat flux (q''_{conv_t}), sensible heat flux due to falling rain (q''_{rf}), latent heat flux due to snow melting (q''_{sm}) and evaporation heat flux of water or melted snow (q''_{evap}). As will be discussed in the following sections, each term in Eq. 3 can be obtained using equations 4 through 20 except evaporation heat flux. Determining the evaporation heat flux is based on the method suggested by ASHRAE (2011).

The bottom surface of the bridge slab is subjected to long radiation (q''_{lw_b}) and convection (q''_{conv_b}) which is given by Eq. 4.

3.3.2.1 Net Radiation (q''_{rad})

The net radiation heat flux at the top surface (q''_{rad_t}) of the bridge includes shortwave radiation (or solar radiation, q''_{sw_t}) and longwave radiation (q''_{lw_t}) as expressed in Eq. 5. Each term in the Eq. 5 can be calculated using Eq. 6 to 9.

Table 3.1 Equations

No.	Equations	No.	Equations
1	$\frac{\partial^2 T}{\partial x^2}+\frac{\partial^2 T}{\partial y^2}=\frac{1}{\alpha}\frac{\partial T}{\partial t}$	15	$\overline{Nu}=0.037\,\mathrm{Re}_L^{\,0.8}\,\mathrm{Pr}^{1/3}$
2	$\alpha=k/\rho c_p$	16	$\mathrm{Re}_L=\frac{\left\|\overrightarrow{V_{nw}}\right\|L_c}{\nu_a}$
3	$q''_t=q''_{rad\_t}+q''_{conv\_t}+q''_{rf}+q''_{sm}+q''_{evap}$	17	$h=1.520\cdot\sqrt[3]{\left\|T_s-T_a\right\|}$
4	$q''_b=q''_{lw\_b}+q''_{conv\_b}$	18	$h=0.760\cdot\sqrt[3]{\left\|T_s-T_a\right\|}$
5	$q''_{rad\_t}=q''_{sw\_t}+q''_{lw\_t}$	19	$q''_{rf}=\rho_w\dot{p}''_{rf}c_{p\_w}(T_a-T_{st})$
6	$q''_{sw\_t}=(1-a)I$	20	$q''_{sm}=\rho_w\dot{p}''_{sf}(c_{p\_sf}(T_a-T_{mp})-L_{hf})$
7	$q''_{lw\_t}=q''_{lw\_t\downarrow}-q''_{lw\_t\uparrow}$	21	$\left\|\overrightarrow{V_{rd}}\right\|=\left\|\overrightarrow{V_v}\right\|-\left\|\overrightarrow{V_{nw}}\right\|\sin\theta$
8	$q''_{lw\_t\downarrow}=\varepsilon^*\sigma T_a^4$	22	$\left\|\overrightarrow{V_{aviw}}\right\|=\frac{N_v t_{viw}\left\|\overrightarrow{V_{eviw}}\right\|}{3600}$
9	$q''_{lw\_t\uparrow}=\sigma\varepsilon_s T_{st}^4+(1-\varepsilon_s)q''_{lw\_t\downarrow}$	23	$\left\|\overrightarrow{V_{ew}}\right\|=\left[\left(\left\|\overrightarrow{V_{aviw}}\right\|-\left\|\overrightarrow{V_{nw}}\right\|\sin\theta\right)^2+\left(\left\|\overrightarrow{V_{nw}}\right\|\cos\theta\right)^2\right]^{1/2}$
10	$q''_{rad\_b}=\varepsilon_e\sigma T_a^4-\varepsilon_s\sigma T_{sb}^4$	24	$q''_v=(OV)\varepsilon_v\sigma(T_{vb}+273.15)^4$
11	$q''_{lw\_t}=\sigma\varepsilon_s(T_{sky}^4-T_{st}^4)$	25	$OV=\frac{N_v}{3600}\times\frac{L_v}{\left\|\overrightarrow{V_v}\right\|}$
12	$q''_{conv\_t}=h(T_a-T_{st})$	26	$q''_{csw\_t}=(1-OV)q''_{csw\_t}$
13	$q''_{conv\_b}=h(T_a-T_{sb})$	27	$q''_{clw\_t}=(1-OV)q''_{lw\_t}$
14	$h=\frac{k_a}{L_{ch}}\overline{Nu}$	28	$\left\|\overrightarrow{V_a}\right\|=\left\|\overrightarrow{V_{rec}}\right\|\cdot\left(\frac{z}{z_{rec}}\right)^{1/7}$

Shortwave radiation (q''_{sw_t})

The shortwave radiation absorbed by the top surface of the bridge can be estimated by Eq. 6. *a* is albedo (reflection coefficient) of the bridge surface ranging from 0.25 to 0.3 for weathered concrete, an average value of 0.275 was used in the model when the surface is dry (Bretz et al., 1998). The albedo of the deck is 0.45 during snow and 0.14 during raining (Dingman,1994; Levinson and Akbari, 2002).

Longwave Radiation (q''_{lw_t})

Incoming longwave radiation ($q''_{lw\_t\downarrow}$) is defined as the total irradiance within the infrared part of the electromagnetic spectrum (4-100 μm). Within this range, atmospheric scattering may be neglected and $q''_{lw\_t\downarrow}$ received by the bridge surface corresponds essentially to radiation emitted by the lower hundred meters of the atmosphere (Zhao et al., 1994; Brown, 1998; Trigo et al., 2010; Moene and van Dam, 2014). In our model, the air temperature measured by weather stations at 2 m above the ground level was used as the radiant temperature of the atmosphere. Following the procedures of Brock and Arnold (2000) and Brown (1998), the longwave radiation at top bridge surface q''_{lw_t} was computed using Eq. 7 to 9. The incoming longwave radiation $q''_{lw\_t\downarrow}$ is estimated by Eq. 8, where ε^* is the effective emissivity of the atmosphere, which ranges from 0.6 to 1 according to Unsworth and Monteith (1975), Prata (1996), and Herrero and Polo (2012) depending on the cloud cover and air temperature (Brock and Arnold 2000), and σ is Stefan-Boltzmann constant (5.67×10^{-8} Wm^2K^{-4}). According to Ryu et al (2008), the outgoing longwave radiation $q''_{lw\_t\uparrow}$ can be estimated by Eq. 9, where ε_s is the deck surface emissivity, which is equal to 0.9 according to Bergman et al. (2011) and Levinson and Akbari (2008).

Net radiation at the bottom surface q''_{rad_b} only includes the longwave radiation, which is estimated using Eq. 10. The incoming longwave at the bottom originates from ambient

environment (ground or water surface). ε_e is the emissivity of ambient environment beneath the bridge, which equals to 0.96 according to Bergman et al. (2011). Air temperature is assumed to be equal to the ambient environment temperature (Chiasson et al. 2000).

Other Formulas for Longwave Radiation

The net longwave radiation at top surface q''_{lw_t} can also be estimated using different procedures including those suggested by Chiasson et al. (2000), Ramsey et al. (1999), ASHRAE (2011), and Qin and Hiller (2013). In those models, the atmosphere was treated as a black body with a uniform sky temperature (mean radiant temperature) T_{sky}. For example, the longwave radiation in ASHRAE (2011) and Qin and Hiller (2013) is expressed as Eq 11.

The emissivity of the atmosphere is assumed the same as the pavement material in Eq. 11. Chiasson et al. (2000) and Qin and Hiller (2013) defined the sky temperature T_{sky} as the longwave radiant temperature which can be over 20 °C lower than the air temperature. The mean radiant temperature T_{sky} used in Ramsey et al. (1999) and ASHRAE (2011) is 15-30 °C lower than the air temperature. The temperature ranges of T_{sky} were carefully calculated by the authors. Larger emissivity of atmosphere (same as the pavement material) was used in those models, and yet the longwave radiation from the atmosphere may still be underestimated. Both Eq. 7 and Eq. 11 were used in the calculation for longwave radiation (q''_{lw_t}), and the results of two methods were compared in this study.

3.3.2.2 Convection (q''_{conv})

The convective heat flux at bridge top surface (q''_{conv_t}) and bottom surface (q''_{conv_b}) was calculated using Eq. 12 and 13, and the convective heat transfer coefficient (CHTC) *h* at the bridge surface for the forced convection is defined as Eq. 14. Nusselt number Nu and Reynolds number Re_L were calculated using Eq. 15 and Eq. 16 according to ASHRAE (2011). ASHRAE (2011)

recommends using the width of the bridge slab as the characteristic length L_{ch} for the calculation of h in Eq. 14 and 16. The CHTC for natural convection coefficient was estimated as Eq. 17 and 18 (Walton 1981; Xiao 2000). For the top bridge surface, Eq. 17 was used when the heat flow is upward (the surface temperature is higher than the air temperature), and Eq. 18 was used when the heat flow is down (the surface temperature is lower than the air temperature). For the bottom surface, conversely, Eq. 17 is for the case that the heat flow is downward, and Eq. 18 is for the case of upward heat flow.

3.3.2.3 Precipitation ($q''_{rf} + q''_{sm} + q''_{evap}$)

The method of estimating the sensible heat and latent heat due to the precipitation recommended by ASHRAE (2011) was used in this study. The maximum depth of liquid water that accumulates on the bridge was assumed as 0.76 mm, which is the average depth of mean texture profile of the concrete pavements in 13 states as reported by Hall et al. (2009). Therefore, the maximal residual liquid water on the bridge surface for evaporation after snowfall and rainfall was set to 0.76 mm. For the heated bridge deck, the snow accumulation was neglected. The sensible heat flux due to falling rain (q''_{rf}) was computed using Eq. 19, and latent heat flux due to snow melting (q''_{sm}) was calculated using Eq. 20.

The snow melting model in ASHRAE (2011) referred to as “ASHRAE model” was used in the simulation and compared with the present “Improved model” without the vehicle effects. The model proposed in ASHRAE (2011) considered only snow periods neglecting the effects of solar radiation. However, the ASHRAE model used in this paper does account for the effects of solar radiation to make it more applicable for the whole year's simulation. In other words, the difference between the ASHRAE model and the present improved model are the contributions of longwave radiation and natural convection as described earlier in this paper.

3.3.3 Vehicle Boundaries

As shown in Figure 3.1b, the vehicle effects include convective heat flux (q''_{conv_t}) combining natural wind and vehicle-induced wind, longwave radiation from vehicle bottom (q''_{v}), and corrected longwave and shortwave radiation (q''_{clw_t} and q''_{csw_t}) blocked by the vehicles. Tire frictional heat was neglected in the model.

3.3.3.1 Vehicle-induced Wind

The vehicle-induced wind speed (VIWS) was calculated following the method proposed by Fujimoto et al. (2008). Figure 3.2 describes the VIWS when a vehicle passing a point (point O in the figure). The VIWS increases linearly to a peak speed at time of t_{vmax}, and decrease exponentially after the peak velocity until time of t_{viw}. The t_{viw} is the lifetime of vehicle-induced wind which alters the convection boundary of the bridge deck surface. During the passing time (t_{pv}) of the vehicle, both the sensible heat (q''_{conv_t}) and longwave radiation (q''_{v}) induced by the vehicle will influence the temperature of the bridge deck top surface. In the post-passing time (t_{pp}), only the sensible heat (q''_{conv_t}) is affected by the vehicle. The equations proposed by Fujimoto et al. (2008, 2012) was used to calculate t_{vmax}, t_{viw}, and t_{pv}.

Fujimoto et al. (2008, 2012) presented the relationship of vehicle speed ($\left|\overrightarrow{V_v}\right|$) and induced wind speed under calm conditions, however, the model does not combine the effects of the natural wind in various direction and vehicle-induced wind. Therefore, the concept of the effective wind velocity was introduced, which uses the concept of the effective pollutant advection velocity proposed by Rao et al. (2002). The effective pollutant advection velocity components can be calculated by adding the natural wind velocity and the total wake velocity deficit components induced by vehicle in x and y directions of the horizontal plane. The wake velocity deficit is a function of the relative velocity ($\overrightarrow{V}_{rd}$) of the vehicle and natural wind in the driving direction which

was studied by many researchers using turbulent dispersion modeling to estimate the carbon monoxide concentration in the vehicle wake of the highways (Eskridge and Hunt 1979; Eskridge and Thompson 1982; Hider et al. 1997). For the heat transfer of the bridge, the related region only includes the turbulent wake of the vehicle close or above the traffic lane. The wake region in the pollutant dispersion models is much larger than the road or pavement area. Therefore, the concept considering the wind direction in the pollutant dispersion model was combined with the vehicle-induced wind model proposed by Fujimoto et al (2008, 2012). The relative velocity ($\vec{V}_{rd}$) of the vehicle and natural wind in the driving direction calculated using Eq. 21 will be used to obtain the VIWS in the driving direction which is different from the model proposed by Fujimoto et al (2008).

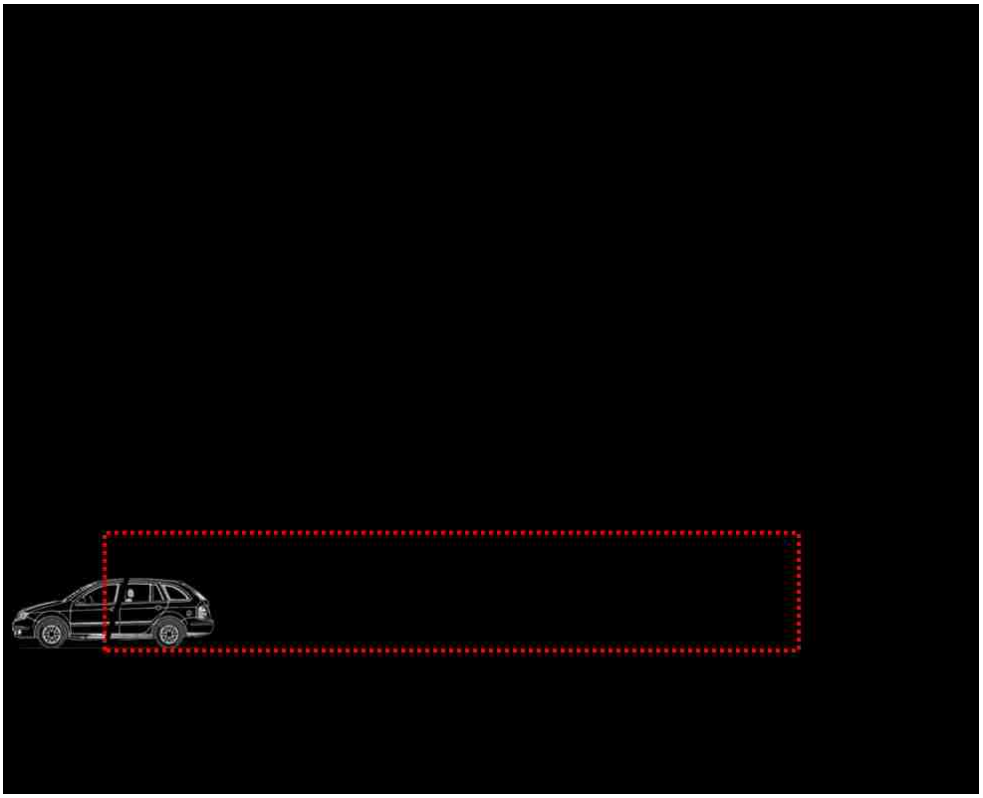

Figure 3.2 Vehicle-induced wind (after Fujimoto et al., 2008)

The following assumptions were made to simplify the model with vehicle-induced effects:

- The VIWS is integrated and equalized to uniform VIWS ($\overrightarrow{V_{eviw}}$) in the period of t_{viw} as represented by the dotted line in Figure 3.2.
- All the vehicle are the automobiles with a normal size (length of vehicles, L_v=4.7 m)
- The effect of traffic from other lanes is neglected, and the traffic flow rate is uniform per unit time (one hour).
- The average temperature at the vehicle bottom (T_{vb}) is assumed as 26.2 °C higher than the air temperature ($T_{vb} = T_a + 26.2$) based on recommendation of Fujimoto et al. (2008).

Once the $\left|\overrightarrow{V_{eviw}}\right|$ by one vehicle is computed, the hourly traffic volume (vehicle/hr) is used to calculate the hourly average vehicle-induced wind speed ($\left|\overrightarrow{V_{aviw}}\right|$) using Eq. 22. The VIWS is combined with the natural wind velocity using Eq. 23 to obtain the effective wind velocity $\overrightarrow{V_{ew}}$ shown in Figure 3.3. In addition, $\left|\overrightarrow{V_{nw}}\right|$ was replaced by $\overrightarrow{V_{ew}}$ to calculate Reynolds number in Eq. 16.

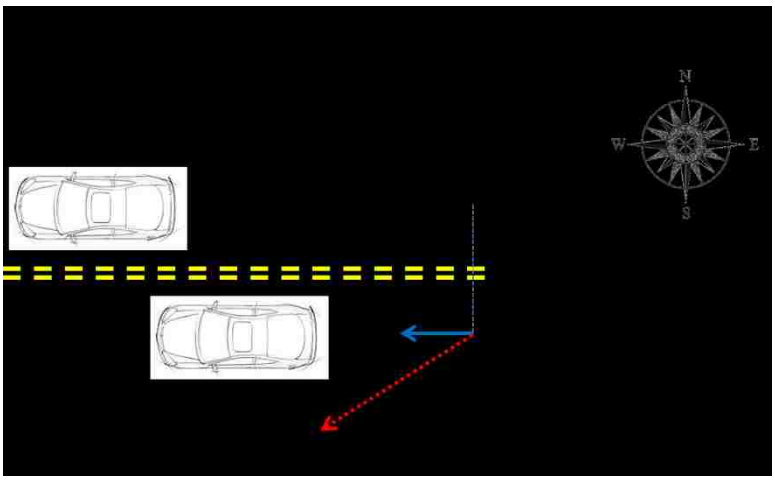

Figure 3.3 Natural wind and vehicle-induced wind

3.3.3.2 Vehicle-induced radiation effect

The temperature of the vehicle undercarriage is 4 to 44 °C higher than the ambient air depending the part position of vehicle and the running time (Ishikawa et al.1999; Fujimoto et al., 2008). The temperature of the bottom of the vehicle (T_{vb}) was assumed as 26.2 °C higher than the air temperature as discussed in the previous section. The vehicle-induced infrared radiation (q''_v) is given by Eq. 24, where ε_v is emissivity of the vehicle bottom (0.95), and *OV* is the occupancy of vehicle (i.e. percent of time for a point on the road to be occupied by vehicles) evaluated by Eq. 25. V_v is vehicle speed which was assumed as 17.9 m/s in the model. Considering the pavement screened by running vehicles, the incoming shortwave and longwave radiations were corrected by Eq. 26 and Eq. 27.

3.4 MODEL VALIDATION

3.4.1 Description of the Bridge

The Jamestown Verrazzano Bridge spans West Passage of Narragansett Bay and links North Kingstown and Jamestown, Rhode Island. The bridge with a width of 22.5 m has four travel lanes separated by a concrete Jersey barrier. The total length of the bridge is 2,240 m with a main center span of 183 m and two side spans of 83 m. The bridge is a double-cell, post tensioned concrete box Girder Bridge. The thicknesses of the top slab and the bottom slab are 0.3 m and 0.2 m separately in main span closure segment. Tsiatas et al. (2002) monitored the strain and temperature of the bridge between 9/17/1997 and 9/23/1998 (approximately one year) in a research report of Rhode Island Department of Transportation. The temperatures of the bridge top slab were monitored at depth increments of 50.8 mm (i.e., 50.8, 101.6, 152.4, and 203.2 mm). Temperatures

of the bottom slab were measured at depth 25.4, 50.8, 101.6, 152.4, 177.6 mm from the bottom surface.

The monitored data summarized by Tsiatas et al. (2002) was compared with the computed results. Tsiatas et al. (2002) presented data over a period of ten days for different weather conditions during the monitoring period for five periods in separate figures. The weather conditions of these 10 days are described in Table 3.2. Both the whole year's data and 10 days data were used for the validation of the model.

Table 3.2 Weather conditions of 10 specific days

Time	Weather Condition
12 pm, 1/13/98 - 12 pm, 1/15/98	Cloudy-rain-clear-cloudy
12 pm, 1/25/98 - 12 pm, 1/27/98	Cloudy (just after snow)-clear-cloudy-clear
12 pm, 5/21/98 - 12 pm, 5/23/98	Clear-cloudy-clear-cloudy-clear
12 pm, 7/21/98 - 11 am, 7/23/98	Clear-light rain-haze-clear
12 pm, 9/5/98 - 12 pm, 9/7/98	Clear-haze-light rain

3.4.2 Finite Element Model

A cross-section of the bridge slab was modeled using a two-dimensional model in ANSYS to simulate the heat transfer of the bridge (ANSYS, Inc., 2014). PLANE55 2-D thermal solid four-node rectangular element was used with heat flux of solar radiation (q''_{sw_t}), infrared radiation (q''_{lw_t}), sensible and latent heat fluxes of precipitation (q''_{rf}, q''_{sm}, and q''_{evap}) applied on the top surface nodes. However, as shown in Figure 3.1, the bridge surface transfers heat through both heat flux and convection boundaries which can override each other on the surface nodes. To model

the heat convection, the SURF151 element was used at the bridge-air interface on which the convection between ambient air and concrete was applied. Because of the complicated boundaries at the bridge surface, the finite element mesh of the model was refined near the bridge slab surface resulting in approximately 0.05 m x 0.05 m elements to yield accurate results (see Figure 3.4).

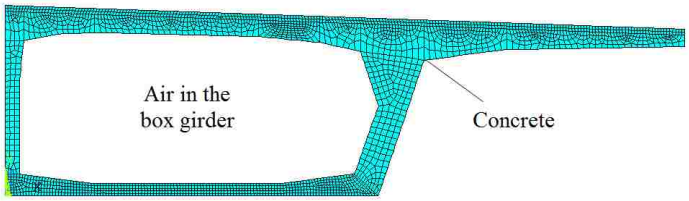

Figure 3.4 Finite element mesh for half of the bridge cross section for the Jamestown Verrazzano Bridge

3.4.3 Material Properties

The thermal properties of concrete and air used in the model are summarized in Table 3.3. Thermal and physical properties of materials. Since the heat transfer of the bridge slab was modeled for a full year, the thermal properties of air at average temperature of 10 °C were used based on the properties reported by Bergman et al. (2011) and were used in the model.

Table 3.3. Thermal and physical properties of materials

	Temperature(°C)	Density (kg/m³)	Specific Heat, c_p (kJ/kgK)	Thermal Conductivity, k $\times 10^{-2}$ (W/Km^2)	Kinematic Viscosity, ν $\times 10^{-6}$ (m^2/s)	Thermal Diffusivity, α ($\times 10^{-6}$ m^2/s)	Pr
Air	10	1.241	1.007	2.494	14.39	20.26	0.705
Reinforced Concrete	10	2500	0.907	198	NA	NA	NA

3.4.4 Input Weather Data

The input weather data were downloaded from Weather Underground (2013) except the cloud cover and solar radiation, which were available at the National Solar Radiation Database (NSRDB, 2012). In order to evaluate the difference between the input weather data and local weather at the Jamestown Verrazzano Bridge, the weather data from two local weather stations were compared. One is a weather station in Newport, RI which is around 8 miles from the bridge. The other one is in Wickford of North Kingstown, RI which is 4 miles from the bridge. The bridge is located between those two weather stations. The recent weather data from of Wickford weather station can be retrieved, but the weather data during the whole simulation period is not available. Therefore, the weather data from Newport were used in the simulation. The weather data difference between those two weather stations are: (1) air temperature and dew point are less than 2 °C; (2) humidity differences are less than 10%; and (3) wind speed differences are less than 25%. Therefore, the input weather data may have ~1 °C air temperature, less than 5% humidity, and less than 15% wind speed differences between the local weather of the bridge and the input weather data. The sensitivity analysis of wind speed was conducted that 15% wind speed difference can lead to ~0.5 °C temperature difference of the bridge deck.

The wind speed obtained from weather station is measured at 10 m above ground surface, therefore, the wind speed at the bridge surface was corrected using the Eq. 28 (Petersen et al. 1998a and 1998b) because the bridge is at elevation of 53.3 m above the sea level. Assuming the wind speed at sea level below the bridge is the same as that at the ground surface of the weather station. The input wind speed is obtained as 1.3 times of the local weather station after the correction.

In the validation case, since the Jamestown Verrazzano Bridge is separated by the Jersey barriers, the characteristic length of the top slab is 11.4 m which is half of the top slab width. The characteristic length for the bottom surface is the width of the bottom slab 12 m. The character length for the free convection can be obtained using the ratio of deck surface area and perimeter

considering the Jersey barriers. During the period of simulation of Jamestown Verrazzano Bridge, the maximum snow precipitation at the site was 2 mm/hour (0.08 in./hour) and the deicing salt was usually used during the snowfall, therefore, the snow accumulation effect on heat transfer was neglected in the validation analysis.

3.4.5 Results and Discussion

Validation of Models

The temperature of the Jamestown Verrazzano Bridge was calculated using both the ASHRAE model and the Improved model. Figure 3.5 shows the comparison between the measured and calculated temperatures at 51 mm below the top surface of the bridge slab (point P1) and 51 mm from the bottom of the bridge (point P2). These results show that the Improved model yields a good estimation of the bridge temperatures especially during the winter time. Results calculated using the ASHRAE model and the Improved model are shown in Figure 3.6 and compared to the measured temperature for ten days. Figure 3.6a shows the comparison at location P1; with the improved model has a root mean square deviation (RMSD) of 1.6 °C compared to 2.6 °C for the ASHRAE model. The predicted temperatures at bottom of the bridge for the two models are almost the same; thus, only the results from the improved model are shown in Figure 3.6 which have the root-mean-square deviation (RMSD) of 1.8 °C. Although, a one degree Celcius difference looks like a minor improvement in the model, however, this temperature difference could result in considerable thermal stresses if the thermal deformation of the bridge components is restrained in the longitudinal direction (Zhou and Yi 2013). Additionally, a one degree Celcius difference temperature can affect phase change of the water on the bridge surface when the temperature of the bridge is close to the freezing point of the water. Thus, it is better to consider the recommendations made in the present improved model that include the effect of longwave radiation and natural convection to predict the bridge temperature.

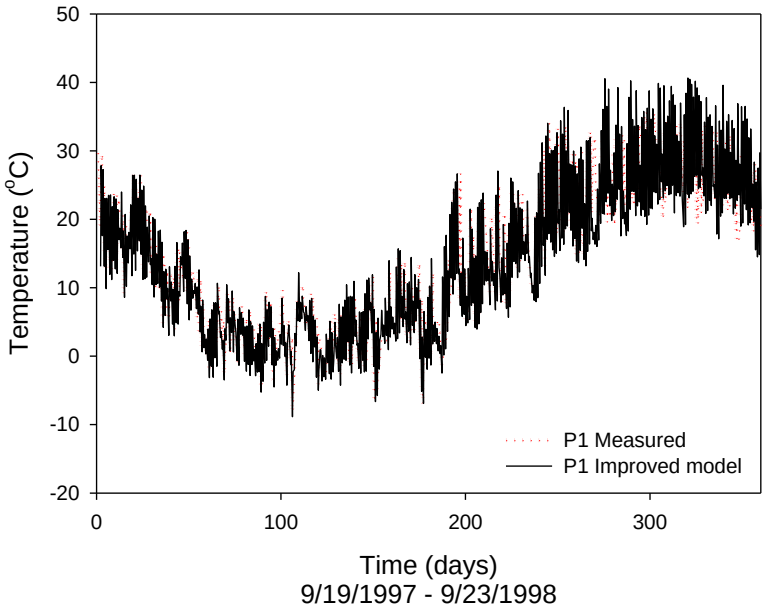

(a)

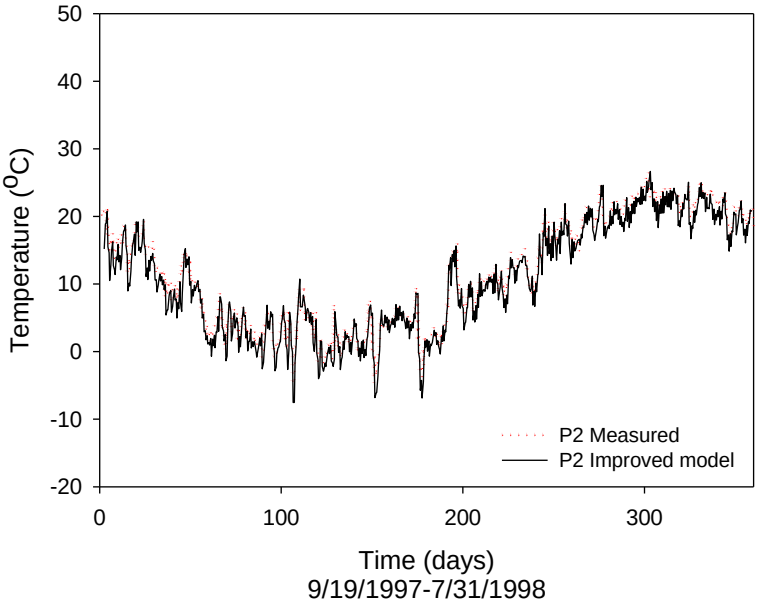

(b)

Figure 3.5 Comparison of the measured data and computed results from the ASHRAE model and improved model in whole year period (a): top slab, (b): bottom slab.

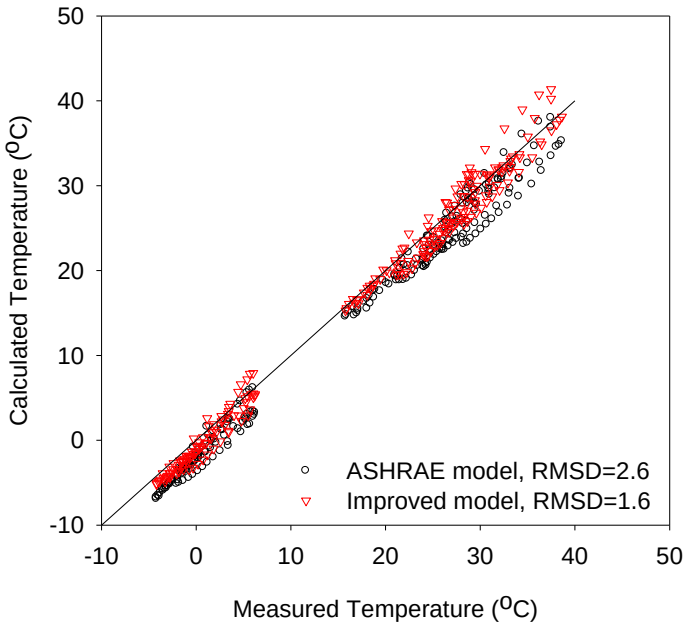

(a)

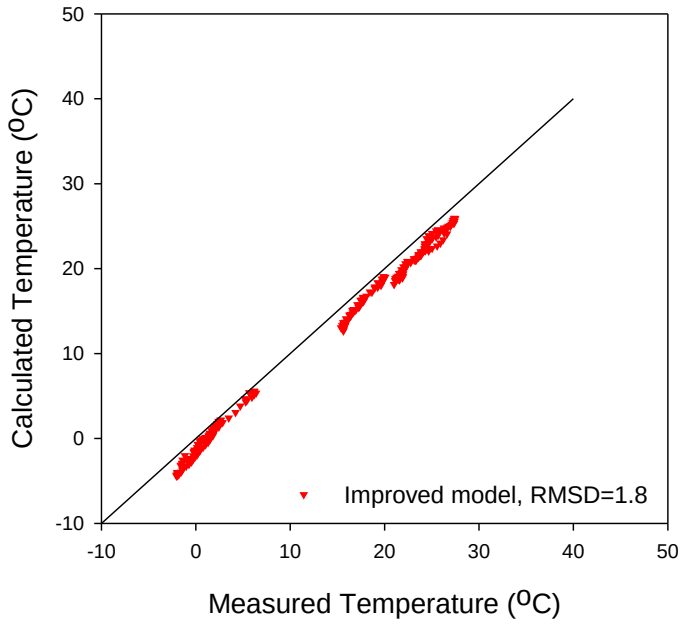

(b)

Figure 3.6 Comparison of the measured data and computed results from the ASHRAE model and improved model in 10 days (a): top slab, (b): bottom slab.

Discussion for the Convection

Figure 3.5 and Figure 3.6 indicate that the calculated results match the measured results very well during the winter time, however, the deviation of temperatures during the summer time is over 3 °C. Some of the deviations may be due to differences of the weather between the location of the bridge and the weather station. Another reason may be that the model underestimates the convective heat transfer coefficient (CHTC) at the lower wind speeds that reduce the convective heat flux contribution in the heat transfer of the bridge based on Eq. 14. Figure 3.7 shows the relation between CHTC and wind speed with different models. Qin and Hiller (2013) investigated the influences of wind speed and CHTC on the pavement temperature prediction. The calculated results from different models for CHTC are compared with one day's measured pavement temperature. Based on the comparisons of Qin and Hiller (2013), the CHTC from Priestley and Thurston (1979) and Bentz (2000) would be overestimated, while the modified Blasius model (Qin and Hiller, 2013) and the model proposed by Sharples and Charlesworth (1993) have a better match with other models. The CHTC obtained from the Eq.14 to 16 (ASHRAE, 2011) is also plotted in Figure 3.7, which increases almost linearly with wind speed. However, the CHTC is smaller than that of other models when the wind speed is lower than 8 m/s and may be underestimated by the equations that were used in the simulation.

The effect of underestimation for CHTC on temperature prediction will be significant when the temperature difference between the air and bridge deck surface is large based on Eq. 12. As shown in the Figure 3.8, the solar radiation and deck-air temperature differences (T_t-T_a) show the similar seasonal variations. The daily average solar radiation during summer time (from June to August) is over twice of the winter time (from December to February). Meanwhile, the temperature of bridge deck surface is higher than surrounding air temperature in most of the summer time, if CHTC is underestimated in the model, the thermal energy stored in the bridge deck is unable to be transferred to the air through the convection which leads to larger predicted temperature of the

bridge deck. Additionally, the wind speed may influence the pavement surface temperature predication in a more pronounced manner if the solar radiation is higher (Qin and Hiller, 2013). As shown in Figure 3.8, the daily average wind speed measured by the weather station during the summer and winter time are 3.4 and 4.4 m/s, respectively, and the instantaneous wind speed is less than 8 m/s during most of the summer time. For this wind speed range, the CHTC may be underestimated using the method in ASHRAE (2011) shown in Figure 3.7. Therefore, the variation of CHTC has a significant influence on convective heat flux during the summer time based on Eq. 12. In other words, if the CHTC is underestimated the predicted deck surface temperature could be larger than the measured data during summer as shown in Figure 3.5. This may be one of the main reasons that the improved model produces the predicted temperature with larger deviation during summer. However, of interest here is that the model produces very good results during the winter time.

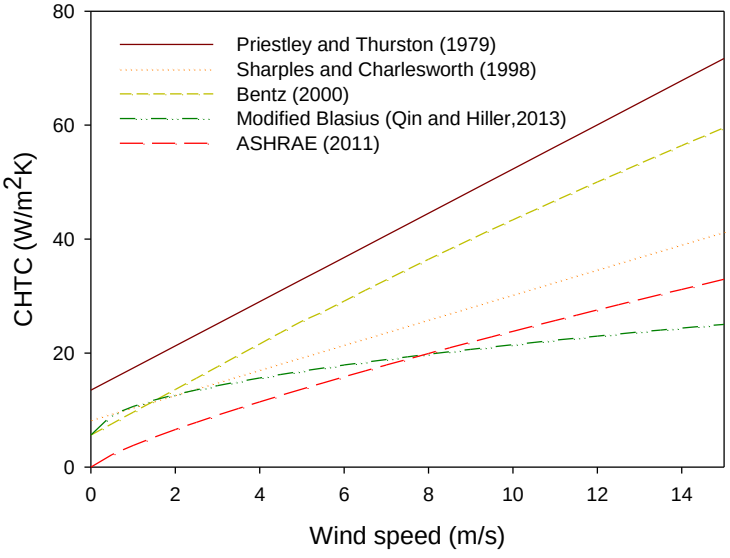

Figure 3.7 Comparisons of CHTC of different models

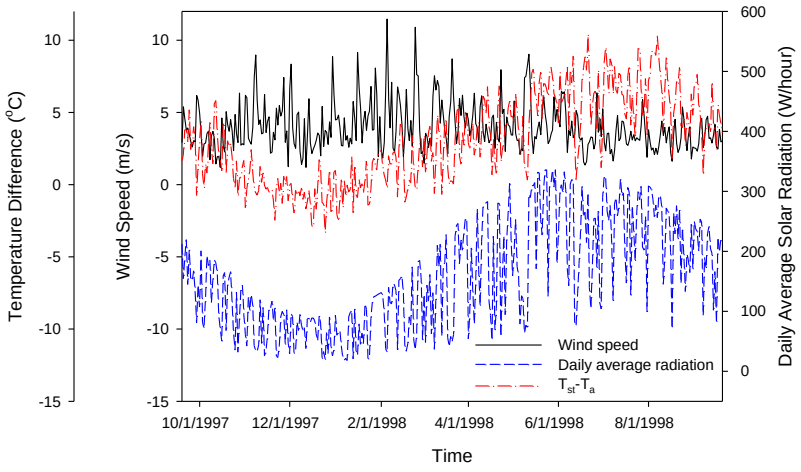

Figure 3.8 Wind speed, solar radiation, and temperature difference between the air and predicted deck surface temperature

3.5 VEHICLE EFFECTS

After validating the 2D improved model for heat transfer analysis, the analysis was extended to evaluate vehicle effects on the bridge temperature. As discussed above, the vehicle effects considered in the model includes the convective heat due to air flow induced by the passage of the vehicle, longwave radiation from vehicle bottom, and longwave/shortwave radiation blocked by the vehicles.

In order to investigate the effects of different traffic flow rates on the energy balance of the bridge, both the low and high traffic rates were simulated with the same local weather conditions of Jamestown Verrazzano Bridge. The average daily traffic (ADT) of the Jamestown Verrazzano Bridge is 30,000 vehicle/day with truck traffic accounting for 10% in 2008 (City-Data 2016). City-Data (2016) also estimated that the ADT would be 36,333 vehicle/day in 2030. Assuming the annul traffic volume increases linearly, the ADT from September, 1997 to September, 1998 can be estimated as 26,977 vehicle/day which is defined as low traffic rate condition. For the analysis, the

traffic condition similar to the Brooklyn Bridge in 2010 was used an example of high traffic rate input in the model.

The model also accounts for the commuting time effect. Laffont et al. (1999) presents six typical daily traffic patterns for a weekday. The traffic volume between 10 pm to the 6 am is usually less than 10% of the total daily traffic. The hourly traffic flow rate in the commuting hour is 1~2 times of the normal time. During the commuting time with heavy traffic flow, the vehicle speed is much lower than the low traffic flow or free flow condition. The Highway Capacity Manual (National Research Council, 2010) classifies the basic freeway speed-flow relationship as a model with three zones: free flow, under-saturated flow with declining speed, and oversaturated flow larger than 2000 passenger vehicles/hour/lane (pv/hr/ln). The congestion is very common during the commuting with heavy traffic such as the Brooklyn Bridge which can be considered as under-saturated flow with declining speed. Therefore, the following assumptions were made:

- The traffic flow during the commuting time (6 to 9am and 4 to 7pm) is twice of the normal traffic time (9am to 4pm and 7 to 10pm).
- The vehicle speed is 17.9 m/s when the traffic flow is low, and 8.9 m/s during the commuting time with heavy traffic.
- There is no traffic in the period from 10 pm to 6 am.

The traffic flow rate and average vehicle speed are shown in the Figure 3.9 during the heavy and light traffic conditions. During heavy traffic period (commuting time), the traffic flow rate is 1800 pv/hr/ln and 900 pv/hr/ln in the period of normal traffic time. The total daily traffic is 198,000 vehicles/lane which is close to 206,000 vehicles/lane of Brooklyn Bridge (NYC DOT, 2010). The total daily traffic of Jamestown Verrazzano Bridge is 6,744 pv/hr/ln (City-Data, 2016), the traffic rate is 614 and 307 pv/hr/ln during the commuting and normal traffic hours. The vehicle speed is assumed to be 17.9 m/s (40 mph).

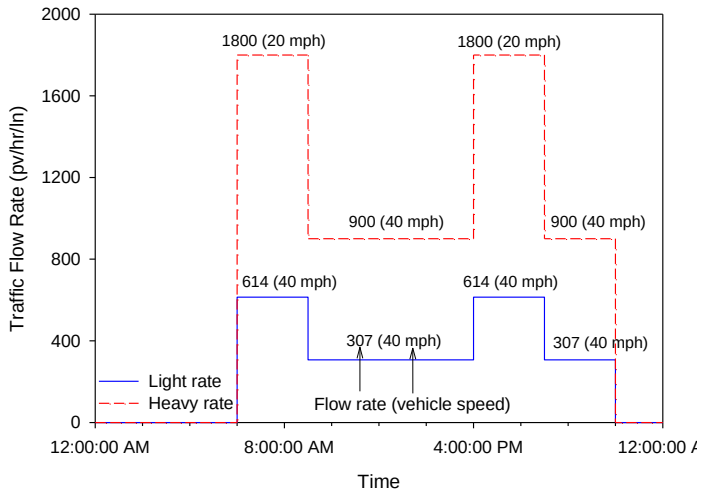

Figure 3.9 Hourly traffic rate and vehicle speed at light and heavy traffic conditions

3.5.1 Results with Local/Light Traffic

Heat transfer of the bridge was conducted for the Jamestown Verrazano Bridge under light traffic conditions. Measured and predicted temperatures at location P1 were compared in Figure 3.10. The RMSD for the temperature comparisons are 1.4 °C for base case compared to 1.6 °C of RMSD for the improved model without vehicle effects. The results of the two models are nearly the same. Though the results of the two models are not that different, it is more appropriate to include the effects of vehicles in these calculations to present a more complete model. It is noted that without including the features of the modified model and conducting a comparison as done here, it would have been difficult to estimate the vehicle-induced effects which are now seen to be small.

The predicted temperature differences of the bridge surface between the Improved model with and without considering vehicle effects are compared in Figure 3.11 in polar coordinates. T_{sv} is the bridge surface temperature obtained by the improved model that includes vehicle effects, and T_s is the bridge surface temperature obtained by the improved model without vehicle effects and

Figure 3.11 depicts the difference (T_{sv} - T_s). The figure shows the traffic effects in 24 hours of a day which presents that the vehicle plays a larger role in the heat transfer of the bridge when the solar radiation is high during the day time between am and pm. The largest temperature differences up to 3 °C of those two models mainly occur around the noon time. This is because the vehicle-induced wind enhances the convection between the bridge deck and air in the vicinity. While 3 °C may not be a large difference, it determines the bridge temperature being below or above the ice point.

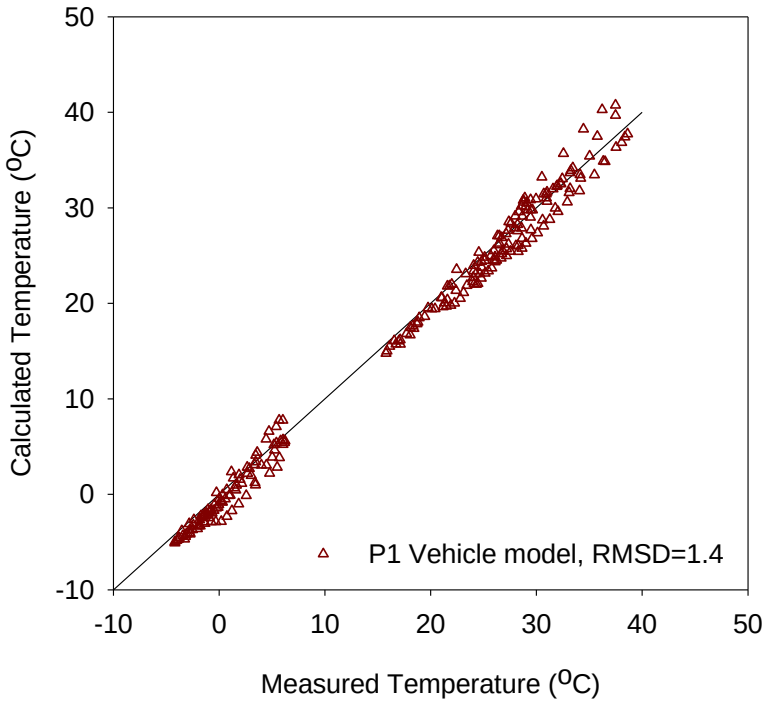

Figure 3.10 Comparison of the measured data and computed temperature at P1 (top slab) from the improved model with vehicle effects in 10 days

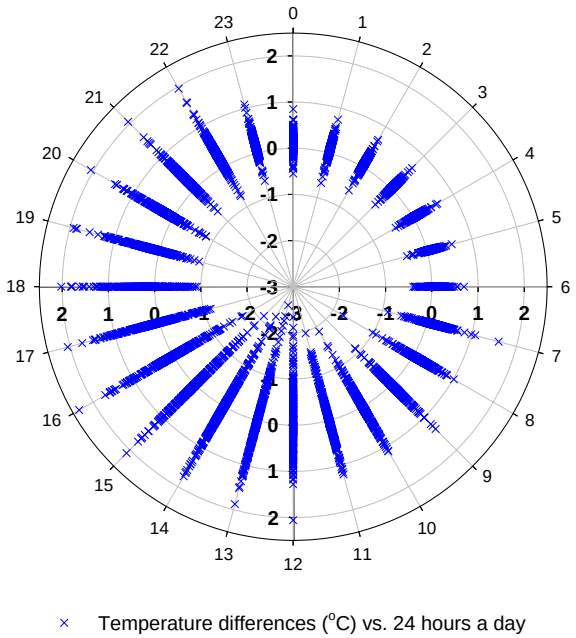

Figure 3.11 Bridge surface temperature differences (T_{sv} - T_s) predicted by improved model with and without vehicle effects in one year's simulation.

3.5.2 Effects of Heavy Traffic

To estimate the effects of heavy traffic, after considering the local traffic conditions, heavy traffic data similar to the Brooklyn Bridge was used as traffic input in the model coupled with the weather data of Jamestown Verrazzano Bridge for the heat transfer analysis. Figure 3.12 represents the results of the top surface temperature difference between the models with and without vehicle effects. Figure 3.12a is the results of the analysis based on the light traffic condition, and Figure 12b is the results for the heavy traffic condition.

As shown Figure 3.12a, the predicted surface temperature differences between the models with and without vehicle effects is less than 1 °C during most of the wintertime, however, the temperature difference can be over 2 °C during the summer. The vehicle plays a more important role during the summer time since the bridge deck receives more solar radiation which leads to a higher temperature difference between the deck surface and ambient air (see Figure 3.8). With the

same CHTC, the heat loss or gain on the bridge surface changes more significantly at larger temperature difference between the deck surface and ambient air.

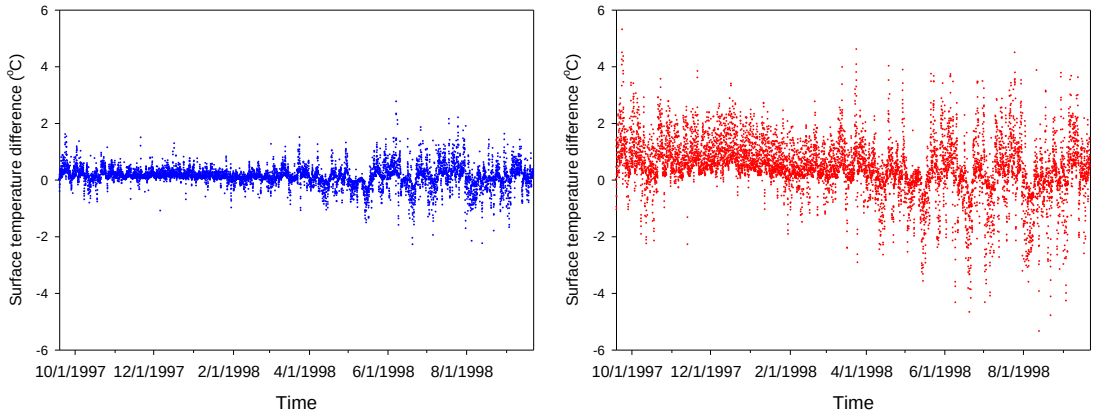

(a) Light Traffic **(b) Heavy Traffic**

Figure 3.12 Surface temperature differences (T_{sv} - T_s) between models with and without vehicle effects

Vehicles can warm up or cool down the bridge surface depending on the weather conditions. Figure 3.12b shows the predicted surface temperature differences between the models with and without vehicle effects with heavy (similar to the Brooklyn Bridge) traffic. During the wintertime, the traffic mainly warms up the bridge by 0 to 4 °C. The temperature differences have a larger variation amplitude of -5 to 5°C during the summertime.

Separate simulations were conducted for two specific days with different weather conditions in January, 1998. The air temperature at 12 am of each day was set as the initial temperature of the whole cross section of the bridge. Figure 3.13 is the results of the bridge surface temperature in the following two days. Figure 3.13a is the bridge surface temperature of different traffic conditions on a clear day, and Figure 3.13b are the results for a day with precipitation. With the comparison of the results in those two days, the bridge surface can be around 1.5 °C warmer in

heavy traffic conditions than that for light traffic during the commuting time and these results are similar those of Chapman (2005). Thus heavier traffic could lead to more significant effects under different weather conditions (see Figure 3.12). Under lighter traffic conditions, (shown in Figure 3.13) surface temperature differences with and without traffic are small for the analyzed weather conditions.

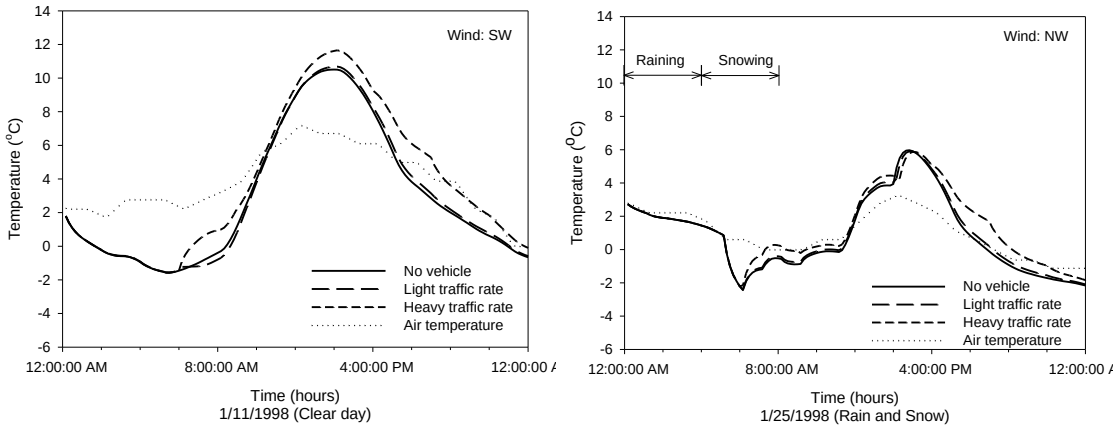

(a) **(b)**

Figure 3.13 Surface temperature of two days under different weather condition.

The heat fluxes at two times in the day are presented in Figure 3.14 based on the simulations discussed in Figure 3.13 for two days with different weather conditions. In early afternoon (~ 1pm), the heat fluxes due to the natural factors (e.g., q''_{conv_t}, q''_{sw_t}, and q''_{lw_t}) are changed by less than 30 W/m^2 by the vehicle effects (see Figure 3.14). However, when it is snowing during the morning commute (~ 7am), heavy traffic makes much more of a difference in the total heat fluxes (see Figure 3.14b). The heat flux of infrared radiation received from vehicle could reach 100 W/m^2 at heavy traffic condition. At the same time, the heat loss through longwave radiation also increases around 60 W/m^2.

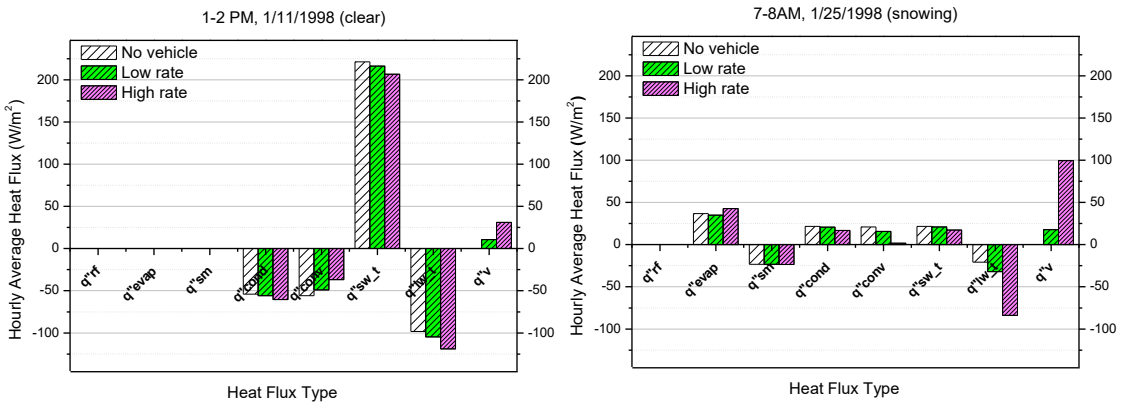

(a) **(b)**

Figure 3.14 The hourly average heat flux of each component

3.6 SUMMARY AND CONCLUSIONS

The development of heat transfer models to predict bridge deck surface temperature and heat flux has been described considering both natural and artificial factors. The model proposed by 2011 ASHRAE Handbook is modified by replacing the longwave radiation formula by Brock and Arnold (2000) and Brown (1998) and adding the effects of solar radiation and natural convection. The effective emissivity of the atmosphere was used in the longwave radiation model considering the cloud cover effect. The improved model with the effects of natural factors represents the heat transfer mechanism of the bridge well and was validated by the comparison of one year's measured results. The comparisons indicate that the used model may underestimate the convective heat transfer coefficient (CHTC) yet produces very good results during the winter time, which is the focus of this paper.

The wind speed influences the bridge deck temperature predication in a more pronounced manner during the noon time of a day and during summer when the solar radiation is higher, because the increase of available solar radiation magnifies the differences between ambient air temperature and the deck surface temperature.

After the validation of improved model with natural factors for heat transfer simulation of the bridge, the analysis was modified to include vehicle effects. The effective wind velocity was used in the model to investigate the vehicle-induced sensible heat on the bridge surface. The predicted temperature of the bridge with vehicle effects has a lower root-mean-square deviation comparing to the measured data.

When the bridge has light traffic rate, the predicted surface temperature differences between the models with and without vehicle effects is approximately 1 °C during most of the winter time. The vehicle movement can cool down the bridge surface. Under the heavy traffic condition, the bridge surface is mostly warmed up by the vehicular traffic during the winter time thus providing an advantage. The cooling down approximately 1 °C of the bridge deck due to vehicular traffic could be used as a recommendation for the design of bridge decks during snowfall periods.

4. INVESTIGATION OF EFFECTS OF TEMPERATURE CYCLES ON SOIL-CONCRETE INTERFACE BEHAVIOR USING DIRECT SHEAR TESTSINTRODUCTION

Thermo-active geo-structures (e.g., energy piles) provide sustainable energy alternative for heating and cooling of buildings and bridge deicing. Energy piles transfer structural loads and exchange heat with surrounding soils using closed-loop ground source heat pump (GSHP) systems (Brandl 2006; Laloui et al. 2006; Xiao 2013). However, the GSHP operates in cycles where it functions for a period of time (running time) then stops for another period of time (stoppage time). The operation (running and stoppage) periods of the GSHP range from 30 minutes to 24 hours (Wood 2009; Montagud et al. 2011; Luo et al. 2015). For energy piles, the temperature at the soil-concrete interface vary between 1°C to 33°C (Brandl 2006; Hamada et al. 2007; Wood et al. 2009; Abdelaziz et al. 2011; Shang et al. 2011; Rouissi et al. 2012; and Akrouch et al. 2013), and could be higher than 40 °C for cooling dominated environment or when energy piles function as solar energy storage sinks (Gabrielsson et al. 2000). The intermittent operation of the GSHP system subjects the piles to expansion and contraction and soils to temperature change and cycles, which affect soil properties (e.g. volume, pore pressure, shear strength) and shaft resistance of the pile. Triaxial and oedometer tests have been developed by different researchers to investigate the behaviors of soil subjected to temperature changes (e.g., Laguros 1969; Noble and Demirel 1969; Houston et al. 1985; Kuntiwattanakul et al. 1995; Cekerevac and Laloui 2004); however, limited investigations have been focusing on evaluating the effects of temperature cycles.

In this paper, the results obtained from the modified direct shear tests (Modified DSTs) were presented to explore the effects of temperature cycles on soil-concrete interface properties. In the Modified DST, two concrete plates with different roughness were used to simulate the pile surface with temperature change and cycles. From the tests, the relationship between shear resistance and vertical displacement (t-z curves) can be directly measured at different temperature cycles.

4.1 BACKGROUND

4.1.1 Temperature Effects on Volume Change and Shear Strength of Soils

Temperature effects on soil properties depend on thermal history, stress history, and hydraulic conductivity of the soil (Graham et al 2001; Burghignoli et al. 2000; Hueckel et al. 2009). Temperature changes induce volumetric strain (volume change) in normally consolidated and overconsolidated saturated soils (Campanella and Mitchell 1968; Demars and Charles 1982; Uchaipichat and Khalili 2009; Tawati 2010). Normally consolidated and slightly overconsolidated saturated clays contract when subjected to drained heating and experience significant irreversible (plastic) volumetric strain when returning to the initial temperature leading to an increased shear strength. When subjected to undrained heating, expansion and thermally-induced excess pore water pressure lead to a reduction in shear strength (Campanella and Mitchell 1968; Mitchell and Soga 2005). Highly overconsolidated clays subjected to drained heating; however, experience irreversible volumetric expansion with the volumetric strain decreasing with overconsolidation ratio (OCR) (Plum and Esrig 1969; Sultan et al. 2002). If heated beyond a threshold temperature, clays may contract (Hueckel and Baldi 1990; Cekerevac and Laloui 2004). Cekerevac and Laloui (2004) and Abuel-Naga, et al. (2007) reported an increase of shear strength for overconsolidated soils when subjected to drained heating. For unsaturated soils, Uchaipichat and Khalili (2009) observed responses similar to those described above for normally and overconsolidated saturated soils. It is worth noting; however, that the critical state shear envelope is independent of temperature change for both saturated and unsaturated soils (Cekerevac and Laloui 2004; Uchaipichat and Khalili 2009; Alsherif and McCartney 2016). When subjected to cyclic heating and cooling, soils experience an accumulated permanent volumetric contraction regardless of stress history due to thermal creep (Campanella and Mitchell 1968; Burghignoli et al. 1992; Vega and McCartney 2015).

For the consolidation behavior, temperature change has minor effect on the compression index of saturated soils (Campanella and Mitchell 1968; Eriksson 1989; Graham et al. 2001) and unsaturated soils (Saix et al. 2000; Uchaipichat and Khalili 2009) which was summarized by Alsherif and McCartney (2016). The preconsolidation pressure increases with decreasing temperature (Eriksson 1989; Tidfors and Sallfors 1989; Uchaipichat and Khalili 2009). The secondary consolidation of soil subjected to temperature change has been investigated by several researchers (Campanella and Mitchell 1968; Plum and 1969; Fox and Edil 1996). Acceleration of the second consolidation due to heating was observed by Plum and Esrig (1969) and Fox and Edil (1996) which could be due to the rearrangement of soil particles (Tsutsumi and Tanaka 2012). Cooling has slight effect on the secondary consolidation rate (Fox and Edil 1996; Burghignoli 2000).

4.1.2 Temperature Effects on Water Migration in Soils

Water migration could be induced due to pore pressure gradient and/or due to temperature gradient. In pores of unsaturated soil, water vapor migrates from higher temperature to lower temperature leading to a reduction of suction at areas of lower temperature and increases at higher temperature. This difference drives the liquid water to migrate from lower temperature to higher temperature. Therefore, water vapor and liquid water could migrate in reverse directions and may theoretically become balanced when equilibrium is reached (Cary 1966; Sakai et al. 2009; Wang and Su 2010). However, temperature gradient is dominant and initial driving force for the moisture migration when the soil is subjected to temperature change. Experimental investigation on effects of temperature gradient on water content has been performed by several researchers (e.g., Romero et al. 2001; Villar and Lloret 2004; Tang and Cui 2005; Gao and Shao 2015) who concluded that moisture content decreases with temperature at constant suction, while suction decrease with temperature at constant moisture content, which could be attributed to the reduction of surface

tension of water and thermal-induced changes in the contact angle at the water-soil particle interface (Bachmann and van der Ploeg 2002; Tang and Cui 2005).

4.1.3 Temperature Effects on Soil-structure Interface

The effects of temperature changes (no temperature cycles) on soil-structure interface properties were investigated by several researchers including Xiao et al. (2014 and 2017b); Murphy and McCartney (2014); Xiao and Suleiman (2015); Di Donna et al. (2015); and Yavari et al. (2016). Xiao and Suleiman (2015) and Xiao et al. (2017b) conducted modified-thermal borehole shear tests for the soil-concrete interface, which combined the effects of radial displacement (due to expansion and contraction of the pile) and temperature change. Preliminary results by Suleiman and Xiao (2015) showed an increase of the shear strength with heating and radial expansion, and significant reduction after the cooling and contraction; however, the effects of temperature cycles were not evaluated. The thermal-borehole shear tests performed in clay and silty sand soils by Murphy and McCartney (2014), which is capable of evaluating the effects of temperature changes only, showed that heating and cooling have negligible effects (< 2%) on the normalized shear stress vs. displacement relationships (t-z curves) of the interface. Xiao et al. (2014), Di Donna et al. (2015), and Yavari et al. (2016) performed direct shear tests to explore the temperature effects on soil-concrete interface properties. For saturated clay-concrete interface, the work of Di Donna et al. (2015) showed an increasing shear strength at soil-concrete interface subjected to heating which may be attributed to thermal consolidation. Yavari et al. (2016) showed that the temperature effects on the friction angle and adhesion are minor for clay/sand-concrete interface. The results of Xiao et al. (2014) showed a slight decrease of the adhesion of the soil-concrete interface when subjected to cooling, and negligible effects on the friction angle for unsaturated soil condition.

Although, the effects of monotonic temperature change (half or one temperature cycle) on the soil-concrete interface properties were investigated in the aforementioned shearing tests, the effects of temperature cycles on the soil-structure interface behavior has very limited data available

in the literatures. In this paper, a modified direct shear test (Modified-DST) device was utilized to evaluate the effects of temperature change and cycles on soil-concrete interface properties.

4.2 TESTING APPARATUS

To evaluate the thermal-mechanical responses of soil-concrete interface subjected to temperature change and cycles, a convectional direct shear device was modified (Figure 4.1). The lower shear box was replaced by a concrete plate with embedded aluminum tubes of 6.4 mm outer diameter to allow for heating and cooling the surface of the concrete (Figure 4.1 and Figure 4.2). The top shear box incorporates a soil specimen with thickness of 13 mm and diameter of 64 mm. Linear variable differential transformers (LVDTs) were used to measure the horizontal deformation of the interface and vertical deformation of the soil sample. Shear force at interface was measured by a load cell.

The dimension of the concrete plate was 127 mm (length) by 102 mm (width) by 21 mm (thickness). Two smooth steel plates with dimension of 102 mm by 16 mm by 1.5 mm were embedded on the sides of the top surface of the concrete plate to minimize friction between the adjustment screws of the top shear box and the concrete plate (Figure 4.1 and Figure 4.2).

Two concrete plates were fabricated; one with a smooth surface and one with rough surface. To make the smooth surface, a glass plate was placed on the top of the cement mortar. For the rough surface, Ottawa 50-70 sand was scattered on the surface of the concrete during casting to create a rougher surface. The two plates are shown in Figure 4.2c and Figure 4.2d.

Aluminum tubes embedded in the concrete plate were connected to two heat pumps to control the cooling and heating that simulate the intermittent field operation of energy pile heat pump systems. Thermocouples (No. 1 to 7 in Figure 4.2) were placed at the soil-concrete interface as well as in the soil to measure the temperature change. Temperature sensor No. 1 is located at the center of the soil-concrete interface, and sensors No. 2-5 were placed at the edge of the interface.

Temperature sensor No. 6 and No. 7 measured the temperature in the middle and at top of the soil specimen, respectively (Figure 4.2a and Figure 4.2b).

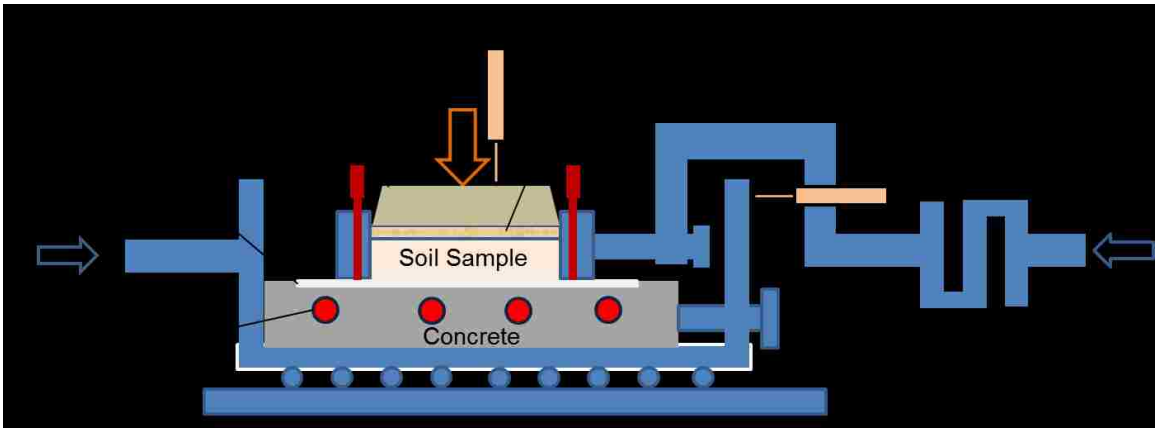

Figure 4.1 Profile of modified direct shear test device

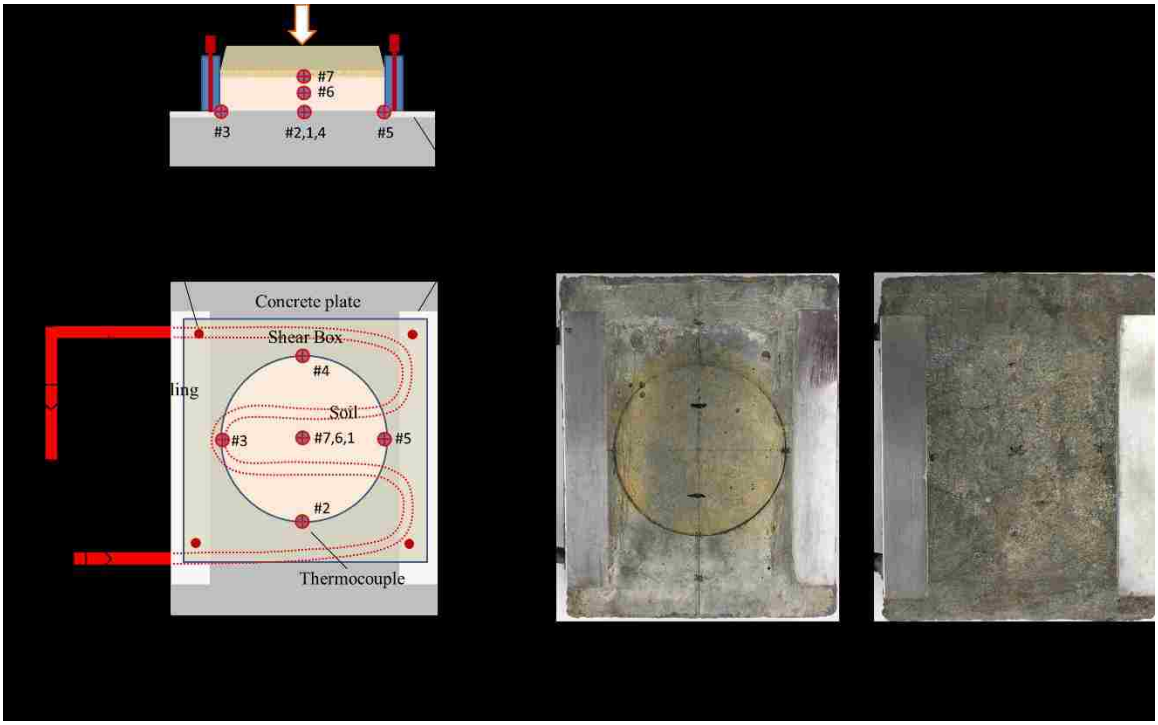

Figure 4.2 Layouts of the heating/cooling tubes in the concrete plate and thermocouples at soil-concrete interface: (a) profile of top shear box and concrete plate; (b) concrete plate with heat pumps; (c) concrete plate with smooth surface; (d) concrete plate with rough surface

4.3 MATERIALS AND PREPARATION

The soil obtained from a construction site in the Lehigh Valley, Pennsylvania was sieved through sieve No. 10 to use in the Modified-DSTs. Using the Unified Soil Classification System (USCS), the soil was classified as sandy silty clay (CL-ML) with 17.9% sand, 55.6% silt, and 26.4% clay. The liquid and plastic limits of the soil were 28% and 22%, respectively. The solid specific gravity was 2.67. Standard Proctor tests were performed and the maximum dry unit weight and optimum moisture content were 17.4 kN/m3 and 14%, respectively.

To prepare the soil samples, oven dried soil was mixed with distilled water to produce the moisture content of 18.9%. To allow moisture equalization throughout the mass, the soil was sealed in a container with a standing time of 24 hours according to ASTM D3080. The soil was compacted in two layers to achieve a target dry unit weight of 13.7 kN/m3. The average soil moisture content after the consolidation stage (12 hours) was ~18.5%. To avoid or minimize water being absorb by concrete plates, the concrete plates were placed in the water for more than 24 hours. The visible water at the concrete surface was dried using cloth prior to placing the soil on top of the concrete plate.

4.4 TEST PROCEDURES

Test consists of three stages, consolidation, temperature change and cycles, and shearing. After the soil was compacted to the target dry unit weight (13.7 kN/m3), preloading of 6.9 kPa was applied on the soil sample. A 0.6 mm gap between the top shear box and concrete plates was generated by adjusting the screws. The target normal stress was applied after 15 minutes of preloading to start the consolidation stage. The duration of the consolidation was 12 hours. The Modified-DSTs were performed under normal stresses of 27.6, 41.4, and 100 kPa.

After the consolidation stage, two heat pumps were utilized for heating and cooling of the concrete plate. The Modified-DSTs were conducted in a lab that has a room temperature of

approximately 22.5 °C. The duration of one temperature cycle was 60 minutes. Figure 4.3 shows the average temperature at soil-concrete interface of tests with 10.5 cooling and heating cycles. The average temperature amplitudes at the interface were 20 °C and 18 °C for heating and cooling cycles, respectively. In the heating cycles, the temperature at the soil-concrete interface were heated from the initial room temperature to the target temperature of 42.5 °C. Once the target temperature of soil-concrete interface was achieved with 30 minutes (i.e., reaching 0.5 heating cycle or TC = +0.5 as shown in Figure 4.3a), the heat pump stopped functioning, and the other heat pump started to cool the plates down to room temperature with another 30 minutes (i.e. reaching 1 heating cycle or TC = +1.0). For the tests with cooling cycles, the temperature at the soil-concrete interface was cooled from the initial room temperature to the target temperature of 4.5 °C. The temperature was decreased by 18 °C instead of 20 °C to avoid the potential freezing at the interface. Once the target temperature of soil-concrete interface was achieved with 30 minutes (i.e., reaching 0.5 cooling cycle, TC = -0.5), the heat pump stopped functioning, and the other heat pump started to warm up the plates back to room temperature with another 30 minutes (i.e. 1 cooling cycle, TC = -1.0). The heating or cooling were repeated to apply temperature cycles.

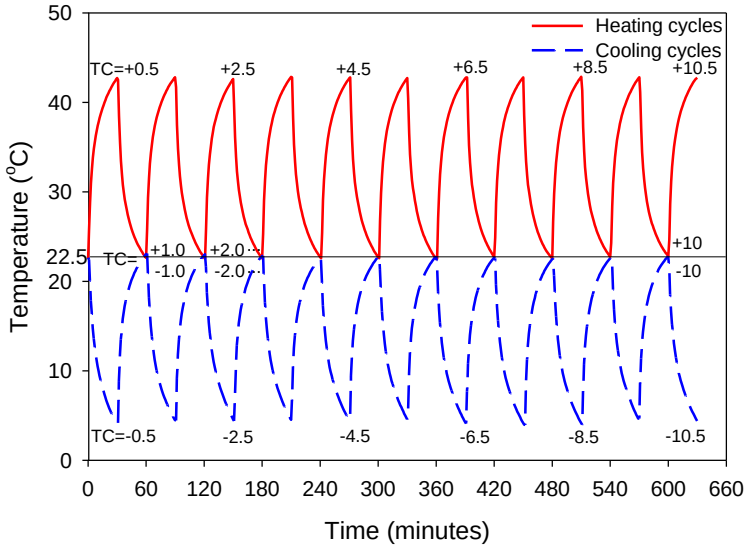

Figure 4.3 Average temperature at soil-concrete interface during heating and cooling cycles

After applying the target temperature cycles, the soil-concrete interface was sheared at a shearing rate of 3mm/min. After finishing the shearing stage, the moisture contents at top and bottom (soil-concrete interface) of the soil were measured by collecting two soil samples from each position.

4.5 RESULTS AND DISCUSSION

4.5.1 Smooth Interface Analysis

Figure 4.4a-f show the shear stress ratio (shear stress/normal stress) – horizontal displacement curves as well as vertical deformation – horizontal displacement curves for smooth interface at different temperature cycles. The shear stress ratio curve of the test with no temperature cycle is the reference line. The effects of temperature cycles on shear strength of smooth interface is negligible at lower normal stresses ($\leq$ 41.4 kPa), and the shear stress ratio changed less than 6% (Figure 4.4a and 4.4c). At normal stress of 100 kPa, 0.5 heating and cooling cycle had no effect on the shear strength, however, the shear strength increased by 12% and 20% after 10.5 cooling and 10.5 heating cycles, respectively (Figure 4.4e). Temperature change and cycles may affect the soil properties as discussed in the background. However, the soil particle-interface interlocking at smooth interface is small at lower normal stress, and the shear zone thickness is negligible, which may induce pure interfacial sliding failure (Nam et al. 2006; DeJong and Westgate 2009), therefore, the temperature effects on the soil may not pronounced in the shearing test of smooth interface at low normal stress. The rearrangement or ratcheting of soil particles under cyclic loading may only occurs at high stress (Pasten and Santamarina 2014) which may also explain that why the temperature effects mainly happen at 100 kPa for the smooth interface.

As shown in Figure 4.4b, 4.4d, and 4.4f, the dilation at normal stresses of 41.4 and 100 kPa was negligible during shearing which was less than 0.01 mm regardless temperature cycles. With this sign convention, dilation is negative and contraction is positive. At normal stress of 27.4 kPa,

slight dilation only presented after larger temperature cycles, which was 0.013 mm and 0.034 mm after 10.5 cooling and 10.5 heating cycles separately.

4.5.2 Rough Interface Analysis

Figure 4.5a-f show the shear stress ratio – horizontal displacement as well as vertical deformation – horizontal deformation curves for the rough interface at different temperature cycles. Subjecting the interface to 0.5 heating cycle resulted in 6% to 11% reduction of the shear strength when compared to the reference tests, which is consistent to the results of thermal borehole shear tests performed by Murphy and McCartney (2014) and Xiao et al. (2017a). The reduction of the shear strength may be attributed to the decreases of suction caused by differential expansion between soil particles and water during undrained heating. The 0.5 cooling cycle caused minimal increase (< 3%) of the interface shear strength which could be due to the increase of suction during the undrained cooling. The interface shear strength increased by 10% to 12% after 10.5 cooling cycles and increased by 14% to 23% after 10.5 heating cycles, which may be attributed to the reduction of moisture contents (increase of suction) and the soil particle rearrangement during the temperature cycles as discussed later in the paper. For rough interface, the interfacial sliding failure plane is located in the soil adjacent to the concrete surface (Nam et al. 2006), the temperature effects on the shear strength of soils may be represented more on the soil-concrete interface with high roughness.

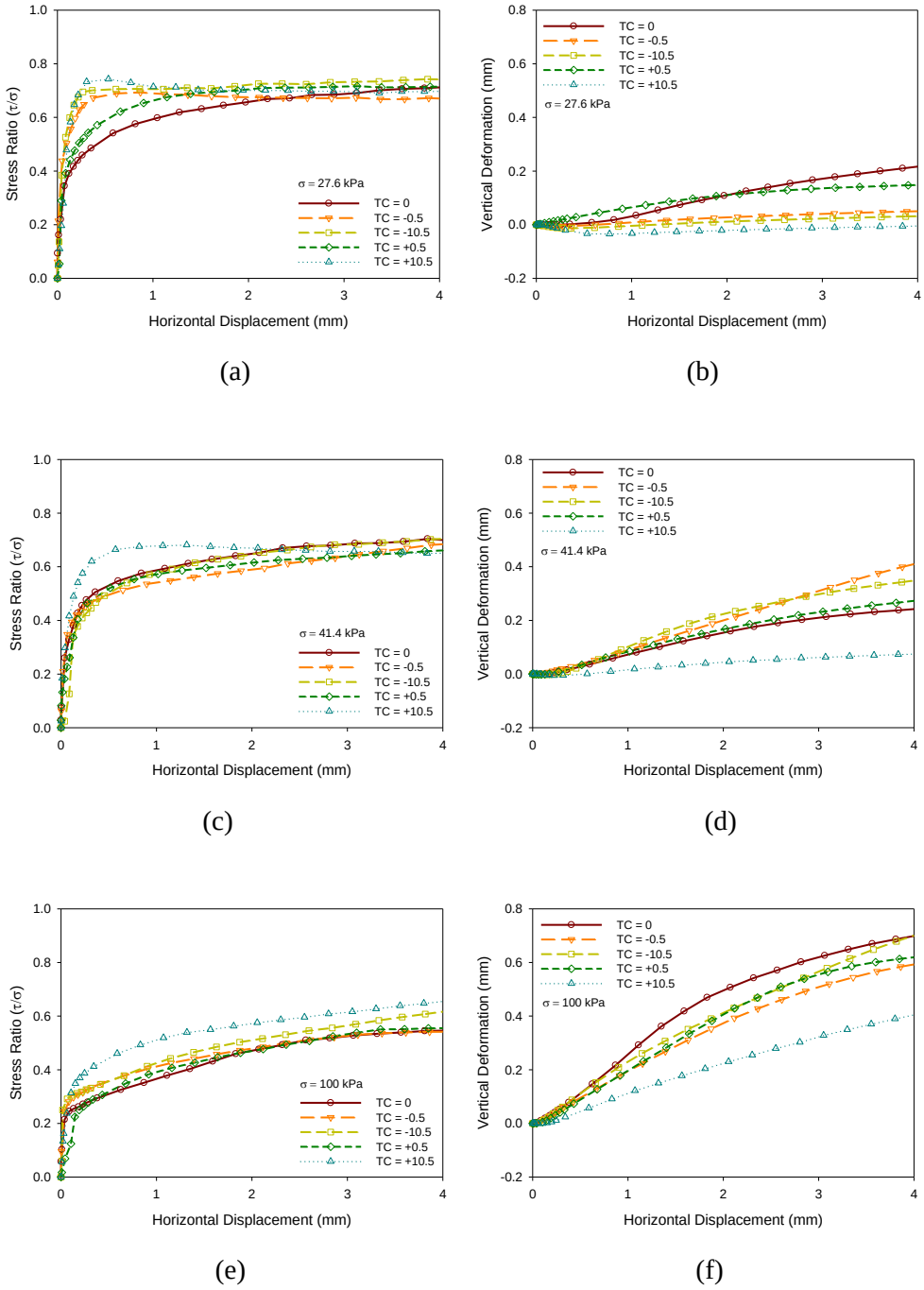

Figure 4.4 Shear stress vs. displacement and volume change with smooth concrete surface

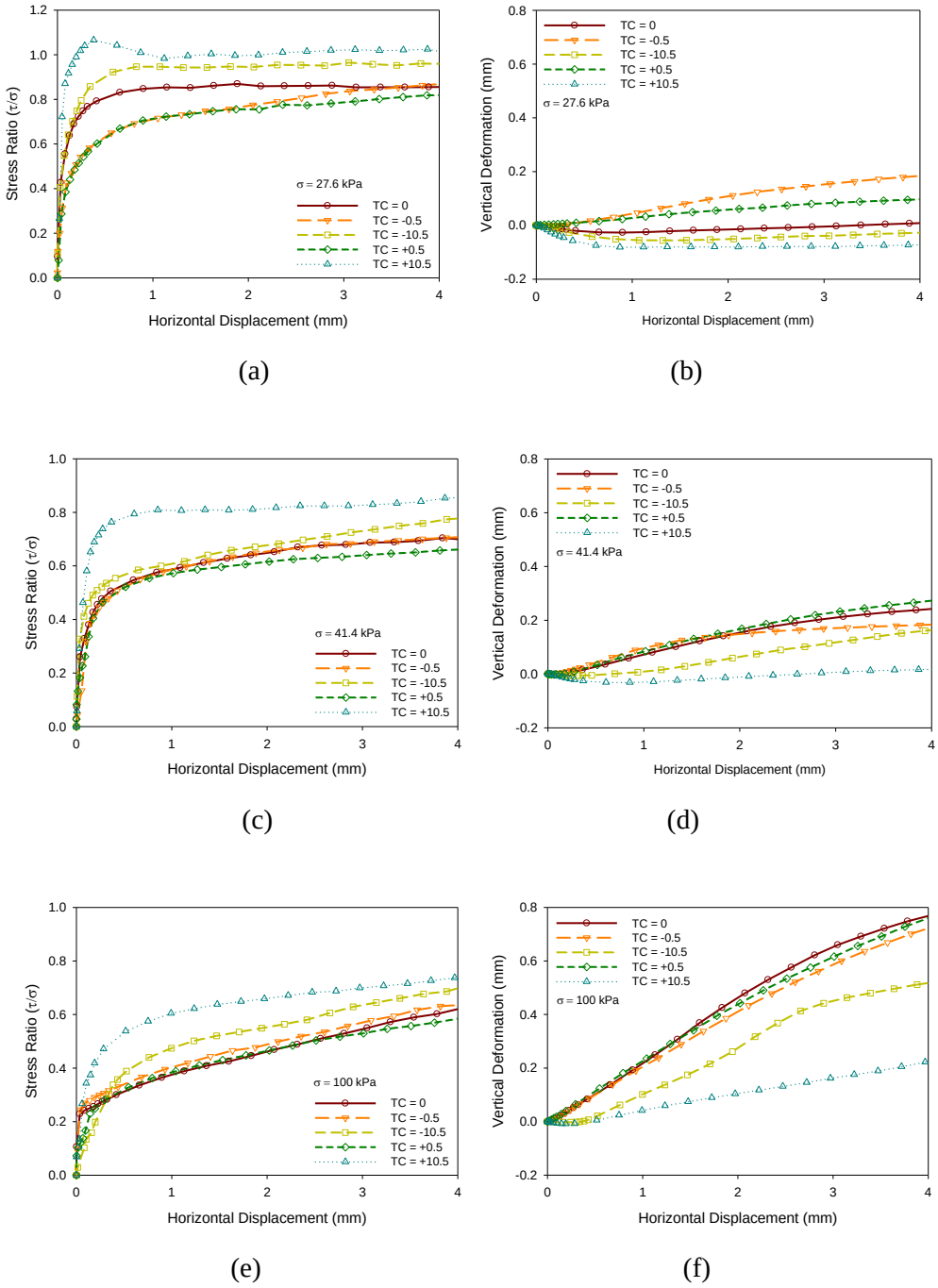

Figure 4.5 Shear stress vs. displacement and volume change of rough concrete surface

The soil dilation at the interface subjected to no temperature cycle and 0.5 temperature cycle was minor at rough interface (Figure 4.5-b, d, f). Dilation of 0.056 and 0.081 mm were observed after 10.5 cooling and 10.5 heating cycles at normal stress of 27.6 kPa (Figure 4.5b),

where the dilation occurred at beginning of shearing stage and then the soil sample contracted. Dilation of 0.031 mm was observed after 10.5 heating cycles at normal stress of 41.4 kPa (Figure 4.5d). The dilation was less than 0.01 mm at the normal stress of 100 kPa regardless of temperature cycles (Figure 4.5f). Therefore, the dilation is decreasing as the normal stress is increasing which was also observed by DeJong and Westgate (2009). The dilation behavior was also consistent to the results of Hossain and Yin (2013) showing that higher interface-dilation was observed at higher suction (smaller moisture content) with lower normal stress. When compared the dilation of tests with smooth and rough interfaces, the dilative behavior was more significant in the tests with rough interface which is consistent to Pra-ai (2013).

Figure 4.6a shows the total stress failure envelopes of the smooth interface after different temperature cycles. The failure envelop without temperature cycle is the reference line which has fiction angle of 25° and adhesion of 8.1 kPa. The results show that 0.5 temperature cycle had no effect on the friction angle and adhesion. Subjecting to the interface to 10.5 cooling temperature cycles, the frictional angle was 29° and adhesion is 5 kPa, and the frictional angle was 32° and adhesion is 3.5 kPa after 10.5 cooling cycles.

Figure 4.6b shows failure envelopes of the rough interface subjected to different temperature cycles. The reference line (no temperature cycles) has fiction angle of 28° and adhesion of 8.3 kPa. 0.5 temperature cycles had minor effect on the friction angle (~ 1° change) of the rough interface, which is consistent to temperature effect on the unsaturated soil (Alsherif and McCartney 2016). However, for 10.5 temperature cycles (both heating and cooling), the friction angle increased by 3 to 4 °. The 0.5 temperature cycle and 10.5 cooling cycles had no effect on the adhesion, while the adhesion increased by 2.8 kPa after 10.5 heating cycles. The effects of temperature change on the adhesion of the soil-concrete interface was negligible in both smooth and rough interfaces, however, the effect of larger temperature cycles on the adhesion of the soil-concrete interface did not show a consistent trend.

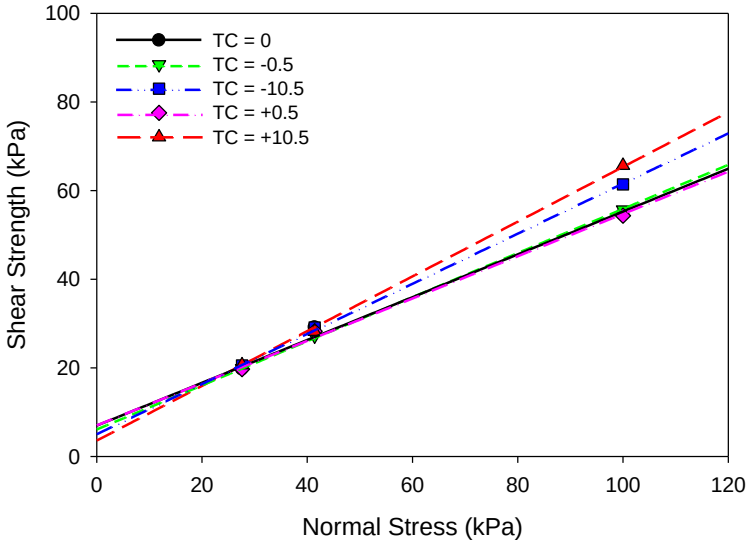

(a)

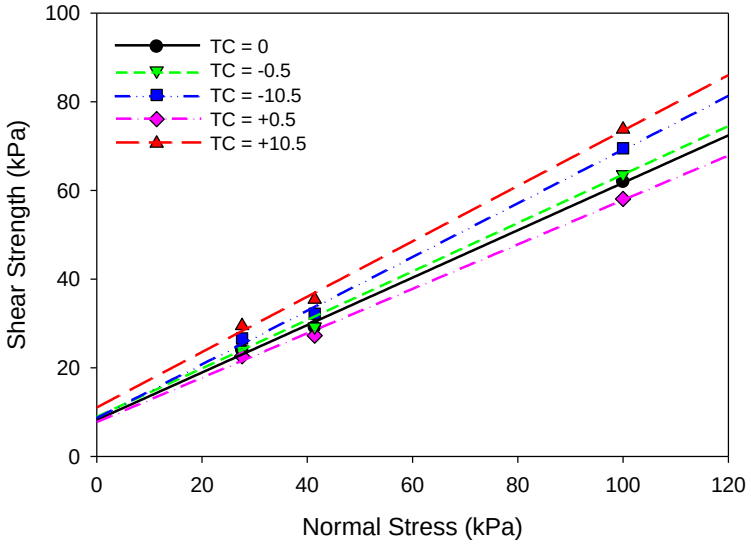

(b)

Figure 4.6 Failure envelopes for soil-concrete interface subjected to different temperature cycles, (a) smooth interface; (b) rough interface

4.5.3 Vertical Deformation

Figure 4.7a illustrates the vertical deformation vs. time at constant normal stress during consolidation stage and heating/cooling cycles. During the heating/cooling cycles, only the

readings of vertical deformation when the interface temperature returned to room temperature were plotted. The deformation rate of the soil specimen in one hour before temperature cycles were around 0.001 mm/hour at normal stresses of 27.6, 41.4, and 100 kPa. Therefore, the primary consolidation had been accomplished in the consolidation stage of 12 hours, and the heating and cooling cycles were applied during the secondary consolidation stage. During the cooling cycles, the average vertical deformation rate is 0.003, 0.003, 0.004 mm/hour at normal stress of 27.6, 41.4, and 100 kPa, respectively. During the heating cycles, the average vertical deformation rate is 0.006, 0.007, 0.007 mm/hour at normal stress of 27.6, 41.4, and 100 kPa, respectively.

Based on the vertical deformation and moisture content changes of the soil specimens, the voids ratios during the consolidation and after temperature cycles were calculated and presented in Figure 4.7b. During the temperature cycles, only the voids ratio at 10 heating and 10 cooling cycles were plotted, although the results of the moisture contents were from the tests with 10.5 temperature cycles. In the calculation, the changing rate of soil moisture contents during the consolidation was assumed to be constant, and the moisture content changes from 10 to 10.5 temperature cycles were neglected. As shown in Figure 4.7b, the initial voids ratio of the soil specimen was 0.91. The voids ratio decreased by 0.03, 0.05, 0.22 after the primary consolidation stage at normal stress of 27.6, 41.4, and 100 kPa, respectively. At three different normal stresses, the void ratio changes were almost the same after 10 temperature cycles, which decreased by 0.01 for cooling and decreased by 0.04 for heating. Therefore, the effects of temperature cycles on the soil volume change is independent of the stress level which is consistent to the triaxial tests performed by Demars and Charles (1981) and to the consolidation test performed by Towhata et al. (1993). The irreversible soil volume may be attributed to the decrease of the moisture content or increase of matric suction (Uchaipichat and Khalili 2009), and soil particles arrangement during the temperature cycles (Ng et al. 2016).

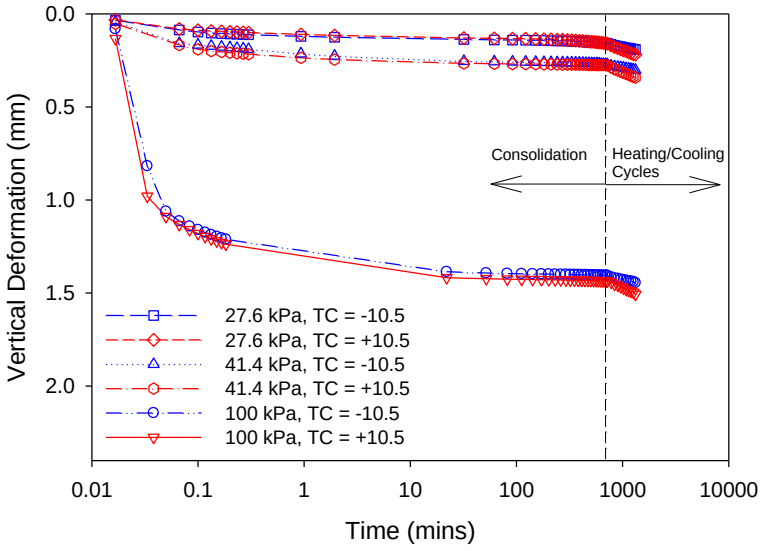

(a)

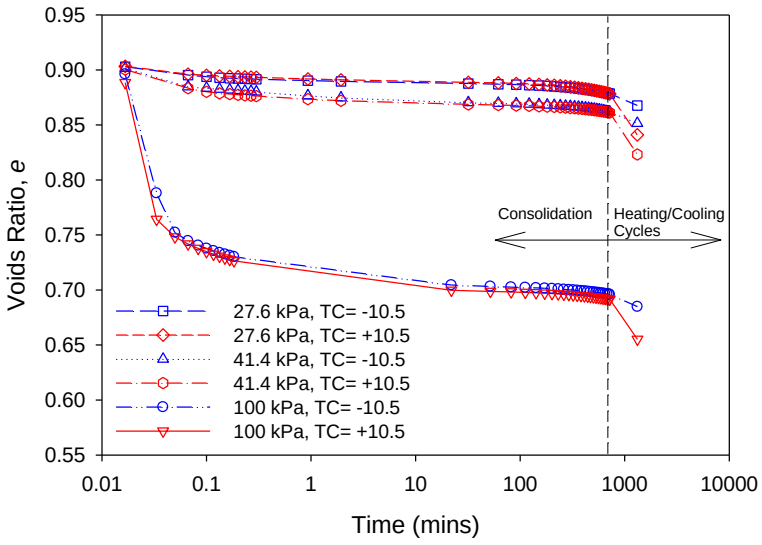

(b)

Figure 4.7 Vertical deformation and voids ratio of the soil specimen during temperature cycles at different normal stresses: (a) vertical deformation; (b) voids ratio

4.5.4 Moisture Contents after Temperature Cycles

Figure 4.8 shows the moisture contents at soil-concrete interface as well as the average moisture contents of the soil specimens during the temperature cycles. For smooth interface, the

moisture content at interface without temperature cycle was 18.5%, the moisture contents were 18.7%, 18.2%, 18.1%, and 16.7% after 0.5 cooling cycle, 10.5 cooling cycles, 0.5 heating cycle, and 10.5 heating cycles, respectively (Figure 4.8a). For rough interface, the moisture content at interface without temperature cycle was 18.6%, and the moisture contents were 18.7%, 18.2%, 17.8%, and 16.4% after 0.5 cooling cycle, 10.5 cooling cycles, 0.5 heating cycle, and 10.5 heating cycles, respectively. The two concrete plates may have different porosity that held different water content in the concrete, which could affect the moisture changes during the temperature cycles. In the 10.5 cooling cycles, the moisture content was expected to be larger than the initial moisture content. However, having a soil sample of 13 mm thick, limit water moves toward the interface during cooling. The lower moisture content after 10.5 cooling cycles could be attributed to evaporation to the surrounding air.

Figure 4.8b is the average moisture contents of the soil specimens which was calculated using the moisture contents at the top and bottom (soil-concrete interface) of the specimens. The largest moisture difference between the soil-concrete interface and soil is 0.26%, which occurred in the test with 10.5 heating cycles for the rough interface. The moisture contents changed 1.75% after 10.5 heating cycles which is ~4 times of the tests after 10.5 cooling cycles. It is interesting to notice that the void ratio change during 10.5 heating cycles was also 4 times that of 10.5 cooling cycles as shown in Figure 4.7b.

4.5.5 Effects of Moisture Contents

As shown in Figure 4.8, the moisture contents changed during the temperature cycles, which could affect the shear behavior of the soil-concrete interface (Hossain and Yin (2013). Furthermore, soil particles rearrangement caused by temperature cycles near the soil-concrete interface may also affect the interface shear strength (Karademir 2011, and Ng et al. 2016).

To separate effects of the moisture content changes from other parameters (e.g., soil particle rearrangement) caused by temperature cycles, tests at different moisture contents were

performed (no temperature cycles) using both smooth and rough interfaces with the same preparation procedure. The tests were conducted with normal stresses of 13.7, 27.6, 41.4, and 100 kPa. Figure 4.9 shows relationships between shear strength and normal stresses or the failure envelopes of the smooth and rough interfaces at different moisture contents including the results of the tests subjected to 10.5 temperature cycles.

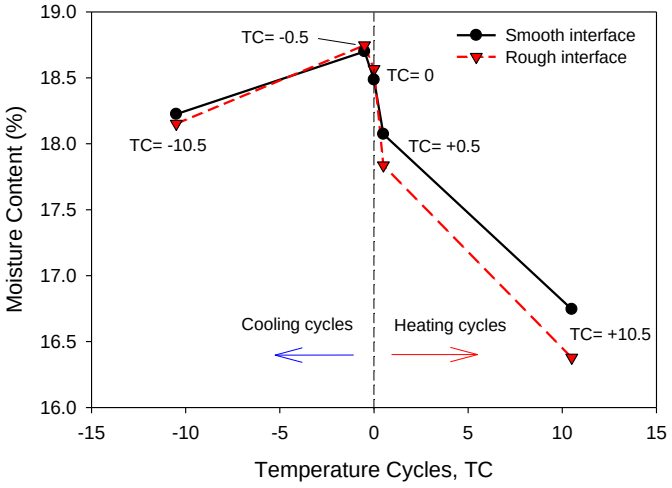

(a)

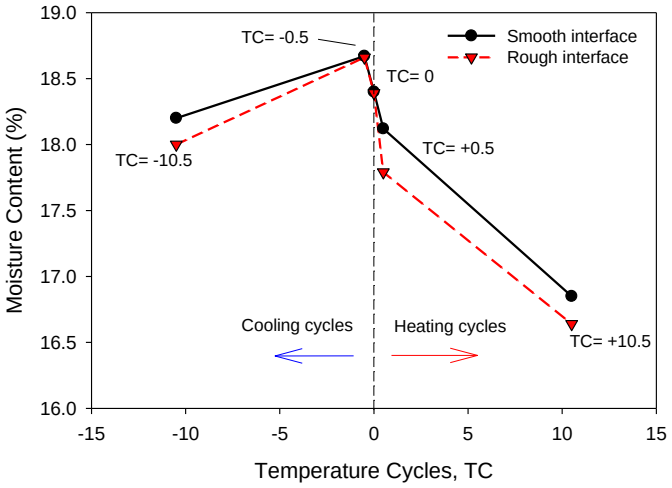

(b)

Figure 4.8 Moisture contents changes during temperature cycles: (a) moisture at interface; (b) average moisture in the soil specimen

For smooth interface, the tests were performed at moisture contents of 15.5%, 16.5%, and 18.3% separately as shown in Figure 4.9a. The results of the smooth interface were presented using symbols in Figure 4.9a to show the difference between the results at lower normal stress (≤ 41.4 kPa) and at 100 kPa. The effects of moisture contents in a range of 15.5% to 18.3% on the interface strength was negligible at lower normal stress (≤ 41.4 kPa); however, the strength increased as the moisture decreased at normal stress of 100 kPa. For example, the shear strength of the smooth interface increased by 21% when the moisture content decreased from 18.3% to 15.5% at normal stress of 100 kPa.

For rough interface, the tests were performed at moisture contents of 15.7%, 16.6%, 18.0%, and 18.6%, and the corresponding friction angles were 34°, 33°, 30°, and 28° (Figure 4.9b). The friction angle and shear strength increased with decreasing moisture contents. The shear strength increased by 17% to 32% when the moisture content decreased from 18.6% to 15.7%. The moisture effects on adhesion of the rough interface was negligible with moisture changes between 15.7% and 18.6%.

During temperature cycles, both moisture contents and other factors (e.g. particle rearrangement) may affect the soil-concrete interface behaviors. The strength of the interface subjected to 10.5 heating cycles was almost same as the strength of the interface without temperature cycle at the same moisture content for both smooth and rough interface as shown in Figure 4.9. Therefore, the effects of the moisture changes during large heating cycles was dominant to the interface properties.

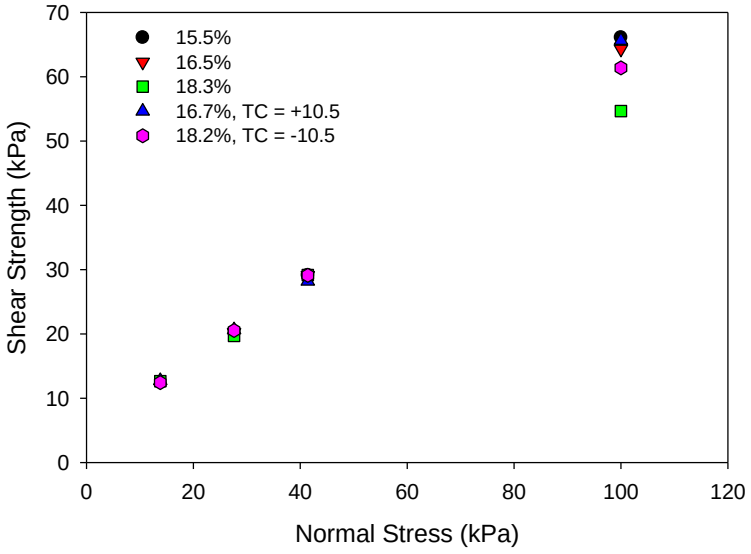

(a)

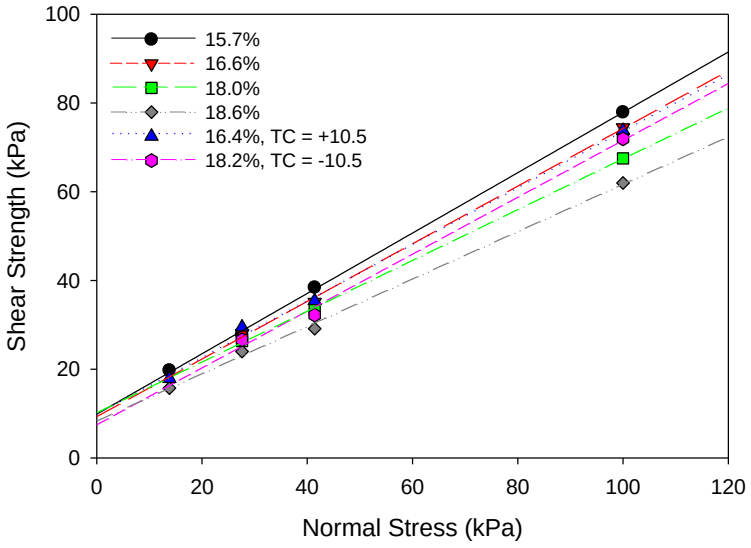

(b)

Figure 4.9 Effects of moisture content and temperature on failure envelope of soil-concrete interface: (a) smooth interface; (b) rough interface)

For the smooth interface at normal stress of 100 kPa, the shear strength is 61.4 kPa after 10.5 cooling cycles, and the moisture content is 18.2%. When the interface was shear at the 18.3%, the strength is 54.7 kPa, which is 11% lower than the tests after 10.5 cooling cycles. The rough

interface showed similar results in Figure 4.9b. The shear strength of the interface after 10.5 cooling cycles is 71.9 kPa, and moisture content is 18.2%. When the interface was shear at 18.0 %, the strength is which is 67.5 which is 6% lower than the tests after 10.5 cooling cycles. Therefore, other parameters could contribute to the increase of the shear strength during the cooling cycles at normal stress of 100 kPa.

For the rough interface at lower normal stresses, the strength of interface was 26.6 kPa and 32.2 kPa at normal stress of 27.6 kPa and 41.4 kPa after 10.5 cooling cycles, which is almost same as the results of the tests without temperature cycles at similar moisture contents. Therefore, the strength increased after 10.5 cooling cycle at lower normal stresses may be mainly attributed to the moisture content changes.

4.6 SUMMARY AND CONCLUSIONS

The ground source heat pumps connected to thermo-active geo-structures (e.g., energy piles) operate intermittently to meet varying heating and cooling loads, which lead to temperature change and cycles and introduces new challenges in the design of geo-structures. For energy piles, the cyclic temperature changes affect soil-structure interface properties, which was investigated by conducting Modified-DSTs in the normally consolidated clay. The shear stress-displacement responses at the soil-concrete interface of different roughness, subjected to cyclic temperature changes were directly measured. Based on the results, the following conclusions were concluded.

For smooth interface, the effects of and temperature cycles are negligible at lower normal stresses (less than 41.4 kPa). The shear strength of smooth interface at normal stress of 100 kPa decreased by increased by up to 20% after 10.5 temperature cycles.

For rough interface, the shear strength decreased by up to 11% after 0.5 heating cycle and slightly increased after 0.5 cooling cycle. The interface shear strength of rough interface increased by up to 23% after 10.5 heating cycles and 10.5 cooling cycles.

The effects of the moisture content changes on soil-concrete interface only happened at smooth interface with normal stress of 100 kPa and rough interface, where the shear strength increased with decreasing moisture contents. The moisture content change is the main reason for the interface strength change in tests of 10.5 temperature cycles. However, for interface subjected to 10.5 cooling cycles at higher normal stress (100 kPa), the increase of the shear strength may also arise from other reasons.

The increase of the shear strength of the soil-concrete interface after large temperature cycles which may be attributed to the reduction of moisture contents and the soil particle rearrangement. The temperature and moisture contents effects on the shear strength of the soil-concrete interface increased with the interface roughness.

The void ratio changes of soil subjected to temperature cycles was independent of stress level and void ratio after the primary consolidation stage. The secondary consolidation rate increased during heating cycles which is around four time of the cooling cycles. For the volume change during shearing, dilation occurred at low normal stresses with larger temperature cycles at beginning of shearing stage and then the soil sample contracted.

5. MODIFIED-THERMAL BOREHOLE SHEAR TEST DEVICE AND TESTING PROCEDURE TO INVESTIGATE THE SOIL-STRUCTURE INTERACTION OF ENERGY PILES

5.1 INTRODUCTION

The use of geothermal deep foundations (energy piles) has been rapidly increasing in Europe, Japan, and China to reduce greenhouse gas emissions (Brandl 2006; Laloui et al. 2006; Ooka et al. 2007; and Gao et al. 2008). When compared to conventional geothermal boreholes, energy piles (with embedded polyethylene pipe heat exchangers connected to a ground source heat pump) are part of the structure and require no additional drilling cost. However, the intermittent operation of the heat pump, which depends on heating and cooling loads of the building, introduces new challenges to the foundation design due to subjecting it and the surrounding soil to daily and seasonal temperature changes and cycles.

Temperature change and cycles alter soil properties and lead to expansion and contraction of the pile in the axial and radial directions, both of which affect the soil-pile interaction of axially loaded foundations (Amatya et al. 2012; Bourne-Webb et al., 2009). Extensive experimental tests have been performed by researchers to investigate the behaviors of soils subjected to temperature changes (e.g., Campanella and Mitchell 1968; Laguros 1969; Noble and Demirel 1969; Houston et al. 1985; Kuntiwattanakul et al. 1995; Cekerevac and Laloui 2004); however, limited investigations focused on evaluating the effects of temperature cycles (TC) on soil properties (e.g., Burghignoli et al. 2000; Mašín and Khalili 2012). Temperature changes and cycles also induce axial and radial expansion and contraction of the pile altering the interaction along the soil-pile interface (Saggu and Chakraborty 2015). Researches have investigated the effects of pile axial expansion and contraction (considering the end-restraint) on shear stresses at the soil-pile interface and on axial stresses in the pile (e.g., Brandl 2006; Laloui et al. 2006, Bourne-Webb et al. 2009; McCartney and Murphy 2012; Suryatriyastuti et al. 2012, Olgun et al. 2014, etc.). However, the effects of thermally-induced radial expansion and contraction on the soil-foundation interaction for energy

piles have not been fully investigated. Attempts to measure the effects of the operation of energy pile systems on the soil-pile interaction and interface properties have been focusing on the effects of temperature changes only. Examples of these investigations include performing modified direct shear tests by Xiao et al. (2014 and 2017a); Di Donna et al. (2015); and Yavari et al. (2016). A modified Borehole Shear Test (m-BST) device was also used to examine this effect by Suleiman and Xiao (2014) and Murphy and McCartney (2014). The thermal-BST (TBST) performed by Murphy and McCartney (2014) only considered temperature changes. Suleiman and Xiao (2014) presented preliminary design and results of a manually-controlled TBST which simulated temperature change and radial expansion, but not accurately simulating the effects of temperature and radial displacement cycles (RDC). In this present paper, a new fully-automated modified-thermal BST (Modified-TBST) device that is capable of simulating temperature changes and cycles as well as radial expansion and contraction displacements and cycles, is described. This paper focuses on detailed description of the device, its capabilities and limitations, and a recommended testing control and procedure. Furthermore, preliminary results of shear stress vs. displacement relationships (t-z curves) are presented.

5.2 BACKGROUND

5.2.1 Operation of Energy Piles

The thermal and mechanical responses of energy piles used as structural support members and heat exchangers have been documented in several case histories (e.g., Laloui et al. 2006; Ooka et al. 2007; Hamada et al. 2007; Adam and Markiewicz 2009; Bourne-Webb et al. 2009; Wood et al. 2009; Amatya et al. 2012; Murphy and McCartney 2015). Energy piles are commonly constructed with diameters ranging from 0.3 to 1.5 m, lengths of 10 to 30 m and with heat exchangers made of polyethylene pipe (Laloui and Di Donna 2013). The net thermal output of energy piles ranges from 18 to 120 W per meter of the foundation length and the system typically

provides 3 to 5 energy units for each unit consumed in operation (Preene and Powrie 2009; Bourne-Webb 2013).

The heat pump connected to energy piles operates in cycles (intermittent operation), in which it functions for a period of time (running time) then stops for another period (stoppage time). The data reported by Amis (2011) indicates that in the U.K., the running time during summer and winter ranges from 8 to 16 hours followed by a stoppage time ranging from 1 to 3 hours. During the month of March, Wood et al. (2009) reported that the typical daily cycle of a heat pump in the U.K. consists of 1.5 hours running time and 30 minutes stoppage time. Similarly, Brandl (2006) reported a running time in the range of 8 to 20 hours during summer in Austria. In Spain, Montagud et al. (2011) reported a running time of 35 minutes for a typical cooling day (summer) and 30 minutes for a typical heating day (winter). These heat pump running and stoppage times (intermittent operation) can be critical for the response of axially loaded energy piles. These running and stoppage times of the heat pump result in heating and cooling cycles of the pile and surrounding soil altering soil properties, effective stresses, and soil-pile interaction, which have not been fully investigated.

The temperature distributions within energy piles and surrounding soils have been investigated by several researchers in different countries (e.g., U.S., Europe, Japan, and China) (Brandl 2006; Hamada et al. 2007; Wood et al. 2009; Bourne-Webb et al. 2009; Amis 2011; Abdelaziz et al. 2011; Shang et al. 2011; Akrouch et al. 2013; Murphy and McCartney 2015; Batini et al. 2015； Loveridge et al. 2016). The temperature change of the pile depends on the heating or cooling loads. Based on the data presented in these references, the following is concluded: (1) the common in-operation temperature of energy piles range from -1 to 35°C; (2) the temperature difference between the pile and the soil is approximately 1 to 2°C, which means that the soil temperature ranges from 1 to 33°C and may rise up to 40°C in cooling-dominated environments, extreme climate conditions, or when the energy piles function as solar energy storage sinks

according to Gabrielsson et al. (2000); (3) the daily temperature changes of energy piles range from 4 to 8 °C (Amis 2011; Batini et al. 2015); (4) the temperature changes throughout a whole year (maximum difference between lowest and highest pile temperature) was approximately 20 °C (Murphy and McCartney 2015; Loveridge et al. 2016); and (5) energy piles alter the soil temperature along most of the total length of the pile. If the intermittent operation (temperature change and cycles) of energy piles affect the soil properties and lead to expansion and contraction of the pile, soil-pile interaction along the interface will be affected. This has been confirmed by field tests and monitoring of energy piles. For example, Amatya et al. (2012) reported that the mobilized shear resistance (per degree change of temperature), which is calculated using axial strain gauge readings under constant mechanical loading, during heating is 1.9 times of that during cooling. In addition, Wang et al. (2015) reported 14% increase in shaft resistance during heating compared to the case with no temperature change; however, Wang et al (2015) did not evaluate the effects of cooling on shaft resistance. Furthermore, analytical study performed by Suryatriyastuti et al. (2012) showed that a temperature change of 15 °C in energy piles result in 21% increase of the normal force on the soil-pile interface during heating and 14% to 65% reduction of the normal force during cooling.

5.2.2 Soil-structure Interaction of Axially Loaded Energy Piles

When an energy pile is heated, it expands in both axial and radial directions, and the pile contracts when it is cooled affecting the shear resistance at the soil-pile interface. The thermal-induced expansion and contraction (or deformation) depends on the load and restraint on the top, toe resistance, and surrounding soil properties. The axial deformation effects were well described by Bourne-Webb et al. (2009) and Amatya et al. (2012) for thermal and mechanical loading conditions. For the effects of radial expansion and contraction, Figure 5.1a shows a pile with soil horizontal (radial) stress distribution normal to the soil-pile interface along the pile with no temperature effects. When subjected to heating, the pile expands radially (horizontally) and the soil

reaction (horizontal stress normal to the soil-pile interface) increases, generating larger shear resistance (Figure 5.1b). When subjected to cooling; however, the pile contracts and the soil reaction decreases leading to a reduction of the shear resistance of the soil-pile interface (Figure 5.1c). With the heat pump running and stoppage cycles described above (intermittent operation), the soil and the pile are subjected to cycles of temperature change and expansion and contraction, the effects of which on soil-pile interface properties have not been directly measured, which are explored using the Modified-TBST in this paper.

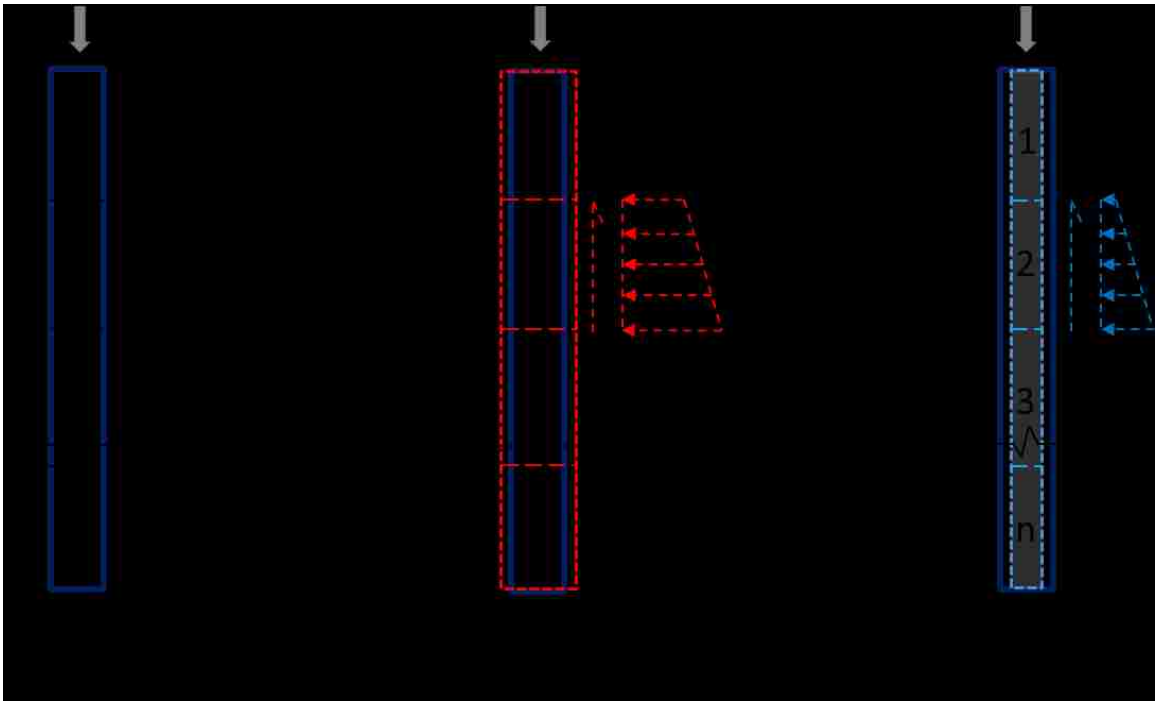

Figure 5.1 Pile subjected to vertical loading showing horizontal stresses normal to the soil-pile interface, (a) Conventional pile; (b) radial expansion of energy pile during heating; and (c) radial contraction of energy pile during cooling

Using modified direct shear and modified borehole shear tests, the effects of temperature changes on soil-pile interface properties have been investigated by several researchers including Xiao et al. (2014); Suleiman and Xiao (2014); Murphy and McCartney (2014); Di Donna et al. (2015); and Yavari et al. (2016). Direct shear test results reported by Di Donna et al. (2015) showed an increase of the shear resistance of the soil-concrete interface (for saturated clay) when subjected to heating (temperature change only), which may be attributed to water migration away from the interface (thermal consolidation). The results reported by Xiao et al. (2014) and Yavari et al. (2016) showed small temperature effects (for both heating and cooling temperature changes but no cycles) on the friction angle and cohesion of the soil-concrete interface for both saturated clay and unsaturated silt soil conditions. Using a thermal borehole shear test (TBST), Murphy and McCartney (2014) also reported very small effects of temperature (heating and cooling with no temperature cycles) on the friction angle, cohesion and shear resistance of unsaturated soil-concrete interface. Suleiman and Xiao (2014), who conducted preliminary tests using manually-controlled TBST combining the effects of radial displacement and temperature change (with no cycles), showed an increase of the soil-concrete interface shear resistance during heating and expansion, and significant reduction after cooling and contraction. The design of this TBST device described by Suleiman and Xiao (2014) did not allow for easy control and application of temperature changes and cycles combined with simulated thermally-induced radial expansion and contraction and the device described by Murphy and McCartney (2014) did not allow for the application and control of thermally-induced expansion and contraction.

5.2.3 Borehole Shear Test Devices

Conventional Borehole Shear Test (BST)

The conventional borehole shear device (BST) developed by Handy and Fox (1967) was used to measure shear strength properties of soils by performing a direct shear test in situ. The BST consists of a bi-lateral expandable shear head with grooved steel plates. The shear head is

lowered into an open borehole, such as the one created by a hollow stem auger. A constant pressure normal to the surface of the borehole is applied by the shear head for typically 5 to 20 minutes to allow for dissipation of any excess pore water pressure after the application of the normal pressure (Lutenegger et al. 1978, Lutenegger and Tierney 1986). When sufficient consolidation time has elapsed, the soil is sheared typically at a displacement rate of 0.05 mm/s by manually applying an upward pulling force, and the shear stress is measured by a dynamometer gauge. In the conventional BST, only the maximum shear stress is recorded (AbdelSalam et al., 2012). The BST is usually conducted three to four times at approximately the same depth using different normal pressures to produce a Mohr-Coulomb failure envelope (Handy and Fox 1967; Handy 1986).

Several modifications have been introduced to enhance the capability and accuracy of the conventional BST and to overcome certain difficulties during soil testing (Lutenegger et al. 1978; Demartinecourt and Bauer, 1983; Lutenegger and Tierney 1986; Lutenegger and Powell 2008,). These modifications include adding pore water pressure sensors and /or load transducer.

Modifications of BST to Measure Interface Properties

BST equipment was also modified to directly measure the shear stress-displacement response (t-z curves) at the soil-pile interface for vertically loaded conventional steel piles (Suleiman et al. 2011; AbdelSalam et al. 2012). The grooved steel plates were replaced by smooth steel plates in a modified-BST device developed by Suleiman et al. (2011) and AbdelSalam et al. (2012) to measure the t-z curves of the interface between a steel pile and surrounding soil. To simulate the soil-pile interaction of energy piles, Suleiman and Xiao (2014) introduced preliminary modifications of BST with manual displacement control to measure the combined effects of temperature and radial displacement on soil-pile interface at temperatures of 2 to 40 °C in the laboratory, and the equipment was called Thermal-BST (TBST). Murphy and McCartney (2014) developed a similar device that can only measure the effects of temperature, and performed tests in Boulder clay and silty sand considering temperature effects ranging from 10 to 45 °C. In the paper

described herein, a Modified-Thermal Borehole Shear Test (Modified-TBST) device that is fully-automated and capable of simulating both temperature change and cycles as well as radial expansion/contraction displacements and cycles of energy piles, is described to directly measure the t-z curves at the soil-pile interface. This paper focuses on detailed description of the device, its capabilities and limitations, testing procedure, and presenting preliminary results.

5.3 DESIGN AND SETUP OF MODIFIED-TBST

5.3.1 Overview

As shown in Figure 5.2, the Modified-Thermal Borehole Shear Test (Modified-TBST) system includes a loading frame to apply pulling vertical force on the shear head using a stepper motor. The shear head, which is connected with the loading frame using steel rods, consists of two concrete plates with embedded aluminum tubes for heating and cooling (Figure 5.3). Two linear potentiometers (displacement gauges) were mounted between the shear plates to measure and control the horizontal displacement simulating the radial expansion and contraction of energy piles.

A data acquisition system was used to record the readings of pulling force, vertical displacement of the shear head, and air pressure of the pneumatic piston applying horizontal pressure normal to the soil-concrete interface (σ_h). The system also includes a unit to control the normal pressure on soil-concrete interface. Two refrigerated/heated circulating baths, connected to the aluminum tubes embedded in the concrete plates, were used to apply temperature change and cycles (heating and cooling) simulating the field intermittent operation of heat pumps connected to energy piles. In addition, thermocouples were installed in the soil and on the surface of the concrete shear plates to measure temperature. In total, eighteen thermocouples were used in the soil at three different depths as shown in Figure 5.2. A tensiometer was also installed in the soil (~5 mm from the interface) to monitor changes of pore pressure.

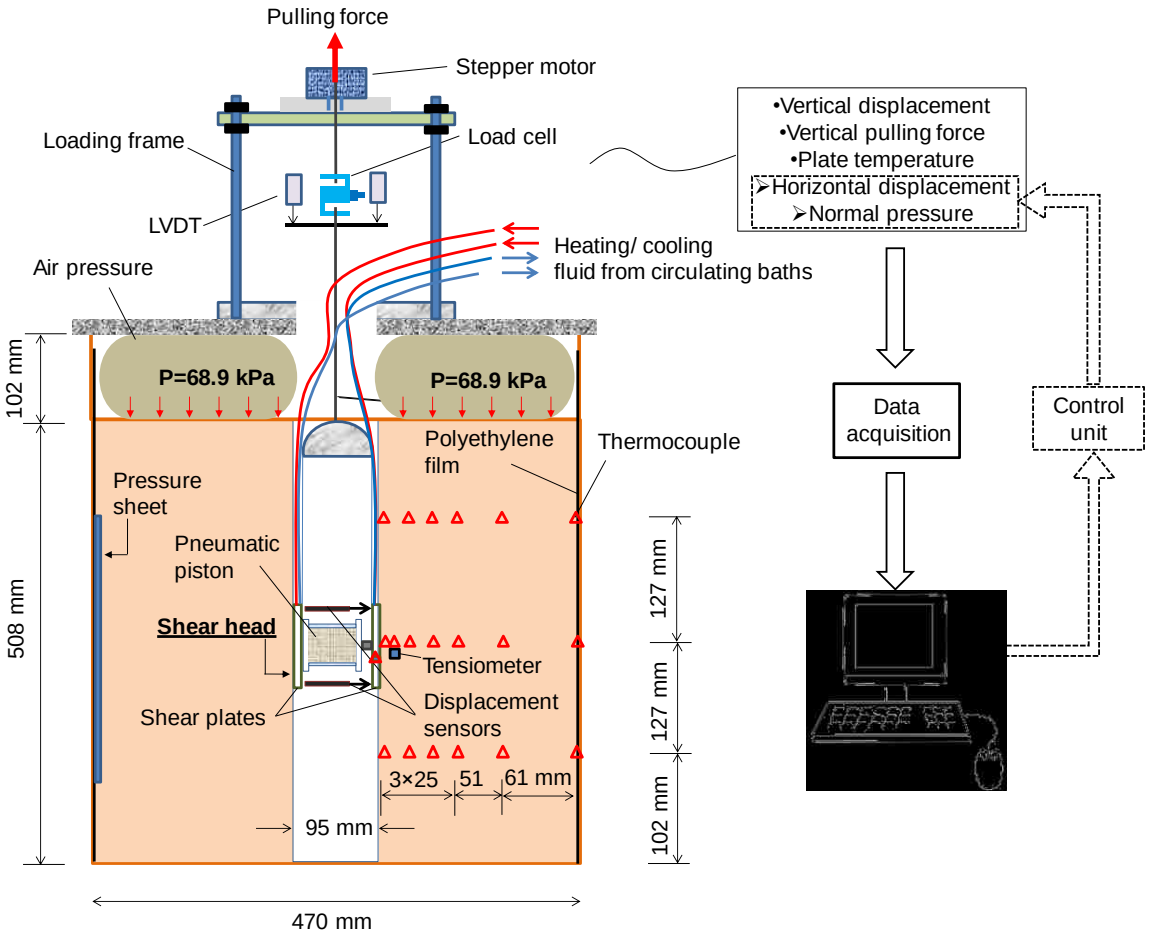

Figure 5.2. Configuration of the Modified-TBST system

Modified-TBSTs were performed in a soil tank filled with compacted soil. The tank was covered by a lid functioning as reaction to apply overburden pressure (p) on the top surface of the soil. An open hole at the center of the lid allows placing the shear head into the borehole. To reduce frictional forces, the inside surface of the tank was covered with a friction-reducing tarp comprised of two thin layers of graphite grease, sandwiched within three layers of thin polyethylene films. Furthermore, tactilus pressure sensors were installed on the inside surface of the tank to evaluate boundary conditions.

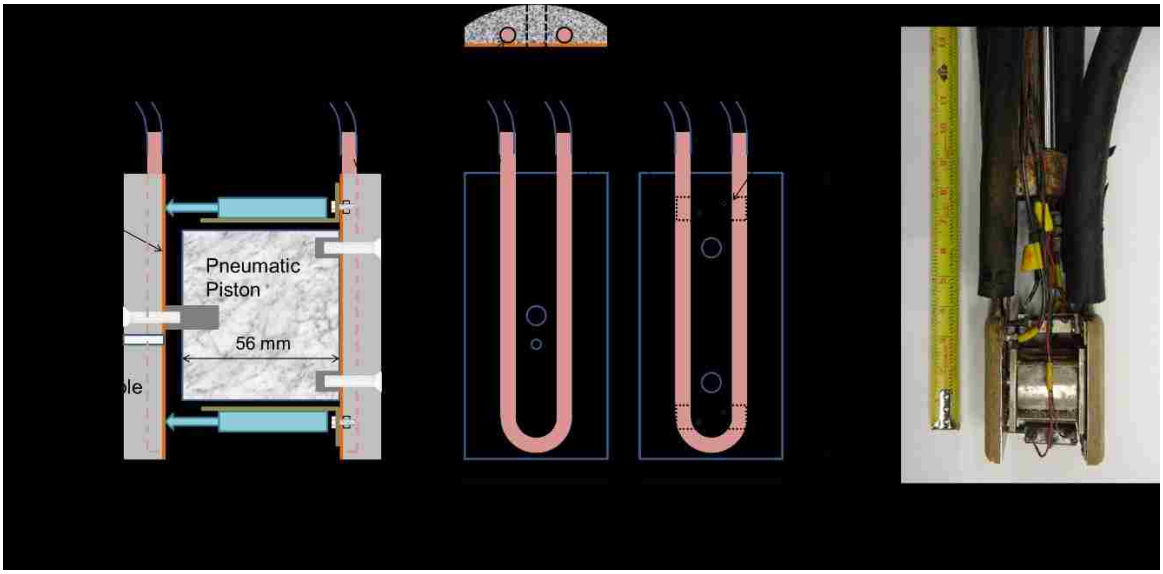

Figure 5.3 Configuration of concrete plates and shear head: (a) side view of the shear head; (b) cross section of concrete plate; (c) left plate and heat exchange pipe; (d) right plate and heat exchange pipe; (e) photo of the shear head with concrete plates.

5.3.2 Design of the Shear Head

The shear head of the Modified-TBST includes two concrete shearing plates with a pneumatic piston in between as shown in Figure 5.2 and 5.3a. Increasing the air pressure of the piston pushes the shear plates toward the soil applying different normal pressures (σh) on the soil-concrete interface. Two displacement sensors with resolution of 1 μm were fixed between the two shearing plates to measure and control the horizontal displacement (radial displacement). The contact area between a concrete plate and surrounding soil is 52 cm2. The concrete plates were casted on high strength stainless steel plates with thickness of 1.2 mm, and U-shaped aluminum heat exchange pipes, with a diameter of 6 mm, were glued on the steel plates as shown in Figure 5.3b, c and d. The heat exchange pipes were connected with circulating pipes outside of the concrete shearing plates and to the two circulating paths to control the temperature. Insulation was used around the circulating pipes to reduce heat loss and minimize condensation and temperature effects on the soil above the concrete plates (Figure 5.3e).

5.3.3 Loading System

An electric worm-gear pulling system, previously used in the manually operated BST device, was coupled with a stepper motor to pull the shear head upward. However, the friction of the worm gear requires a motor with a higher power and also influences the shearing rate. Therefore, a new loading frame was built using four aluminum T-slotted framings and two steel plates (see Figure 5.2). The T-slotted framings are standing on a 305 by 356 mm aluminum plate with thickness of 19 mm. The stepper motor was placed on a 305 by 305 mm steel plate, the elevation of which is adjustable along the T-slotted framing using end-feed fasteners. The stepper motor, which has a pulling capacity of 2200 N, was connected to the control system to target a vertical displacement rate (shearing rating) of 0.05 mm/s during the shearing stage (applying pulling force on the shear head), which is similar to the rate used in the conventional BST. An S-beam load cell with 2200 N capacity was used to measure the pulling force. Three LVDTs were mounted on the pulling rod to measure the vertical displacement of the shear head during shearing to minimize any tilting effect on measured displacements.

5.3.4 Heating and Cooling System

Two refrigerated/heated circulating baths were used to simulate temperature changes. One circulating bath was used for heating the soil-concrete interface to the target temperature, while the other was used for cooling. The heating and cooling baths had liquid reservoirs of 8 and 28 liters, respectively, and a mixture of 50% distilled water and 50% glycol was used. The working temperature of the liquid ranges from -30°C to +200°C.

5.3.5 Control System

The shear head radial expansion and contraction displacement and cycles were controlled by a National Instruments PXI series real-time controller using a LabView-based graphical user interface, INERTIA, developed by Wineman Technology Inc. During preliminary tests, a Proportional-Integral-Derivative (PID) closed-loop control method was used to conduct the tests.

As shown in Figure 5.4, the total target displacement (radial expansion or contraction of the pneumatic piston) and the displacement increment (y_{sp}) were specified and sent to the PID controller. Then, a voltage command was sent to the piston to adjust the pressure targeting to achieve the first displacement increment and the actual displacement was measured. The error, which is defined as the difference between the command (target displacement increment) and feedback (measured displacement) was calculated and used by the controller to send a new voltage command. Once the error is very small (less than 1 μm), a new displacement increment was targeted and the same process was repeated until the total target displacement was achieved. This is a continuous running closed-loop application (loop rate is 1000 scans a second).

Figure 5.4 Block diagram of PID control system

After performing few preliminary tests, it was observed that the PID system with closed-loop displacement control to simulate expansion and contraction does not function accurately at very small target displacements. To achieve a specific displacement increment, the system tends to set a larger piston pressure, which caused overshooting of the displacement followed by a reduction of the pressure to adjust the displacement. This process occurred several times for each displacement increment resulting in frequent oscillation of the pressure and applying cyclic loading on the soil, which may result in changes of the soil stiffness leading to larger pressure needed to

achieve the total target displacement and plastic soil displacement when achieving the total target displacement. This issue will be discussed later in the paper.

In order to avoid this issue of the PID control system after performing the first few tests, loading control with displacement tracking (LCDT) method was followed to apply expansion and contraction displacements. LCDT was achieved by programing the loading procedure in INERTIA to perform the expansion and contraction displacements and cycles, which will be described later in the experimental procedure.

5.4 CALIBRATION OF MODIFIED-TBST

The heating or cooling of the fluid circuiting through the aluminum tubes embedded in the concrete plates alters the temperatures of the plates and the pneumatic piston, which changes the readings of the radial displacement sensors between the two shearing plates and the pressure normal to the soil-concrete interface. To account for all these changes, a calibration of the device was performed at temperatures ranging from 2 to 40 °C.

5.4.1 Effect of Temperature on Displacement Reading

The heating and cooling effects on the reading of the sensors measuring the radial expansion and contraction of the shear head were evaluated by subjecting the shear head to temperature changes. The results of the calibration tests are shown in Figure 5.5. It was observed that the readings of the radial displacement sensors, used to control and measure the expansion and contraction of the shear head, change due to temperature change only, which is attributed to the expansion and contraction of different parts and materials of the shear head. The total change of the displacement reading divided by the temperature change at the surface of the shearing plate provides a displacement correction factor of the shear head per unit temperature change. Based on six temperature calibration tests, the average displacement correction factor of the shear head was -1.1μm/°C.

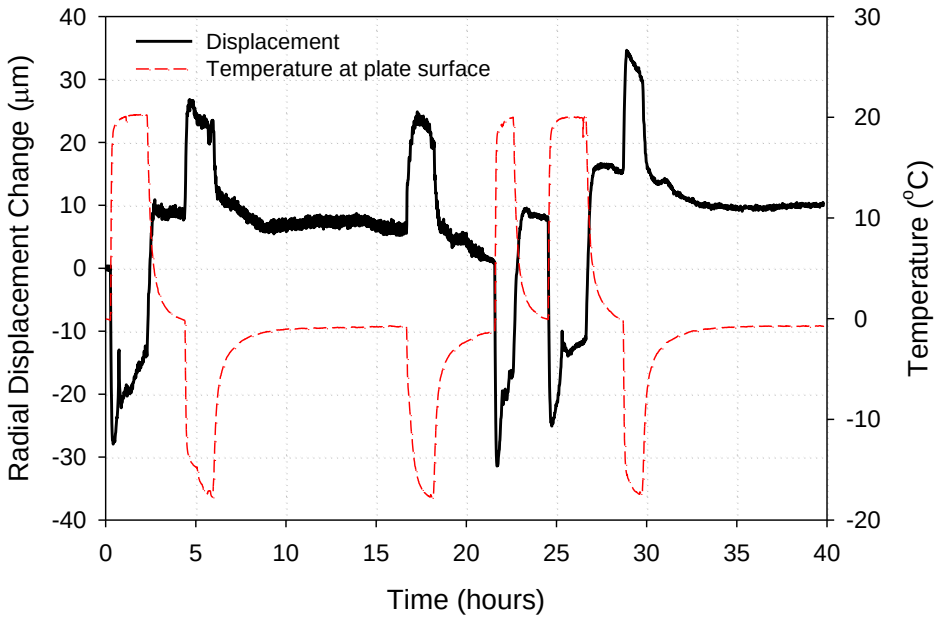

Figure 5.5 Calibration of the change of radial displacement sensor readings due to temperature effects on the shear head

5.4.2 Temperature Effects on Horizontal Force

The horizontal (normal) force applied on the soil-concrete interface is controlled by the air pressure in the pneumatic piston. The relationship between the horizontal force and the air pressure in the pneumatic piston was calibrated using a compression machine at different temperatures as shown in Figure 5.6. Comparing the results at different temperatures, Figure 5.6 shows that the temperature effect on the measured horizontal force is minimal. It is also worth noting that the air pressure has a linear relation with the horizontal force, except for air pressures smaller than 20 kPa, which correspond to a normal force of 12 N. A coefficient (slope) of 0.81 N/kPa was used to calculate the normal pressure on the soil-concrete interface when the air pressure was larger than 20 kPa. When the air pressure was smaller than 20 kPa, a coefficient of 0.5 N/kPa was utilized.

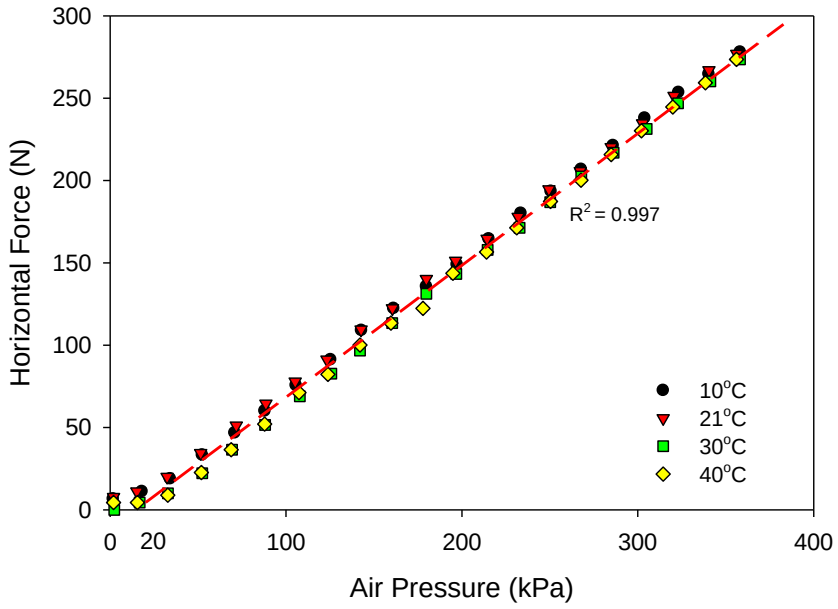

Figure 5.6 Relationship between the horizontal (normal) force of pneumatic piston and air pressure at different temperatures

5.5 MATERIALS AND PREPARATION

5.5.1 Soil Properties

Soil obtained from a construction site in the Lehigh Valley, Pennsylvania was used to conduct the Modified-TBSTs. Using the Unified Soil Classification System (USCS), the soil was classified as sandy silty clay (CL-ML) with 17.5% sand, 54.3% silt, and 25.8% clay. The liquid and plastic limits of the soil were 28% and 22%, respectively, and the solids specific gravity was 2.67. Standard Proctor tests were performed and the maximum dry unit weight and optimum moisture content were 17.4 kN/m^3 and 14%, respectively. To perform the Modified-TBSTs inside the soil tank, the soil was compacted in layers to achieve target moisture content of 18% and dry unit weight of 13.8 kN/m^3. The measured thermal conductivity of the soil was ~1.1 W/mK and the volumetric heat capacity was ~ 2100 kJ/m^{3}K.

5.5.2 Soil Preparation

The soil was mixed at the target moisture content in a concrete mixer. During preliminary tests, it was observed that the average moisture loss during preparation and waiting times was less than 0.5%, which was compensated for during soil preparation. As shown in Figure 5.2, thin polyethylene films placed on the inside surface of the tank were used to reduce the friction between the soil and the tank. Tactilus pressure sheet sensors were also used on the inside surface of the tank to check for boundary effects (Figure 5.2). The soil was filled in the tank in 7 layers and compacted using a tamper with targeted compaction energy per unit volume of ~54 kN-m/m^3. This consistent procedure was utilized in all experiments and resulted in soil dry unit weight of 13.7 kN/m^3. During compaction, an aluminum pipe with a diameter of 95 mm was installed in the middle of the tank to create the borehole needed to perform the Thermal-TBSTs. Thermocouples were installed at different locations in the soil as the tank was being filled and the locations of these sensors are shown in Figure 5.2.

After filling the soil in the tank, an overburden pressure (p) of 68.9 kPa was applied on the top surface of the soil for two days to consolidate it (see Figure 5.2). Then the overburden pressure was released, the aluminum pipe was pulled out of the soil, and the overburden pressure (p) of 68.9 kPa was applied again for another two days. The top lid of soil tank was covered by plastic film to avoid or minimize the loss of the soil moisture during the test.

5.6 TESTING PROCEDURE

After preparing the soil and consolidating it under vertical overburden pressure (p), the test proceeded using three major stages; the consolidation stage, the temperature and/or displacement stage, and the shearing stage. The details of each of these stages are discussed below.

5.6.1 Consolidation Stage

After the soil preparation, the shear head was lowered in the borehole and a constant horizontal (or normal) pressure (σ_h) was applied normal to the soil-concrete interface. The horizontal pressure was increased from 0 kPa to the target pressure value at a rate of 1.55 kPa/s. This constant pressure is called the initial radial consolidation pressure. Initially, the constant pressure was applied for different time intervals to determine the time required for the radial consolidation stage. When subjected to this consolidation pressure, the soil consolidates laterally and the displacement of the shear plates was measured with time. The horizontal pressure vs. radial displacement of the plates of the shear head during the increase of horizontal pressure is presented in Figure 5.7a, which shows a displacement of 0.71 mm and 0.94 mm for tests with target horizontal pressures of 41.4 and 69.0 kPa, respectively. During the consolidation stage, the radial displacement of the plates increased to 0.98 mm and 1.27 mm for consolidation pressure of 41.4 and 69.0 kPa, respectively. Figure 5.7b presents the radial displacement rates of the shear plates for 24 hours at applied horizontal consolidation pressure (σ_h) of 41.4 and 69.0 kPa. Based on the results from different consolidation time intervals and consolidation pressures, it was noticed that after 12 hours of consolidation, the rate of radial displacement is very small (< 2 μm/hour), which reduces the creep effect of soil during temperature and displacement change stages. Therefore, the initial constant radial consolidation pressure was applied for 12 hours during this stage for other tests. Modified-TBST tests were conducted at radial consolidation pressures of 13.8, 27.6, and 41.4 kPa. It is worth noting that the pressure at the inside wall of the soil tank, which was measured using a Tactilus pressure sheet, showed pressure increase smaller than 0.5 kPa (i.e. ~1% of the pressure applied at borehole) during the tests confirming the minimal effects of the boundary.

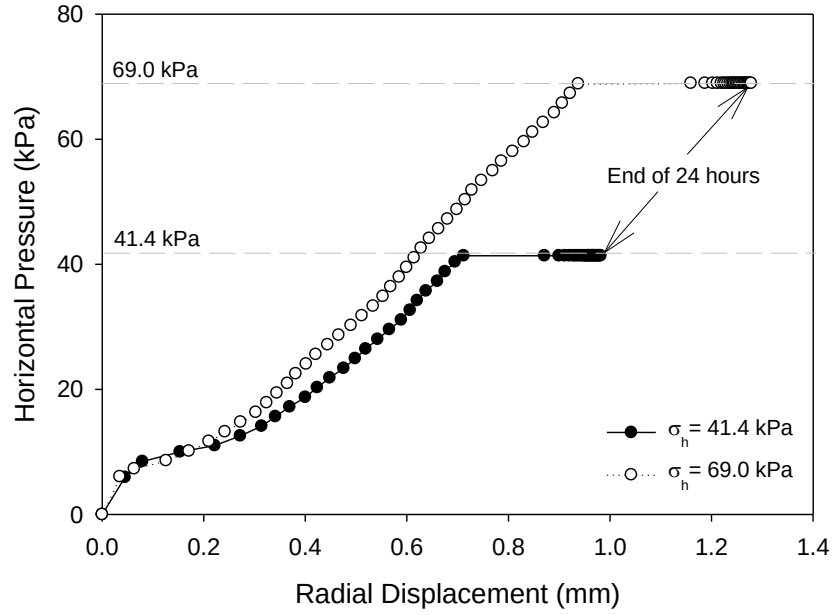

(a)

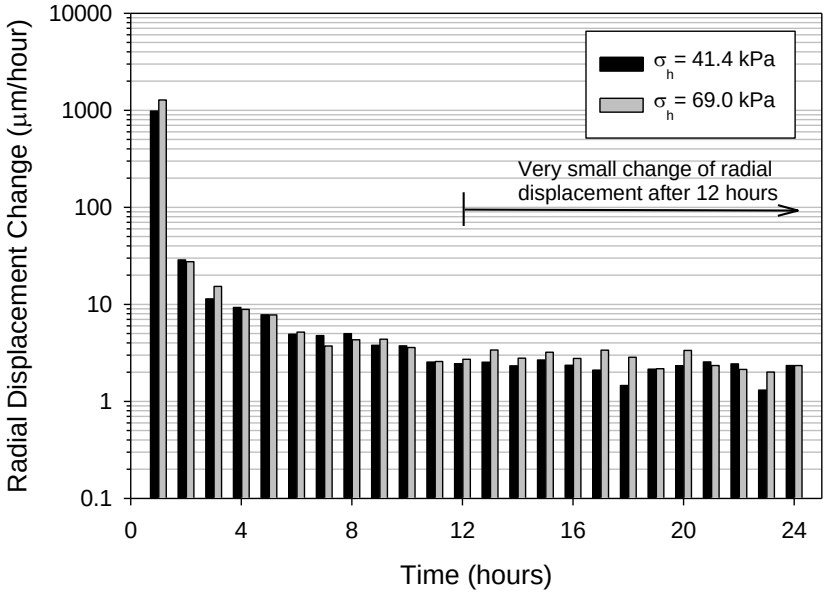

(b)

Figure 5.7 Radial displacement at consolidation pressure of 41.4 and 69.0 kPa during consolidation stage, (a) horizontal pressure vs. radial displacement; (b) change of radial displacement as a function of time

5.6.2 Applying Temperature Change and Cycles

For tests with temperature change and/or cycles, the shear plates were heated or cooled by circulating a fluid with different temperatures. For heating cycles, one circulating bath was used and the fluid temperature was set to ~8 °C higher than the target temperature of the soil-concrete interface (to account the heat loss) measured using a thermocouple on the shearing plate surface. The soil-concrete interface was heated to the target temperature (i.e., reaching 0.5 temperature cycle or TC = 0.5 as shown in Figure 5.8). Then, the circulating bath was stopped, and the other bath started to cool the plates down to room temperature (i.e. reaching 1 heating cycle or TC = 1 as shown in Figure 5.8). For cooling cycles, the fluid temperature was set to ~12 °C below the target temperature. The soil-concrete interface was cooled to the target temperature (i.e., reaching 0.5 cooling cycle or TC = −0.5 as shown in Figure 5.8). Then, the circulating bath was stopped and the other bath started to warm up the plates back to the room temperature (i.e. 1 cooling cycle or TC = −1). This process could be repeated to apply the target number of heating or cooling cycles. This process was used to better control the interface temperature and to allow for applying several cycles within one testing/working day.

Based on the discussion provided in the background section related to the daily running and stoppage times of heat pumps installed in different environments and to allow for applying several cycles within one testing/working day, heating or cooling cycles of 1 hour was targeted in our investigation. Temperature change (ΔT) of 20 °C was used for heating and temperature change of -18 °C was used for cooling. It is worth noting that the target temperature change of 20 °C or 18 °C is higher than the practical case for the daily operation of energy piles which may alter pore pressure of surrounding soil. However, the pore pressure change was measured during tests with temperature cycles (tests with 10 cycles). For the test conditions presented in this paper (silty clay with 17.5% sand, unsaturated condition), the change of pore pressure within 30 min (0.5 cycle) and

20 °C temperature change was ~4%. The details of the pore pressure measurements will be discussed in a future paper that focuses on effects of temperature and displacement cycles.

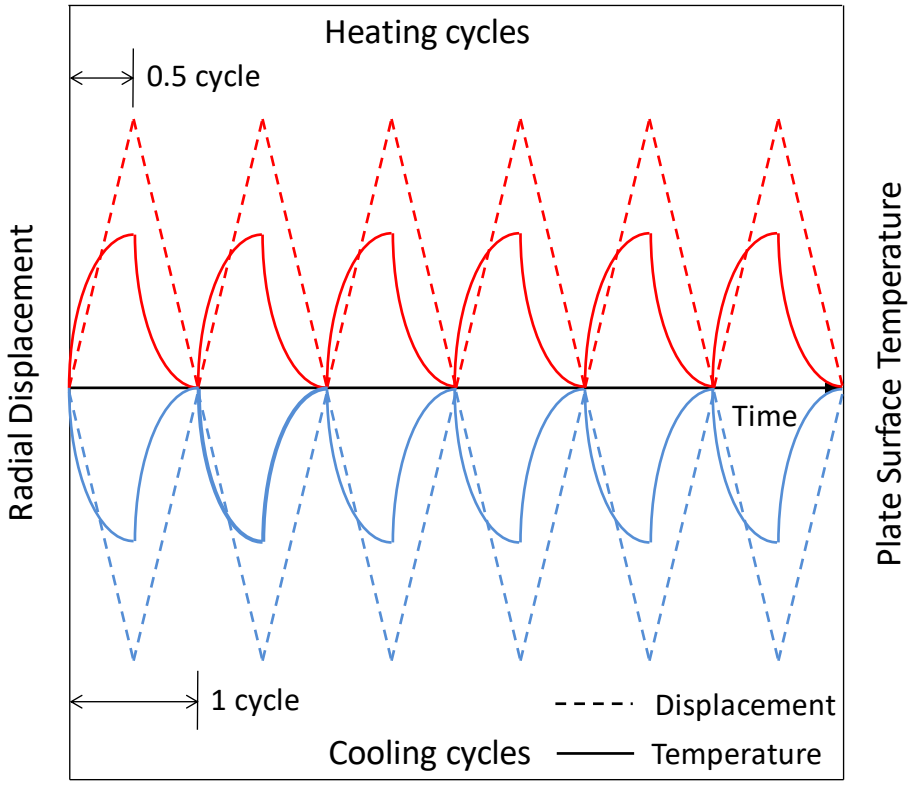

Figure 5.8 Temperature and displacement cycles of the test device

5.6.3 Applying Radial Displacement Change and Cycles

As previously discussed and will be discussed later, a LCDT displacement control approach was used to address oscillation under PID control. Using the LCDT displacement control approach, the control system adjusts the air pressure of the pneumatic piston to change the normal pressure applied on the soil-concrete interface. The adjusted piston pressure changed the position of the shear plates relative to the surrounding soil [i.e., pushed forward into the soil (simulating pile expansion) or pulled backward (simulating pile contraction)]. As shown in Figure 5.8, the expansion to a target displacement is defined as 0.5 expansion cycle (radial displacement cycle or

RDC = 0.5) and returning the plates to the original position completes a displacement cycle (1 expansion cycle or RDC = 1). Similarly, for contraction cycles the plates contract to a target displacement from the original position (0.5 contraction cycle or RDC = −0.5) followed by returning the plates to their original position, which completes 1 contraction cycle (RDC = −1).

To calculate the target radial expansion and contraction of energy piles, the pile diameter, temperature difference, and coefficient of thermal expansion (α) of concrete are needed. For example, an energy pile with 0.6 m diameter, $\alpha = 10^{-6}$ $\mu\varepsilon$/°C subjected to 20 °C temperature changes is expected to expand and contract by 120 μm, which was used in our tests. This target displacement can be achieved using the PID control or the LCDT control systems. The performance of the device using both of these systems will be compared in the results section. It is worth noting that confinement from surrounding soil may affect the radial strain of energy piles. For example，Mimouni and Laloui (2015), based on results of field test, concluded that radial strain was partially restrained, while Wang et al. (2015), who performed an O-cell test on an energy pile, reported that the pile expanded freely in the radial direction. During the tests presented in this paper, a free radial expansion was assumed.

5.6.4 Shearing Stage

After temperature and/or radial displacement change/cycles were applied, the shear head was pulled upward shearing the soil-concrete interface and the applied pull out force and the vertical displacement were measured (i.e., producing shear stress vs. vertical displacement curves or t-z curves). Shearing was applied at a constant rate of 0.05 mm/s. During the shearing stage, control in the radial direction can use displacement control (DC) or load control (LC). If displacement control is used, the radial displacement of the concrete plates is maintained constant by adjusting the horizontal pressure. If load control is used, the horizontal pressure at the soil-concrete interface is maintained constant. The difference between the two control procedures during the shearing stage will be discussed later. It is important to note that the tests without

temperature change were conducted first to avoid any temperature effects on surrounding soil. Furthermore, the shear head was rotated between tests so each position was only sheared once.

5.7 PRELIMINARY RESULTS AND ANALYSIS

5.7.1 PID vs. LCDT Control

To evaluate the performance of the PID control, the radial displacement and the corresponding horizontal pressure at the interface for trail tests with 10.5 expansion cycles (RDC = 10.5, TC = 0) are presented in Figure 5.9a. The tests were performed at room temperature using both PID closed-loop control and LCDT methods. At the beginning of the expansion cycles (Point A in Figure 5.9a), the initial radial consolidation pressure was 41.4 kPa. At the end of first half expansion cycle (RDC = 0.5, Points B and B' in Figure 5.9a) with target expansion of 120 μm, the horizontal pressure increased from 41.4 kPa to 49.7 kPa for the LCDT method and to 63.0 kPa for the PID control method. When the plates returned to the initial position at 1 expansion cycle (RDC = 1, Points C and C' in Figure 5.9a), the horizontal pressure was 16.0 kPa for LCDT and 8.5 kPa for PID control. The horizontal pressure-displacement response of these two control methods also have a significant difference during the following expansion cycles (Figure 5.9a). Using the LCDT method, the horizontal pressure at 10 and 10.5 expansion cycles (Points D and E in Figure 5.9a) were 11.4 and 40.4 kPa, respectively. However, using the PID control, the horizontal pressure at 10 and 10.5 expansion cycles (Points D' and E' in Figure 5.9a) were 4.4 and 54.3 kPa, respectively. As discussed before, the differences between the two systems could be attributed to the frequent oscillation of pressure (applying cyclic loading on the soil), which resulted in changes of the soil stiffness leading to larger pressures and plastic soil deformations. This pressure oscillation of the PID control is clearly shown in Figure 5.9b, which focus on the collected data for the first 60 seconds of the control systems. While the pressure with LCDT method was stable compared to that with PID control. The horizontal pressure increased from 41.4 to 44.4 kPa in 60 seconds. The

corresponding expansion of the plates increased around 6μm in the first 60 second using LCDT method compared to 4μm in the test with PID closed-loop displacement control.

5.7.2 Effect of Radial Consolidation Time Interval

The effect of radial consolidation time on the shear stress-vertical displacement response of the soil-concrete interface (i.e., t-z curves) was investigated. Figure 5.10 shows the t-z curves of the soil-concrete interface with radial consolidation times of 15 minutes, 1 hour and 12 hours for an initial consolidation pressure of 41.4 kPa. Peak strengths of 26.9, 27.6, and 26.7 kPa were measured at consolidation times of 15 minutes, 1 hour and 12 hours, respectively. Figure 5.10 shows that the effect of consolidation time on interface shear strength was not significant (only 3.3% maximum difference). However, the values of the stiffness of the soil-concrete interface at 50% of the peak shear strength (G_{50}) were also compared. The stiffness (G_{50}) was calculated using by Equation 1

$$G_{50} = \frac{\tau_{50}}{d_{50}} \tag{1}$$

where τ_{50} is 50% of the shear strength, and d_{50} is the vertical displacement of the shear plates corresponding to τ_{50}.

The G_{50} of soil-concrete interface with consolidation time of 15 min, 1 hour, and 12 hours were 182.2, 194.3, and 212.2 kPa/mm, which shows a maximum difference of ~16%. Based on these results, and those shown in Figure 5.7, a radial consolidation time of 12 hours was used in all other tests.

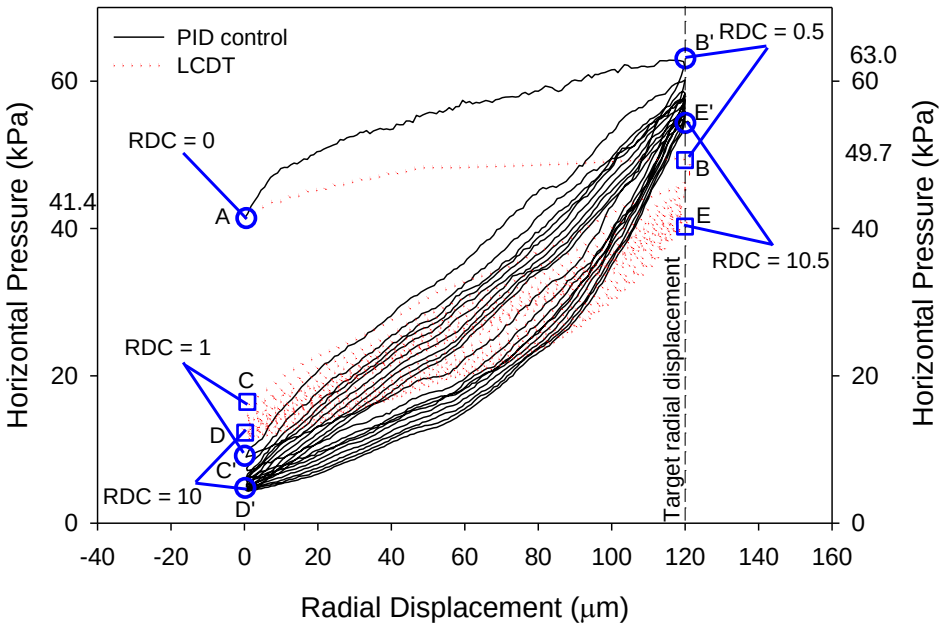

(a)

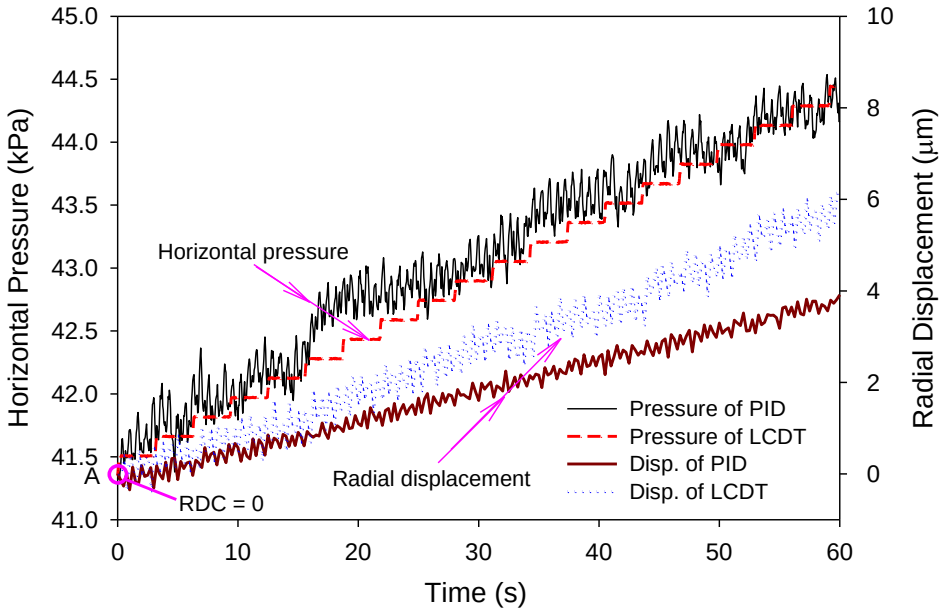

(b)

Figure 5.9 Comparison of PID control and LCDT, (a) horizontal pressure vs. displacement for expansion cycles; (b) horizontal pressure and radial displacement at the beginning of PID control and LCDT

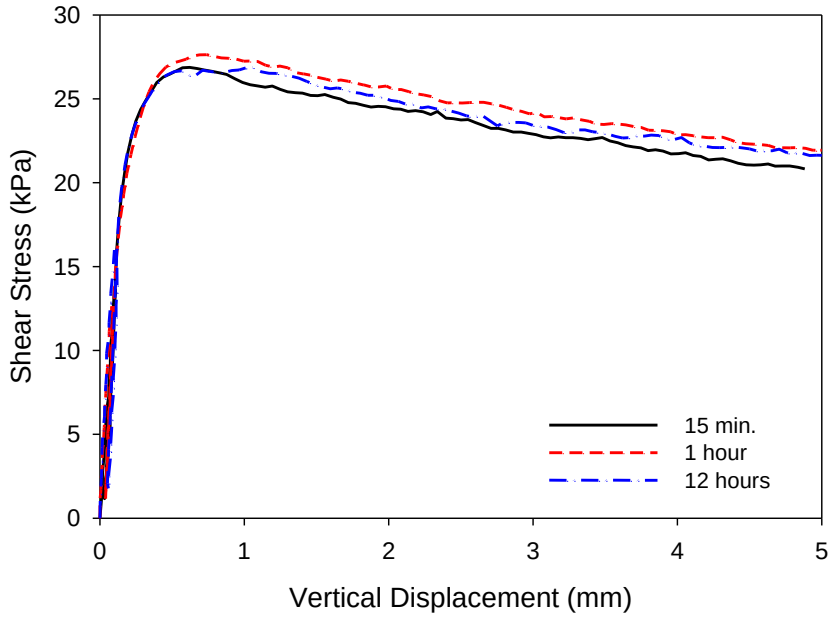

Figure 5.10 t-z curves of soil-concrete interface at different consolidation times

5.7.3 Load Control vs. Displacement Control during Shearing Stage

Figure 5.11 shows the measured t-z curves of tests subjected to initial consolidation pressures of 13.8, 27.6, and 41.4 kPa without temperature or displacement cycles. After finishing the radial consolidation stage, the control in the radial direction was changed to a displacement control (DC) keeping the plates at the same radial (horizontal) distance as that at the end of radial consolidation, while the other set of tests was performed by keeping the horizontal pressure constant using load control (LC). In both sets of tests, the shearing was performed using a constant rate of displacement of 0.05 mm/s. Figure 5.11 illustrates that the measured t-z curves with DC show a softening response after achieving the peak strength. Furthermore, the peak and ultimate shear strength of the soil-concrete interface for tests performed with LC was higher than those performed with DC. This difference could be attributed to the reduction of the horizontal pressure when the system was trying to keep the same radial distance between the two plates in DC. For example, for the tests with initial radial consolidation pressure of 27.6 kPa, the horizontal pressure decreased significantly from 27.6 kPa to 14.7 kPa during shearing when the radial distance between

the plates was kept constant during shearing. During shearing, the plates could rotate very slightly when subjected to pull out force changing the radial displacement readings triggering a change of the horizontal pressure. This very small rotation of the plates may cause the tilt of a horizontal displacement sensor or the tip of the displacement sensor to slide of the back of the shearing plate. Because of the issues and to allow for comparing the responses of tests at different conditions, the LC is recommended and was used for future tests.

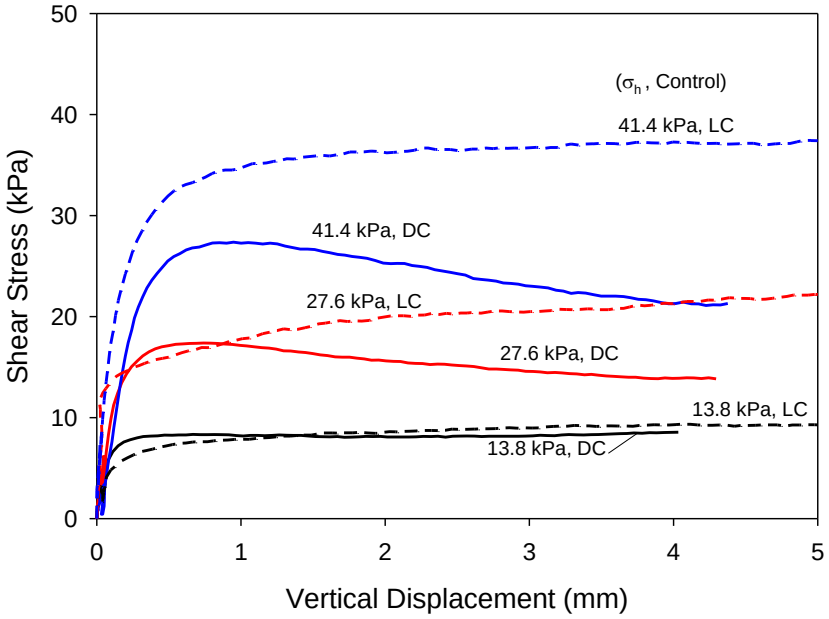

Figure 5.11 Comparison of t-z curves with load control and displacement control in radial direction during shearing

5.7.4 Preliminary Test Results

After finalizing the testing procedure and calibration based on the tests discussed before, a series of Modified-TBSTs were performed with radial consolidation pressure of 41.4 kPa. A reference test was conducted without temperature or displacement cycles (RDC = 0, TC = 0). The strength of the shear stress-vertical displacement (t-z curve) for this reference test was 35.8 kPa. Figure 5.12 shows the t-z curves after 0.5 heating cycle (RDC = 0, TC = 0.5), 0.5 expansion cycle (RDC = 0.5, TC = 0), and the combination of 0.5 expansion and 0.5 heating cycles (RDC = 0.5 and

TC = 0.5). When compared to the reference test, the interface strength decreased by 9% for the test with RDC = 0 and TC = 0.5. According to Murphy and McCartney (2014), this difference could be attributed to undrained heating which may increase thermally-induced pore pressures resulting in thermal softening. However, for the test conditions presented in this paper (silty clay with 17.5% sand, unsaturated condition), the change of pore pressure within 30 min (0.5 cycle) and 20 °C temperature change was ~4%. For the test with half cycle heating and expansion (RDC = 0.5, TC = 0.5), the interface strength was 40.6 kPa (13.4% increase) and it was 43.6 kPa (21.8% increase) for the test with half cycle expansion (RDC = 0.5, TC = 0). During expansion, the concrete plates expand toward the soil and the horizontal pressure at the interface increases. For the test with half expansion cycle, the horizontal pressure increased from 41.4 kPa to 49.5 kPa. For the test with half heating and expansion cycle, the horizontal pressure increased to 46.7 kPa. The difference between the two radial pressures during these two tests could be attributed to the effects of temperature on soil properties (stiffness), which could be as high as 30% according to the stress relaxation tests performed by Murayama (1969) for a saturated clay subjected to temperature change. The decrease of stiffness with increasing temperature was also observed by Zhou and Ng (2015) for unsaturated fine soils.

Figure 5.12 also show the t-z curves after 0.5 cooling cycle (RDC = 0, TC = -0.5), 0.5 contraction cycle (RDC = -0.5, TC = 0), and the combination of 0.5 contraction and 0.5 cooling cycles (RDC = -0.5 and TC = -0.5). For the test with RDC = 0 and TC = -0.5, the interface strength was 38.4 kPa (increased by 7% compared to the reference test). The interface shear strength was 9.2 kPa for the test with half cycle contraction (RDC = -0.5, TC = 0), which decreased by 74% when compared to the reference tests due to the reduction of horizontal pressure at the interface. For the test with RDC = -0.5 and TC = -0.5, the shear strength was 8.8 kPa. Based on the results for the test conditions (unsaturated cohesive soil), the effect of expansion and contraction on the interface shear strength is significantly larger than that of temperature change only.

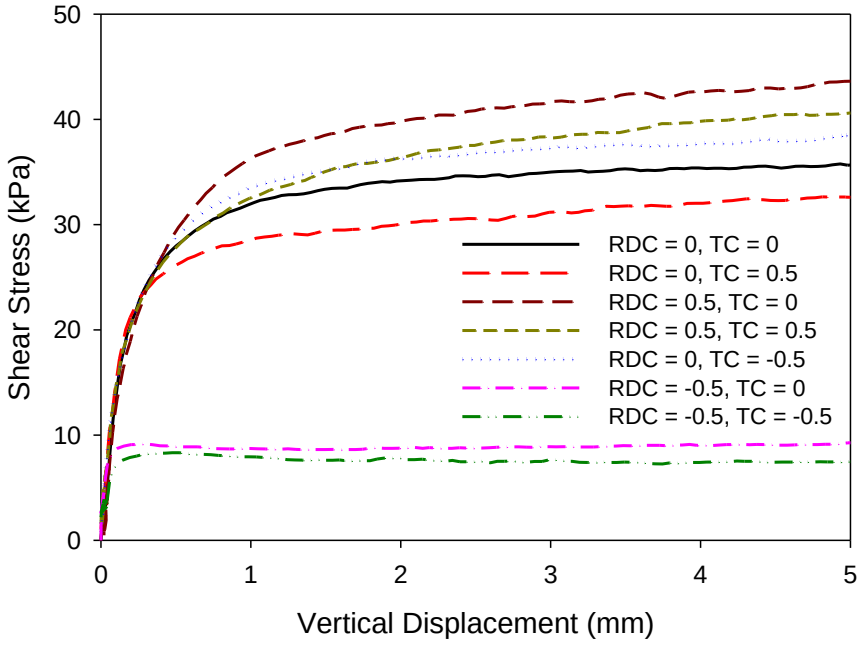

Figure 5.12 t-z curves at initial consolidation pressure of 41.4 kPa

5.8 SUMMARY AND CONCLUSIONS

This paper presents a detailed description of a new fully-automated Modified-TBST device. To simulate the effects of intermittent operation of the heat pump on soil-foundation interaction of energy piles, this device is capable of combining the effects of temperature change and cycles with radial expansion/contraction (displacement) cycles, or separating those effects. Based on the preliminary tests and calibration, LCDT method was proposed for simulating the expansion and contraction displacements and cycles of energy piles. The LCDT method is based on the load control with stable output and it eliminates the oscillation of horizontal pressure, which was observed with the PID closed-loop displacement control. The tests performed at different radial consolidation time intervals showed small difference in interface strength. However, adequate radial consolidation time is required to minimize the soil creep effect on simulated expansion and

contraction cycles. Therefore, a radial consolidation time of 12 hours is recommended to perform the Modified-TBST. During the shearing stage, both displacement control (DC) and load control (LC) methods were used to control the system in the radial direction. The LC method showed better results allowing for comparing different tests and evaluating the effects of temperature and displacement changes and cycles. Based on the preliminary results of t-z curves, thermal softening was observed in the test with 0.5 temperature cycle. Although the temperature change (20 °C) does not reflect the daily temperature change in energy piles, the maximum effect of temperature only (with no cycles) on the interface shear strength was 9% for the tested soil conditions. However, the effects of expansion and contraction were significant (up to 74%). Compared to the reference test, the test with half cycle of heating and expansion (RDC = 0.5, TC = 0.5) showed a 13.4% increase, while for the test with half cycle expansion (RDC = 0.5, TC = 0), the strength increased by 21.8%. The difference between these two tests could be attributed to the effect of temperature on soil properties. For the tests with half contraction cycle (RDC = -0.5, TC = 0) and the test with half cycle of cooling and contraction (RDC = -0.5, TC = -0.5), the interface shear strength experienced more than 70% reduction due to the decrease of horizontal pressure. The measured changes presented in this paper are consistent with those reported by Wang et al. (2015) and Suryatriyastuti et al. (2012). Future tests will focus on evaluating the effects of temperature cycles simulating the intermittent operation of heat pumps connected to energy piles.

6. EFFECTS OF TEMPERATURE AND RADIAL DISPLACEMENT CYCLES ON SOIL-CONCRETE INTERFACE PROPERTIES USING MODIFIED THERMAL BOREHOLE SHEAR TEST

6.1 INTRODUCTION

The ground source heat pump (GSHP) connected to thermo-active geo-structures (such as energy piles) operates in cycles where it functions for a period of time (running time) then stops for another period of time (stoppage time) as shown in Figure 6.1. This intermittent operation subjects thermo-active geo-structures and surrounding soil to changes of temperature and temperature cycles (Shang et al. 2011; Xiao et al. 2017a). In practice, the daily running and stoppage times of GSHP ranges from 30 minutes to 24 hours depending on the heating and cooling loads (Hamada et al. 2007; Wood et al. 2009; Montagud et al. 2011; Luo et al. 2015). As shown in the schematic diagram of Figure 6.1, if the soil temperature during stoppage time does not return to the original ground temperature, the soil will experience a cumulative increase of temperature with number of cycles (Plum and Esrig 1969). Temperature change and cycles also induce volume changes of soil components and affect their interaction (Campanella and Mitchell 1968; Romero et al. 2001; Uchaipichat and Khalili 2009). The effects of temperature change on soils have been well explored in the literature using triaxial and oedometer tests; however, limited investigations have been focusing on evaluating the effects of temperature cycles.

For energy piles, temperature changes and cycles also induce axial and radial expansion and contraction of the pile altering the interaction along the soil-pile interface (Saggu and Chakraborty 2015). Researches have investigated the effects of pile axial expansion and contraction (considering the end-restraint) on shear stresses at the soil-pile interface and on axial stresses in the pile (e.g., Brandl 2006; Laloui et al. 2006, Bourne-Webb et al. 2009; McCartney and Murphy 2012; Suryatriyastuti et al. 2012, Olgun et al. 2014, Xiao et al. 2015, 2017b). However, the effects of thermally-induced radial expansion and contraction and their cyclic effects on the soil-foundation interaction for energy piles have not been fully investigated.

In this paper, Modified Thermal Borehole Shear Tests (Modified-TBSTs) were performed to explore the effects of temperature and radial expansion/contraction cycles on soil-concrete interface properties (shear stress vs. vertical displacement responses or t-z curves). In the Modified-TBSTs, two concrete plates, which were used to simulate the pile surface, were subjected to temperature and expansion/contraction cycles. Utilizing the Modified-TBSTs, t-z curves were directly measured at different radial displacement and temperature cycles.

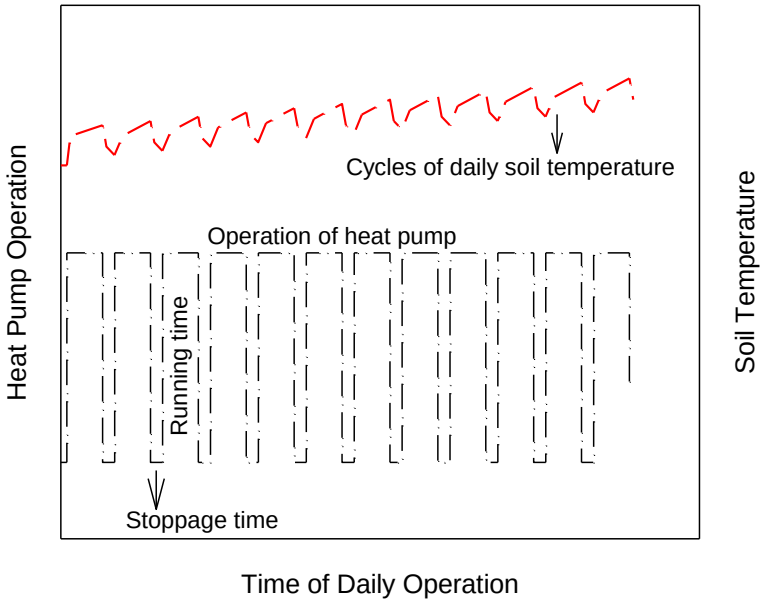

Figure 6.1 Schematic diagram of the daily operation of ground source heat pumps and the changes of surrounding soil temperature

6.2 BACKGROUND

6.2.1 Temperature Effects on Volume Change and Shear Strength of Soils

Temperature effects on soil properties depend on its thermal history, stress history, and hydraulic conductivity (Graham et al 2001; Burghignoli et al. 2000; Hueckel et al. 2009). Temperature changes induce volumetric strain (volume change) in normally consolidated and overconsolidated saturated soils (Campanella and Mitchell 1968; Demars and Charles 1982;

Cekerevac and Laloui 2004; Uchaipichat and Khalili 2009; Tawati 2010). Normally consolidated and slightly overconsolidated saturated clays contract when subjected to drained heating and experience significant irreversible (plastic) volumetric strain when returning to the initial temperature leading to an increased shear strength (e.g., Cekerevac and Laloui 2004). When subjected to undrained heating, expansion of soil components and thermally-induced excess pore water pressure lead to a reduction in shear strength (Campanella and Mitchell 1968; Mitchell and Soga 2005). Highly overconsolidated saturated clays subjected to drained heating; however, experience irreversible volumetric expansion that decreases with overconsolidation ratio (OCR) (Plum and Esrig 1969; Sultan et al. 2002). If heated beyond a threshold temperature, saturated overconsolidated clays may contract (Hueckel and Baldi 1990; Cekerevac and Laloui 2004). Cekerevac and Laloui (2004) and Abuel-Naga, et al. (2007) reported an increase of shear strength for overconsolidated soils when subjected to drained heating. For unsaturated soils, Uchaipichat and Khalili (2009) reported responses similar to those described above for normally and overconsolidated saturated soils. It is worth noting; however, that the critical state shear envelope is independent of temperature change (not cycles) for both saturated and unsaturated soils (Cekerevac and Laloui 2004; Uchaipichat and Khalili 2009; Alsherif and McCartney 2016). When subjected to cycles of heating and/or cooling, soils experience an accumulated permanent volumetric contraction regardless of stress history due to thermal creep (Campanella and Mitchell 1968; Burghignoli et al. 1992; Vega and McCartney 2015; Xiao et al. 2017a).

6.2.2 Temperature Effects on Water Migration in Soils

Water migration could be induced due to pore pressure difference and/or temperature gradient. When soils are subjected to temperature gradient water migrates from high temperature to low temperature (Sakai et al. 2009; and Cary 1966). Experimental investigation on effects of temperature gradient on water content has been performed by several researchers (e.g., Romero et al. 2001; Villar and Lloret 2004; Tang and Cui 2005; Gao and Shao 2015). These researchers

concluded that moisture content decreases with temperature at constant suction, while suction decrease with temperature at constant moisture content, which could be attributed to the reduction of surface tension of water and thermal-induced changes in the contact angle at the water-soil particle interface (Bachmann and van der Ploeg 2002; Tang and Cui 2005). These factors could lead to volume change where soils with low density contract (collapse) when wetted (referred to as wetting collapse) due to the reduction of suction whereas dense soils expand when subjected to temperature change at a constant mechanical load (Remero et al. 2003; Fredlund and Gan 1995).

6.2.3 Temperature Effects on Soil-Pile Interaction and Interface

Temperature change and cycles lead to expansion and contraction of the pile in the axial and radial directions, both of which affect the soil-pile interaction of axially loaded energy piles. The axial deformation effects were well described by Bourne-Webb et al. (2009) and Amatya et al. (2012) for thermal and mechanical loading conditions.

In addition to temperature effects on the surrounding soils, the radial expansion and contraction of geothermal foundations alter the normal (horizontal) pressure (σ_h) at the soil-pile interface and affect the axial thermo-mechanical responses of the piles (Suleiman and Xiao 2014; Minouni and Laloui 2015). During heating, radial expansion of the pile leads to an increase of normal pressure at the soil-pile interface, generating larger shear resistance. However, when subjected to cooling, the pile contracts and the soil reaction decreases leading to a reduction of the shear resistance. A three-dimensional numerical investigation performed by Suryatriyastuti et al. (2012), which considered both temperature and radial displacement, showed that a temperature change (no cycles) of 15 °C in energy piles resulted in 21% increase of the normal force on the soil-pile interface during heating and 14% to 65% reduction of the normal force during cooling. Wang et al. (2015) reported 14% increase in shaft resistance during heating compared to the case with no temperature change; however, Wang et al (2015) did not evaluate the effects of cooling on shaft resistance.

The effects of temperature change and cycles on soil-pile interface properties have been investigated by Xiao et al. (2014 and 2017a), Suleiman and Xiao (2014), Murphy and McCartney (2014), Di Donna et al. (2015), and Yavari et al. (2016) using modified direct shear tests and modified borehole shear tests. However, the combined effects of temperature cycles and expansion/contraction cycles on the soil-pile interface properties have been rarely investigated. In this study, a fully-automated Modified-TBST device was used to directly measure the shear stress-vertical displacement response (t-z curves) of the soil-concrete interface subjected to cyclic temperature changes and to radial expansion/contraction cycles.

6.3 EXPERIMENTAL SETUP

Modified-TBSTs were performed in the laboratory inside a soil tank with dimensions of 470 mm in diameter and 610 mm height (Figure 6.2). The shear head, which is connected to the loading frame using steel rods, consists of two concrete plates with embedded aluminum tubes for heating and cooling. Three linear variable displacement transformers (LVDTs) were used to measure the vertical displacement of the shear head, and a load cell was used to measure the axial pull out force (shear force at the interface). Two linear potentiometers (displacement gauges) were also mounted between the two shear plates to measure and control the horizontal displacement simulating the radial expansion and contraction of energy piles. The system also includes a unit to control the normal pressure on soil-concrete interface by adjusting the air pressure in the pneumatic piston shown in Figure 6.2. Two refrigerated/heated circulating baths, connected to the aluminum tubes, were used to apply temperature change and cycles (heating and cooling) simulating the intermittent operation of heat pumps connected to energy piles. In addition, thermocouple sensors were installed in the soil and on the surface of the concrete shear plates to measure and monitor temperatures. As shown in Figure 6.2, temperature sensors were located at distances of 2, 10, 25, 50, 75, 126, and 188 mm from the interface. The pore pressure was measured using a tensiometer installed at ~10 mm from the interface. As shown in Figure 6.2, thin polyethylene films placed on

the inside surface of the tank were used to reduce the friction between the soil and the tank. Tactilus pressure sheet sensors were also used on the inside surface of the tank to evaluate boundary effects, if any. All the readings were recorded using a data acquisition system. More details of the device design and control, and experimental setup can be found in Xiao et al. (2017b).

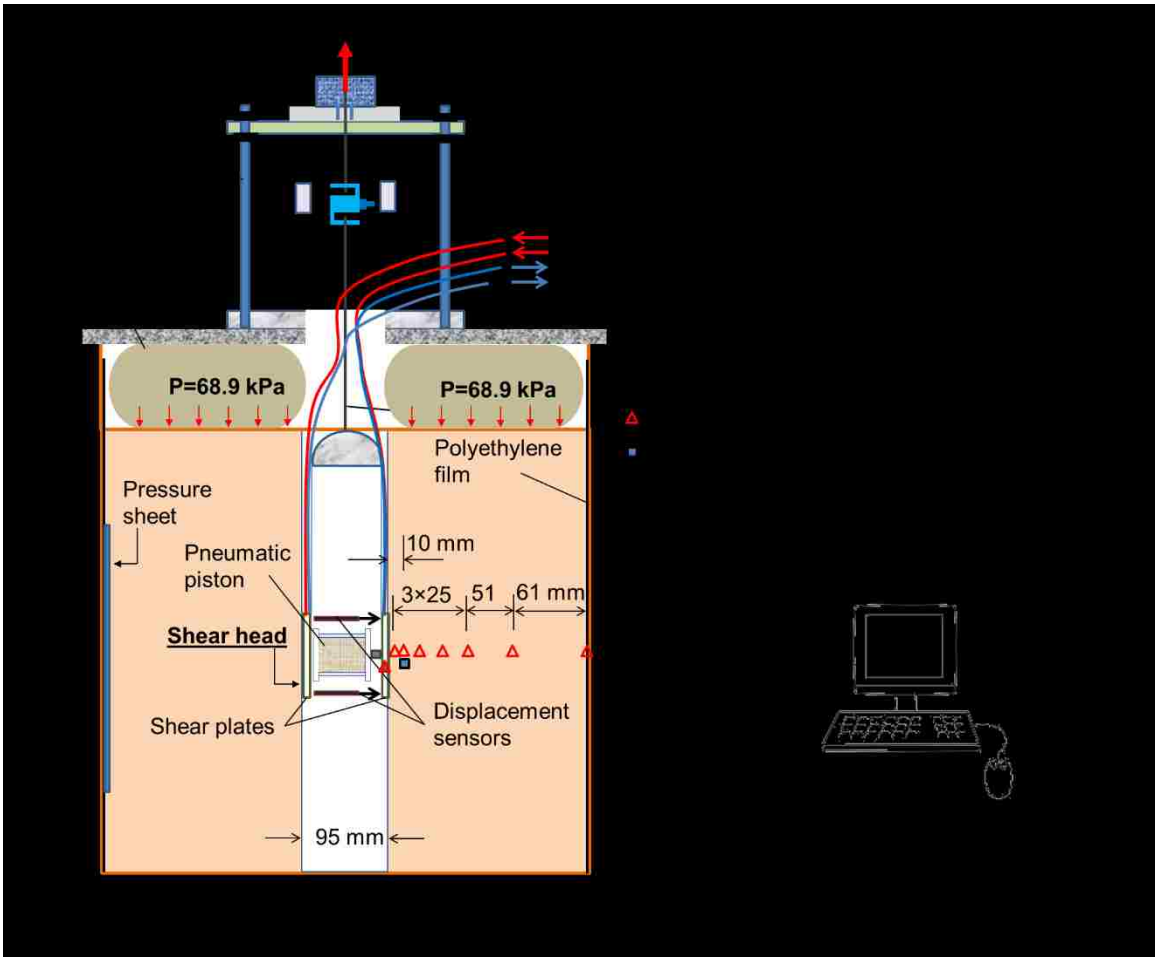

Figure 6.2 Configuration of the Modified-TBST system

6.4 TEST SOIL AND TESTING PROCEDURE

To perform the Modified-TBSTs, soil obtained from a construction site in the Lehigh Valley, Pennsylvania was compacted in 7 layers to achieve a dry unit weight of 13.8 kN/m^3 and a target moisture content of 18% (degree of saturation of 52%). Standard Proctor tests were performed and the maximum dry unit weight and optimum moisture content of the soil were 17.4 kN/m^3 and 14%, respectively. The particle size distribution curve of the used soil is shown in Figure 6.3. Using the Unified Soil Classification System (USCS), the soil was classified as sandy silty clay with fines content of 80% and 17% sand.

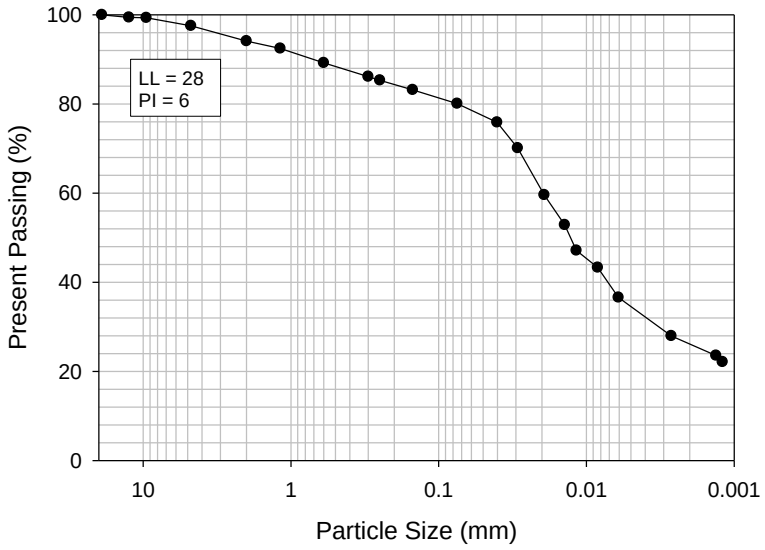

Figure 6.3 Grain size distribution curve of the test soil

The soil was mixed at the target moisture content in a concrete mixer. During preliminary tests, it was observed that the average moisture loss during preparation and waiting times was less than 0.5%, which was compensated for during soil preparation. The soil was filled in the tank in 7 layers and compacted using a tamper with targeted compaction energy per unit volume of ~54 kN-m/m^3. This consistent procedure was utilized in all experiments and resulted in an average soil dry

unit weight of 13.7 kN/m^3. During compaction, an aluminum pipe with a diameter of 95 mm was installed in the middle of the tank to create the borehole needed to perform the Modified-TBSTs. After preparation, the soil was consolidated under vertical overburden pressure (P) of 68.9 kPa for ~48 hours. Then the test started where three major stages were utilized: (1) the horizontal consolidation stage; (2) the temperature and/or displacement stage; and (3) the shearing stage.

During the horizontal consolidation stage, the shear head was lowered in the borehole and a constant horizontal (or normal) pressure (σ_h) was applied normal to the soil-concrete interface for 12 hours.

For the temperature or thermal loading stage, circulating baths were used for heating or cooling the soil-concrete interface to the target temperature change and cycles. Temperature change (ΔT) of 20 °C was used for heating and ΔT of -18 °C was used for cooling with a room temperature of ~21 °C. For heating cycles, one circulating bath was used and the fluid temperature was set to ~8 °C higher than the target temperature of the soil-concrete interface (to account the heat loss) measured using a thermocouple on the shearing plate surface. The soil-concrete interface was heated to the target temperature (i.e., reaching 0.5 temperature cycle or TC = 0.5). Then, the circulating bath was stopped, and another bath started to cool the plates down to the room temperature (i.e. reaching 1 heating cycle or TC = 1). For cooling cycles, the fluid temperature was set to ~12 °C below the target temperature. The soil-concrete interface was cooled to the target temperature (i.e., reaching 0.5 cooling cycle or TC = −0.5). Then, the circulating bath was stopped and the other bath started to warm up the plates back to the room temperature (i.e. 1 cooling cycle or TC = −1). This process was repeated to apply the target number of heating or cooling cycles. Utilizing two circulating baths provide better control of the interface temperature. The time for 1 cycle (e.g. 30 min heating and 30 min cooling) was selected to represent practical cases (as discussed in the introduction) and to allow for applying several cycles within one testing/working day.

To apply radial displacement change and cycles, the horizontal pressure applied on the soil-concrete interface was adjusted to achieve the target displacement. A radial displacement magnitude of 120 μm was used. After temperature and/or radial displacement change/cycles were applied, the shear head was pulled upward shearing the soil-concrete interface and the applied pull out force and the vertical displacement were measured (i.e., producing directly measured shear stress vs. vertical displacement curves or t-z curves). Shearing was applied at a constant rate of 0.05 mm/s. The results of the tests with initial radial consolidation pressure of 27.6 kPa are presented in this paper. More details about the testing device, control and testing procedure were described by Xiao et al. (2017b).

6.5 TESTING PLAN

To better describe the testing plan, a sign convention system was adopted. The number of radial displacement cycle (RDC) is positive for expansion cycles and negative for contraction cycles. The number of temperature cycles (TC) is positive for heating and negative for cooling. A non-integer RDC (e.g., RDC = 0.5, 1.5, -2.5) means that the plates were expanded or contracted to the target displacement and shearing was applied at that condition. Similarly, a non-integer TC (e.g., TC = 0.5, 1.5, -2.5) means the plates were heated or cooled to the target temperature and shearing was applied at that condition. When RDC and TC are integers (e.g., 1, 2, or -3), the displacement and temperature of the plate return to the initial conditions and shearing applied at those conditions.

As shown in Table 1, a reference test (Test No. 1) was conducted without temperature change/cycles (TC = 0) or displacement change/cycles (RDC = 0). To investigate temperature effects on the soil-concrete interface properties, three heating and three cooling tests were performed with temperature change and cycles (Tests No. 2 to 7). Generally, the duration of one temperature cycle was one hour (i.e., heating to a target temperature for 30 minutes and back to original temperature for another 30 minutes with a total time per cycle of 1 hour) except for Tests

No. 3 and 6, for which 10 hours of heating or cooling were used. For Test No. 2, 0.5 temperature cycle was applied where the interface was heated from the room temperature to the target temperature in 30 minutes (RDC = 0, TC = 0.5, and called undrained heating). For Test No. 3; however, 0.5 temperature cycle was applied where the interface was heated from room temperature to the target temperature in 30 minutes and the target temperature was kept for a total of 10 hours (RDC = 0, TC = 0.5, and called drained heating). Test No. 4 is similar to Test No. 2 but with 10 heating cycles (RDC = 0 and TC = 10). Tests No. 5 and 6 are similar to Tests No. 2 and 3 but subjected to 0.5 cooling cycle (RDC = 0, TC = -0.5, Test 5 and 6 called undrained and drained cooling, respectively) and Test No. 7 is similar to Test No. 4 but with 10 cooling cycles (RDC = 0 and TC = -10).

Table 6.1 Testing plan of Modified Thermal-BSTs

Test Conditions	Test No.	TC	ΔT (°C)	RDC	ΔD (μm)
Reference test	1	0	0	0	0
Temperature change (ΔT) and cycles (TC)	2	0.5	20	0	0
	3*	0.5	20	0	0
	4	10	20	0	0
	5	-0.5	-18	0	0
	6**	-0.5	-18	0	0
	7	-10	-18	0	0
Radial displacement (ΔD) and cycles (RDC)	8	0	0	0.5	120
	9	0	0	1	120
	10	0	0	10	120
	11	0	0	10.5	120
	12	0	0	-0.5	-120
	13	0	0	-1	-120
	14	0	0	-10	-120
	15	0	0	-10.5	-120
Temperature and displacement cycles	16	0.5	20	0.5	120
	17	-0.5	-18	-0.5	-120
	18	10	20	10	-120
	19	-10	-18	-10	-120

*10 hours drained heating, **10 hours drained cooling

Tests No. 8 to 15 evaluate the effects of radial displacement (with no temperature change or cycles) where expansion cycles of 0.5, 1, 10, and 10.5 (RDC = 0.5, 1, 10, or 10.5 with TC = 0;

Tests No. 8 to 11) and contraction cycles of 0.5, 1, 10, and 10.5 (or RDC = -0.5, -1, -10, or -10.5 with TC = 0; Tests No. 12 to 15) were targeted. To apply one displacement cycle, the displacement was changed from 0 to the target displacement (120 or -120 μm) and returned to the initial position in 1 hour (similar to the times of temperature cycles).

Combined radial displacement and temperature cycles were applied in Tests No. 16 to 19 where 0.5 and 10 temperature and radial displacement cycles were targeted for cooling/contraction and heating/expansion tests. The temperature changes, radial displacement changes, and number of TC and RDC for all tests were summarized in Table 6.1.

6.6 RESULTS AND ANALYSIS

6.6.1 Effects of Temperature Change and Cycles (Tests No. 2 to 7)

6.6.1.1 Temperature distribution

Figure 6.4 shows the temperature at the soil-concrete interface and in the surrounding soil for Tests No. 4 and 7 (10 heating or cooling cycles). As shown in Figure 6.4, the temperature distribution in the soil was initially uniform (before starting the tests). When the interface was heated or cooled to 0.5 cycle and then returned to original temperature at 1 cycle, the soil close to the interface (< 25 mm from interface) experienced a temperature change smaller than 1 °C. The temperature- active zone surrounding the heated/cooled concrete plates (i.e., soil zone experiencing temperature changes) extended to approximately 50 mm for TC = 0.5 and TC = 1 and it increased with number of cycles. At the end of the 10 heating/cooling cycles, the temperature-active zone extended to approximately 75mm with temperature change of 1.8 °C at this location.

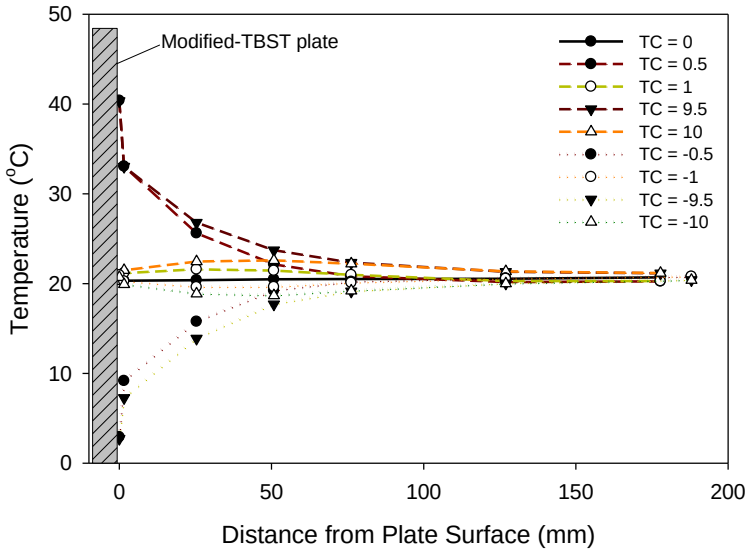

Figure 6.4 Temperature distribution with distance during heating and cooling cycles

6.6.1.2 Pore water pressure

The negative pore pressure (soil suction) near the interface was measured utilizing a tensiometer located at ~10 mm from the concrete interface during Tests No. 4 and 7 (10 heating or cooling cycles). Figure 6.5a andFigure 5.5b show the measured temperatures and the soil suction during heating and cooling cycles. As shown in Figure 6.5a, the temperature measured at 10 mm during the heating cycles varied by ~9 °C during initial cycles; however, this temperature sensor stopped working after the fourth cycle. Figure 6.5a illustrates that suction near the interface increased from 50.6 to 62.7 kPa during the 10 heating cycles and decreased from 46.8 to 33.8 kPa during the 10 cooling cycles. These changes of the soil suction could be attributed to thermally-induced water migration during heating and cooling cycles and to the differential thermal-expansion of water and soil particles (Philip and Vries 1957; Cary 1965). When subjected to temperature change, water migrates from high temperature to low temperature increasing suction (pore pressure becomes more negative) during heating and decreasing suction (pore pressure

becomes less negative) during cooling. However, the expansion coefficient of water is ~15 times that of soil particles (Cui et al. 2000) causing the increase of saturation (leading to a decrease of suction) during heating and decrease of saturation (increase of suction) during cooling (Mitchell and Soga 2005). It is worth noting that the measured values of soil suction incorporate the effects of both thermally-induced water migration and differential expansion and contraction of soil components.

Unlike their general trends shown in Figure 6.5a andFigure 6.5b, soil suction near the interface decreased at 0.5 heating cycle and increased at 0.5 cooling cycles. This could be attributed to the differential expansion/contraction between soil particles and water since small thermal-induced water migration is expected to occur during 30 minutes (time of 0.5 cycle) of heating or cooling. At one cycle (returning to room temperature), soil suction had very minor change when compared to original reading (before heating/cooling). As the number of cycles increased, suction increased with heating cycles and decreased with cooling cycles. This could be attributed thermally-induced water migration and change of water content near the interface. Figure 6.5c summarizes the change of suction per temperature cycle during heating and cooling showing a general increasing trend with number of cycles followed by a reduction. During heating, the maximum change of suction per temperature cycle was 1.6 kPa/cycle at the 7th heating cycle and 2.8 kPa/cycle at the 9th cooling cycle. In addition to creating a temperature change, subjecting the soil to temperature cycles creates a pore pressure difference. Therefore, the reduction of the suction change per temperature cycle after the 7^{th} cycle during heating could be attributed to the conflicting effects of thermally-induced water migration (from high temperature at the interface to low temperature away from the interface) and difference in pore pressure-induced water migration (from high pore pressure away from the interface to low pore pressure at the interface). These conflicting effects of the thermally-induced water migration and pore pressure-induced water migration were discussed by Cary (1966) and Sakai et al. (2009) who concluded that thermally-induced water migration is dominant.

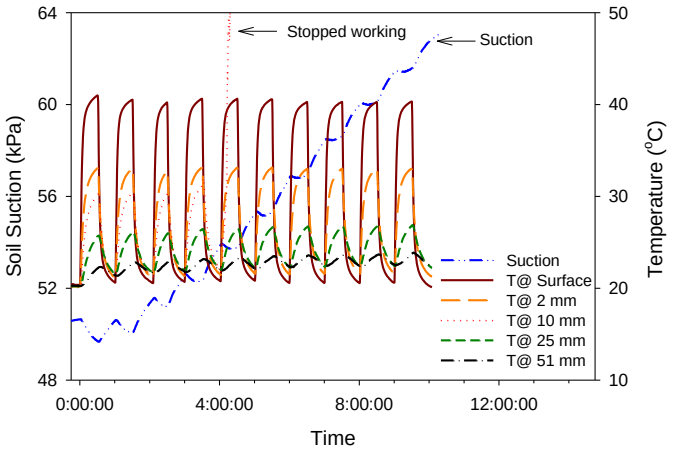

(a)

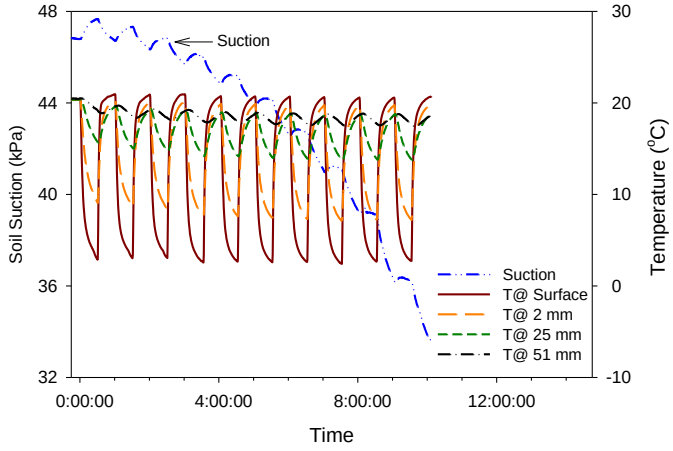

(b)

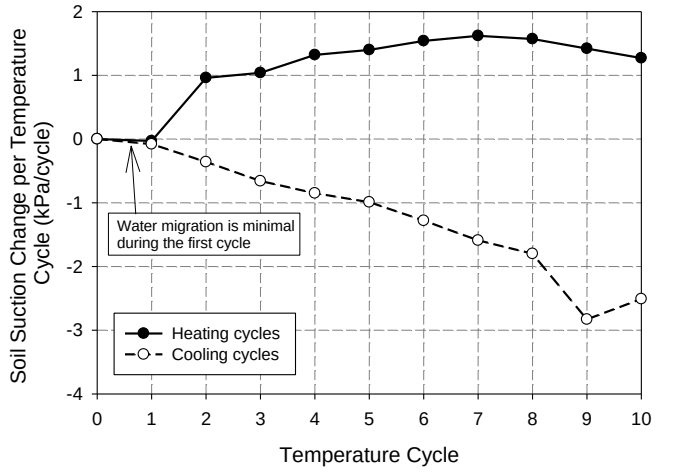

(c)

Figure 6.5 Suction and temperature changes during heating and cooling cycles; (a) TC = 10, (b) TC = -10, and (c) suction change per temperature cycle

6.6.1.3 T-z curves and interface shear strength

Figure 6.6 shows that for the reference test (Test No. 1; RDC = 0, TC = 0), the interface shear strength and shear stiffness were 19.6 kPa and 86 kPa/mm, respectively. The shear stiffness was calculated using the data at shear stress levels (τ/τ_{max}) between 10% and 50%. Figure 6.6 also summarize the t-z curves for Tests No. 2 to 7 with different heating and cooling cycles. Figure 6.6a illustrates that Test No. 2 (TC = 0.5, undrained heating) showed ~2% increase of the interface shear strength. For Test No. 3 (TC = 0.5, drained heating), the peak interface shear strength increased by ~8%, and the t-z curve of the soil-concrete interface shows a strain-softening response with the residual shear strength ~10% lower than the peak strength. This strain-softening response could be caused by the increase of the suction due to water migration for drained heating condition, which is similar to the observation reported by Hossain and Yin (2013). After 10 heating cycles, the interface shear strength increased by 8% which could also be attributed to the 24% increase of suction (see Figure 6.5a).

Figure 6.6b shows the results of Tests No. 5 to 7 (subjected to cooling cycles). When compared to the reference test, the interface shear strength increased by 9% for Test No. 5 (TC = -0.5, undrained cooling) which could be attributed to the increase of suction (see Figure 6.5b). For Test No. 6 (TC = -0.5, drained cooling), the interface shear strength increased by 18% when compared to the reference test, which is similar to results obtained for Test No. 7 (TC = -10). The increase of interface shear strength for Tests No. 6 and 7 may be attributed to the wetting collapse of soil aggregates due to water migration resulting in larger contact area between the soil and concrete according to Shakir and Zhu (2009). It is worth noting that cooling affects the interface shear strength, which is consistent with the measurements reported by Gu et al. (2014).

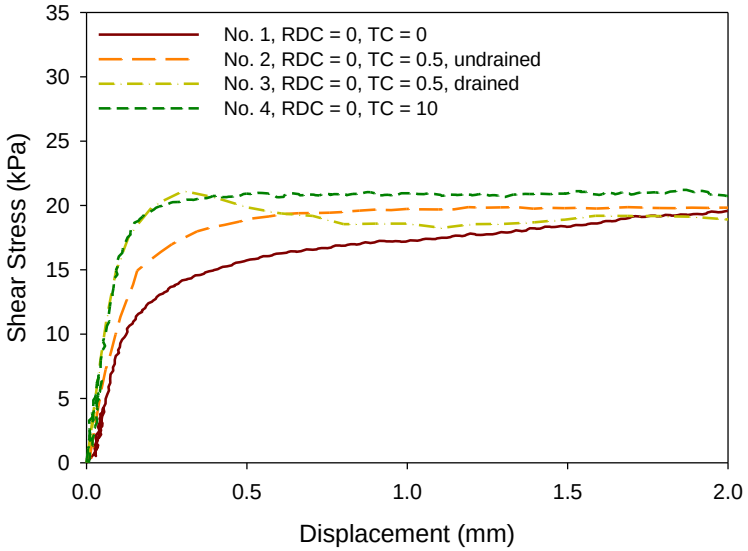

(a)

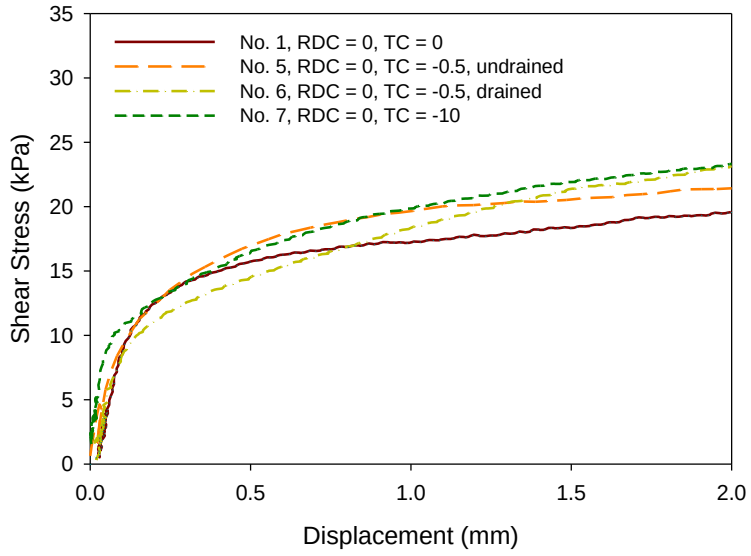

(b)

Figure 6.6 Temperature effects on the measured t-z curves of soil-concrete interface; (a) heating cycles, (b) cooling cycles

6.6.1.4 Moisture content and interface stiffness

The interface shear stiffness and the moisture content at the end of Tests No. 2 to 7 are summarized in Figure 6.7. For Test No. 2 (TC = 0.5, undrained heating), the moisture content decreased from 18.0% to 17.4%, while it increased from 18.0% to 18.7% for Test No. 5. (TC = -0.5, undrained cooling). After 10 cycles, the moisture contents of the soil at the interface were 16.2% for heating cycles (Test No. 4) and 21.4% for cooling cycles (Test No. 7). For the tests with drained heating or cooling (Tests No. 3 and 6), the moisture contents changed by 4% (changed to 14% after 10 hours heating and 22% after 10 hours cooling).

Figure 6.7 indicates that the interface shear stiffness decreases with increasing moisture content. The interface shear stiffness for Test No. 2 (TC = 0.5, undrained heating) was 32.6% higher than that of the reference test. For Test No. 3 (TC = 0.5, drained heating), the interface shear stiffness was 180 kPa/mm, which is more than twice that of the reference test. After 10 heating cycles (Test No. 4), the shear stiffness was 161.3 kPa/mm, which is 86.8% higher than the reference test. For tests with cooling cycles (Tests No. 5 to 7), the interface shear stiffness decreased by 13% after 0.5 cycle (Test No. 5, undrained cooling), 45.2% (Test No. 6, TC = -0.5, drained cooling), and 28.5% after 10 cycles (Test No. 7). These results are consistent with the power law for moduli of unsaturated soil proposed by Lu and Kaya (2014), where the Young's and shear moduli decrease with increasing water content.

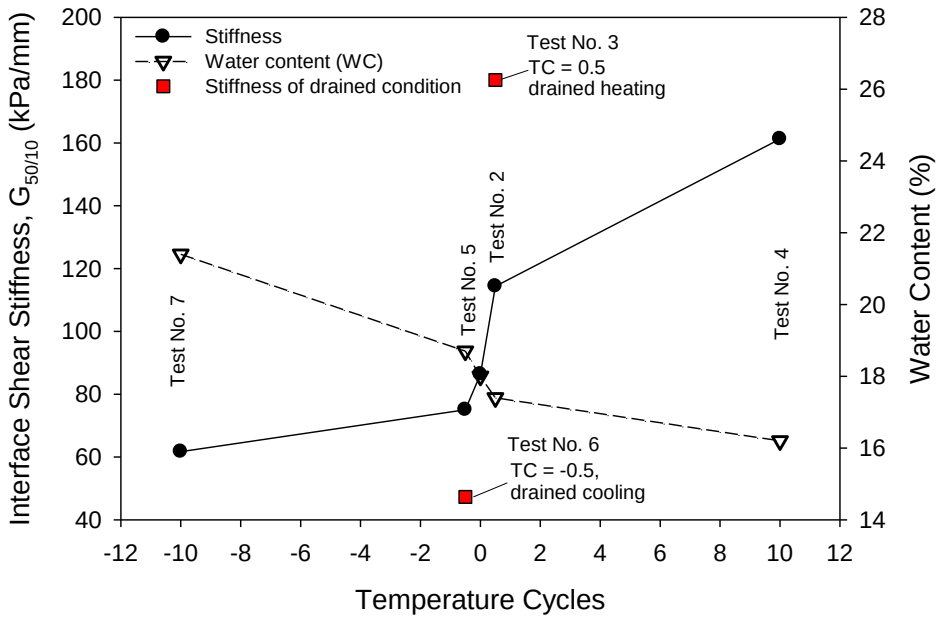

Figure 6.7 Interface shear stiffness and moisture at different temperature cycles

6.6.2 Effects of Radial Displacement Cycles (Tests No. 8 to 15)

6.6.2.1 Radial displacement vs. horizontal pressure

To apply the radial displacement simulating energy piles expansion and contraction cycles, the horizontal (normal) pressure (σ_h) applied on the soil-concrete interface was adjusted to achieve the target displacement. Figure 6.8 shows the relationships between the horizontal pressure and radial displacement in Test No. 10 (10 expansion cycles or RDC = 10) and Test No. 14 (10 contraction cycles or RDC = -10). For Test No. 10 (10 expansion cycles), the horizontal pressure (soil reaction) increased from the initial value of 27.6 kPa (point A in Figure 6.8) to 37.9 kPa at the first half expansion cycle (point B in Figure 6.8). When the concrete plates returned to the initial position at 1 cycle, the horizontal pressure decreased to 7.9 kPa (point C in Figure 6.8). This reduction in horizontal pressure when the plates returned to the initial position at 1 expansion cycle was attributed to irreversible volume change of the normally consolidated soil when subjected to 0.5 expansion cycle (pressure increased from 27.6 kPa to 37.9 kPa), which is consistent with the results reported by Ng. et al (2014) where significant plastic strain occurred during the first loading

cycle. At 9.5 and 10 expansion cycles, the horizontal pressures were 30.9 kPa (point D in Figure 6.8) and 5.3 kPa (point E in Figure 6.8). Generally, the horizontal pressure slowly decreased with number of expansion cycles after the first expansion cycle (Figure 6.8).

For contraction cycles, the horizontal pressure at the interface decreased from the initial value of 27.6 kPa (point A) to 5.2 kPa at 0.5 contraction cycle (point F in Figure 6.8) and to 4.2 kPa at 9.5 contraction cycles (point G in Figure 6.8). The horizontal pressures were 28.4 kPa after 1 cycle and 26.9 kPa (point H in Figure 6.8) after 10 cycles, which differ by less than 3% from the initial horizontal pressure of 27.6 kPa. These results show that the soil primarily experienced elastic strains during contraction cycles, while plastic strains were experienced during expansion cycles leading to the reduction of the horizontal pressure.

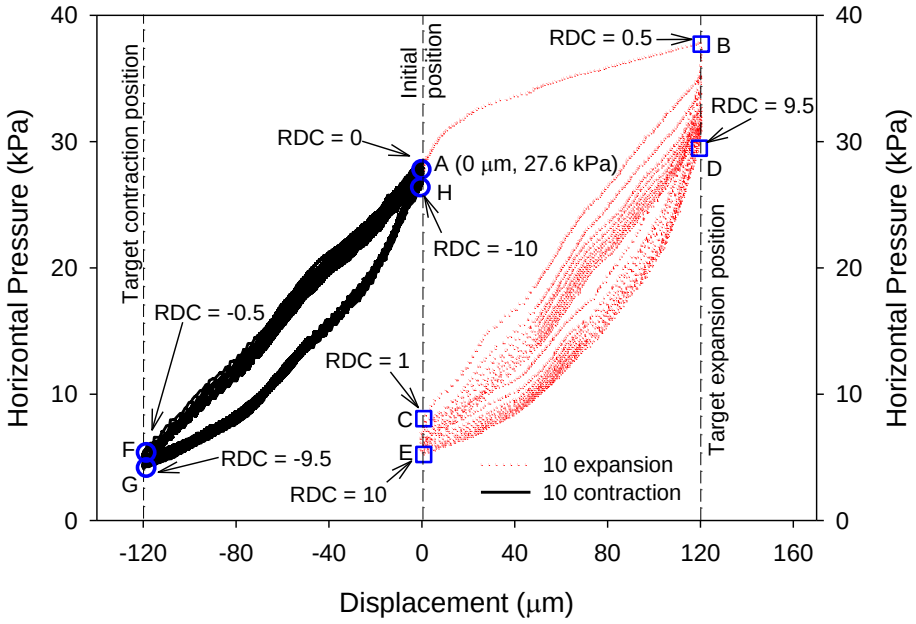

Figure 6.8 Measured horizontal displacements and corresponding pressures during radial expansion and contraction cycles

6.6.2.2 T-z curves and interface shear strength

Figure 6.9 presents the t-z curves for Tests No. 8 to 15 with different radial displacement cycles (RDC) of expansion and contraction (i.e., 0.5, 1, 10, and 10.5). The radial displacement used in all cycles was 120 μm. If RDC is an integer, the shearing pull out force was applied when the concrete plates returned to the original position. If the RDC is not an integer, the shearing pull out force was applied when the plates expanded into the soil (positive RDC) or contracted from the soil (negative RDC). When compared to the reference test (Test No. 1), Test No. 8 (RDC = 0.5 or the shearing pull out force is applied when the plates are expanded) shows an interface shear strength of 29.5 kPa (51% increase). At 10.5 expansion cycles (Test No. 11) the interface shear strength was 22.4 kPa (14% increase). For Tests No. 9 and 10 (at 1 and 10 expansion cycles where the shearing pull out force was applied when the plates returned to the original position after 1 and after 10 expansion cycles), the interface shear strength was 6.8 kPa (65% reduction) and 5.4 kPa (72% reduction), respectively.

When compared to the reference test (Test No. 1), Test No. 12 (RDC = -0.5 or the shearing pull out force is applied when the plates are contracted from the soil) shows an interface shear strength of 5.1 kPa (74% reduction), while Test No. 15 has an interface shear strength of 4.2 kPa (79% reduction) after 10.5 contraction cycles (RDC = -10.5). For Tests No. 13 and 14 (at 1 and 10 contraction cycles where the shearing pull out force was applied when the plates returned to the original position after 1 and 10 contraction cycles), the interface shear strengths were approximately equal (21.0 kPa).

When subjected to radial displacement only (expansion or contraction), the interface shear strength is mainly proportional to the horizontal pressure at the soil-concrete interface; therefore, the effects of radial expansion and contraction cycles on the interface shear strength can be generally explained by the relationships between the horizontal pressure and radial displacement shown in Figure 6.8.

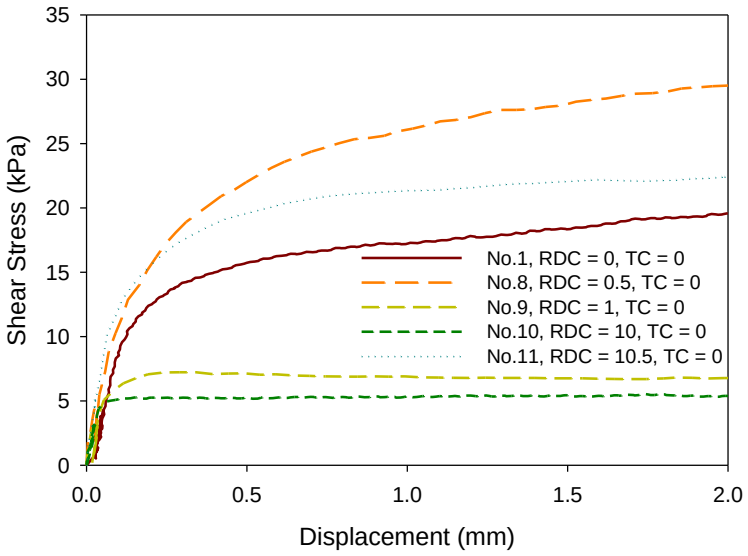

(a)

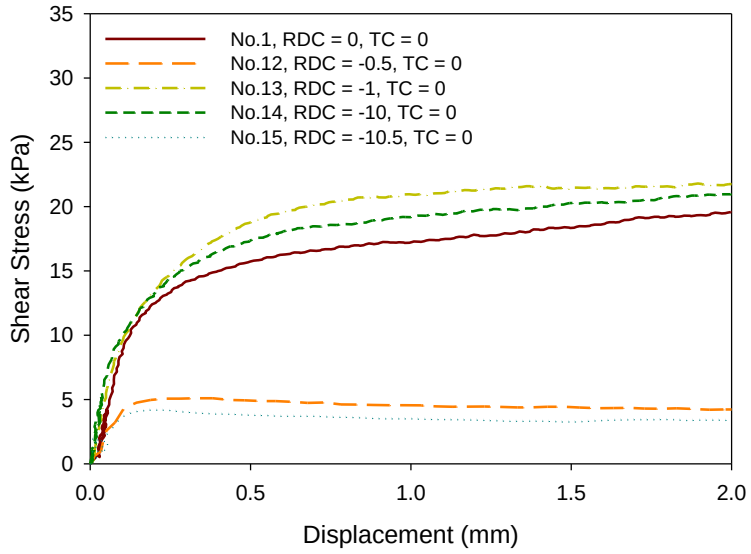

(b)

Figure 6.9 Effect of displacement cycles on the measured t-z curves, (a) expansion cycles; and (b) contraction cycles

6.6.3 Combined Effects of Temperature and Radial Displacement Cycles

Figure 6.10, Figure 6.11, and Figure 6.12 present the combined effects of temperature cycles and radial displacement cycles compared to the results of tests with radial displacement cycles only (no temperature cycle). Figure 6.10 shows the t-z curves when the interface is subjected to 0.5 radial displacement cycle combined with 0.5 temperature cycle. Test No. 16 (RDC = 0.5, TC = 0.5) showed an interface shear strength of 26.1 kPa (33% increase compared to the reference test). When compared to Test No. 8 with 0.5 expansion cycle only (RDC = 0.5, TC = 0), the interface shear strength for Test No. 16 (RDC = 0.5, TC = 0.5) showed an interface shear strength that is ~12% smaller. This difference could be attributed to the decrease of soil suction (i.e., increase of pore pressure and decrease of effective stress) near the interface at 0.5 heating cycle (see Figure 6.5a) due to the differential expansion between soil particles and water. Another reason is the smaller horizontal pressure at 0.5 cycles of displacement and temperature (Test No. 16) compared to 0.5 displacement cycle (Test No. 8) (see Figure 6.11b at 0.5 cycle) because of the increase in compressibility of normally consolidated soil as the temperature increase (Plum and Esrig 1969). For Test No. 17 with 0.5 contraction cycle combined with 0.5 cooling cycle (RDC = -0.5, TC = -0.5), the interface shear strength was 3.3 kPa (83% reduction compared to the reference test). When compared to Test No. 12 with 0.5 contraction cycle only (RDC = -0.5, TC = 0), the interface shear strength for Test No. 17 (RDC = -0.5, TC = -0.5) showed an interface shear strength that is ~46% smaller. These values are similar to those reported by Suryatriyastuti et al. (2012) based on numerical analyses of energy piles.

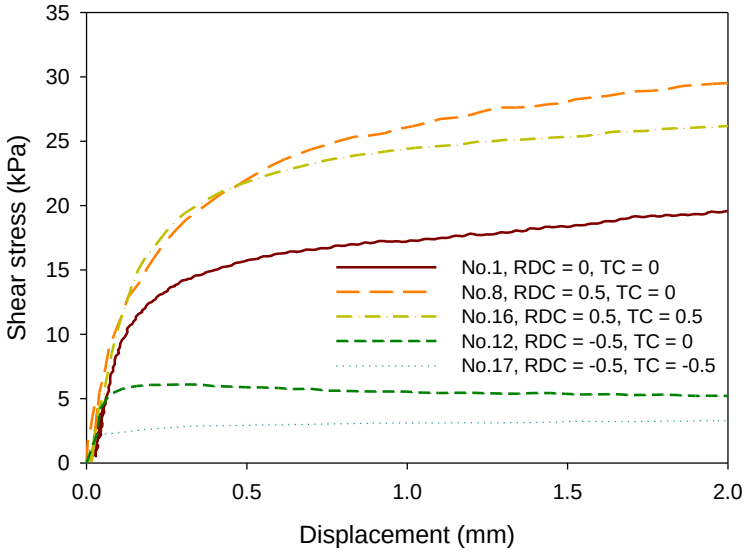

Figure 6.10 Combined effects of ±0.5 displacement and temperature cycles on measured t-z curves

Figure 6.11 shows the t-z curve when the interface is subjected to 10 radial expansion cycles combined with 10 heating cycles (Test No. 18; RDC = 10, TC = 10) compared to Test No. 10 with 10 radial expansion cycles and no temperature cycles (RDC = 10, TC = 0) and Test No. 1 (reference test). Test No. 18 showed an interface shear strength of 2.0 kPa (~90% decrease compared to the reference test). When compared to Test No. 10 with 10 expansion cycles only (RDC = 10, TC = 0), the interface shear strength for Test No. 18 (RDC = 10, TC = 10) showed an interface shear strength that is ~63% smaller. These reductions could be attributed to the significant decrease of the horizontal pressure with number of heating cycles for Test No. 18 compared to Test No. 10 (Figure 6.11b).

Figure 6.12 shows the t-z curve when the interface is subjected to 10 radial contraction cycles combined with 10 cooling cycles (Test No. 19; RDC = -10, TC = -10) compared to Test No. 14 with 10 radial contraction cycles and no temperature cycles (RDC = -10, TC = 0) and Test No. 1 (reference test). Test No. 19 showed an interface shear strength of 6.1 kPa (~69% decrease compared to the reference test). When compared to Test No. 14 with 10 contraction cycles only

(RDC = -10, TC = 0), the interface shear strength for Test No. 19 (RDC = -10, TC = 10) is ~71% smaller. These reductions could be attributed to the thermally-induced water migration and reduction of horizontal pressure with number of cooling cycles (Figure 6.12b).

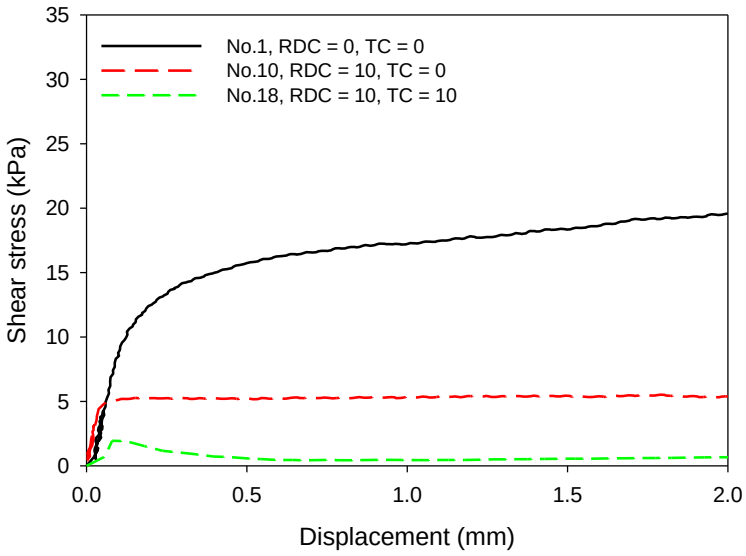

(a)

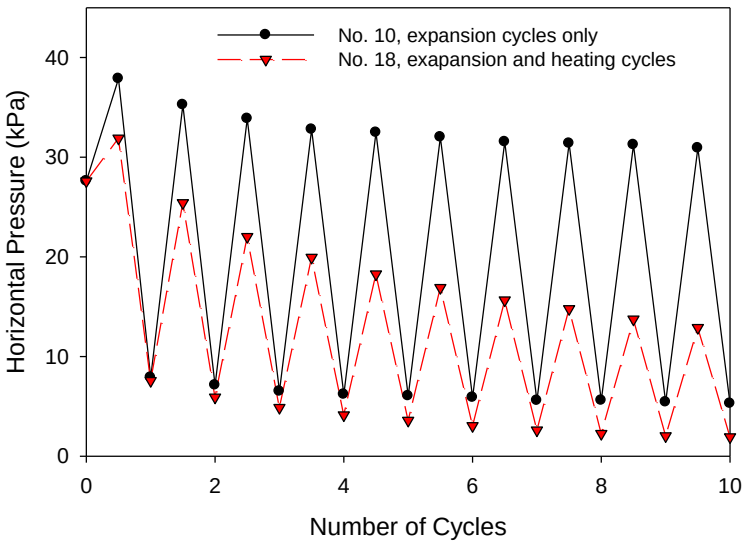

(b)

Figure 6.11 Measured t-z curves and horizontal pressures with heating cycles; (a) t-z curve, and (b) horizontal pressure

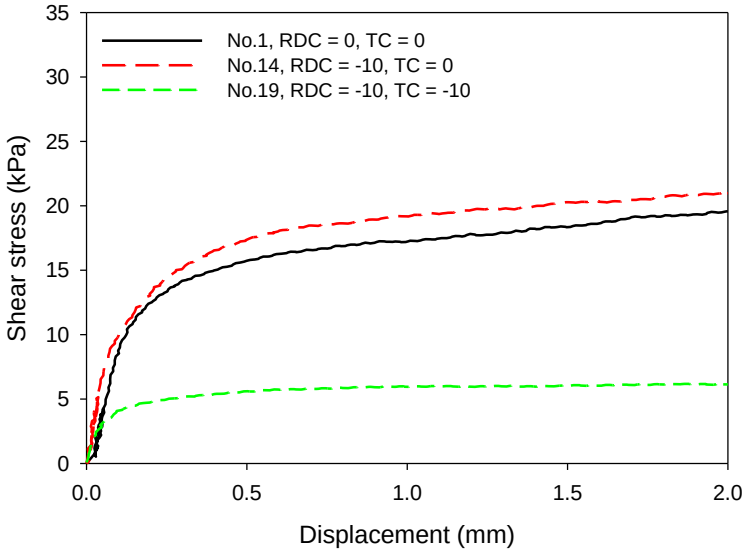

(a)

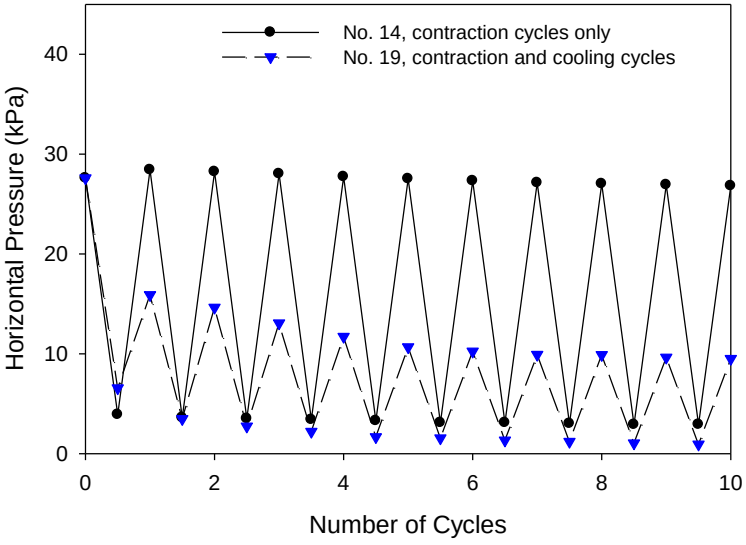

(b)

Figure 6.12 Measured t-z curves and horizontal pressures with cooling cycles; (a) t-z curve, and (b) horizontal pressure

6.7 SUMMARY AND CONCLUSIONS

The intermittent operation of heat pumps connected to thermo-active geo-structures creates temperature change and cycles, which introduce new challenges in designing of these structures. For energy piles, the cyclic temperature changes affect soil properties and produce expansion and

contraction in both axial and radial directions of the pile. Those thermal-induced effects alter the shaft resistance of energy piles. In this paper, a recently developed device called the Modified Thermal Borehole Shear Test (Modified-TBST) device was used to evaluate the effects of temperature and displacement cycles on soil-concrete interface properties. The Modified-TBSTs were performed in a normally consolidated compacted clay. The shear stress-vertical displacement responses at the soil-pile interface (t-z curves), subjected to cyclic temperature changes and radial expansion/contraction, were directly measured using the Modified-TBST device. Based on the results, the following conclusions were drawn.

- The extent of temperature-active soil zone surrounding the heated/cooled concrete plates (soil experiencing temperature changes) increased with number of cycles and was approximately 75mm with temperature change of 1.8 °C at this location.
- The soil suction measured near the soil-concrete interface increased with heating cycles and decreased with cooling cycles. The suction change per temperature cycle generally increased with number of temperature cycles then decreased.
- The interface shear strength increased when subjected to drained heating or to larger heating cycles. The t-z curve of the soil-concrete interface subjected to drained heating showed strain-softening response due to thermally-induced water migration and increase of suction. The increase of the interface strength during the cooling cycles could be attributed to the wetting collapse of soil aggregates due to water migration resulting in larger contact area between the soil and concrete.
- The radial expansion and contraction (with no temperature changes) have significant effects on the measured t-z curves. For expansion cycles, the interface shear strength increased by up to 51% at the expansion position because of the increase of horizontal pressure at the interface. A significant reduction (~65%) of the interface shear strength was observed due to the plastic strain (deformation) induced during the first expansion

cycle. During contraction cycles (with no temperature cycles), the soil plastic strain was very small; therefore, the shear strength was not affected by the contraction cycles when the plates returned to the initial position. However, the interface shear strength decreased by up to 79%, when the plates were sheared at contraction position due to the reduction of the horizontal pressure at the interface.

- The interface shear strength had larger reduction when subjected to the combined effects of temperature and radial deformation and those effects increased with number of cycles.

Based on the results of the Modified-TBST, radial expansion/contraction cycles and temperature cycles are expected to have significant effects on the shaft resistance of energy piles installed in normally-consolidated clays.

7. CONCLUSIONS AND FUTURE RESEARCH

This PhD dissertation research focused on the use of geothermal energy piles for bridge anti-icing and on the thermo-mechanical response of soil-energy pile subjected to temperature cycles. In this final chapter, the research contributions of this dissertation are summarized, and directions for future research are discussed.

7.1 CONTRIBUTIONS

This research advances the research on feasibility on using geothermal pile foundations for bridge anti-icing in different weather condition and its thermo-mechanical behavior towards practical applications based on the conclusions shown below.

A new modelling approach of heat transfer of bridges considering different meteorological factors (e.g., air temperature, wind speed/direction, precipitation, solar radiation, and infrared radiation) was proposed and validated using measured data. The effects of radiation and convection on the bridge surface temperature were also assessed. The comparisons indicate that the improved model may underestimate the convective heat transfer coefficient yet produces very good results during the winter time.

The wind speed influences the bridge deck temperature predication in a more pronounced manner during the noon time of a day and during summer when the solar radiation is higher, because the increase of available solar radiation magnifies the differences between ambient air temperature and the deck surface temperature. The vehicle-induced effects were also considered in the analysis. The vehicle movement can cool down the bridge surface with smaller traffic rates. Under the heavy traffic condition, the bridge surface is mostly warmed up by the vehicular traffic during the winter time thus providing an advantage. A cooling of approximately 1 °C of the bridge deck due to vehicular traffic could be used as a recommendation for the design of bridge decks during snowfall periods.

The results of the modified direct shear tests for the soil-concrete interface indicated that the interface shear strength increased by up to 23% after 10.5 heating cycles and 10.5 cooling cycles. The temperature and moisture contents effects on the shear strength of the soil-concrete interface increased with the interface roughness. The changes of soil void ratio when subjected to temperature cycles was independent of stress level and void ratio after the primary consolidation stage. The temperature cycle-dependent consolidation rate increased during heating cycles which is ~ 4 times that of the cooling cycles.

Fully-Automated Modified Thermal Borehole Shear Test (Modified-TBST) device was developed to evaluate the effects of temperature and radial displacement cycles on soil-concrete interface properties. The results show that both the temperature cycle and the radial expansion and contraction cycles have significant effects on the measured t-z curves. For effects of temperature cycle only, the shear strength of the soil-concrete interface increased by up to 18% after 10.5 heating cycles and 10.5 cooling cycles. For expansion cycles, the interface shear strength increased by up to ~50% at the expansion position because of the increase of horizontal pressure at the interface. A significant reduction of the interface shear strength was observed due to the plastic strain (deformation) induced during the first expansion cycle. During contraction cycles (with no temperature cycles), the soil plastic strain was very small; therefore, the shear strength was not affected by the contraction cycles when the plates returned to the initial position. However, the interface shear strength decreased by up to 79%, when the plates were sheared at contraction position due to the reduction of the horizontal pressure at the interface. The interface shear strength had larger reduction when subjected to the combined effects of temperature and radial deformation and those effects increased with number of cycles.

7.2 FUTURE RESEARCH

The proposed heat transfer model of bridges can be used in the feasibility analysis of bridge anti-icing using energy piles with more weather data at different locations. In the applications, the

primary loop in the energy piles and the secondary loop in the decks could be connected by a conventional circulating pump or a heat pump. With a heat pump, the circulating fluid in the bridge can be kept at a much higher temperature, and electric energy can also be combined with geothermal energy to melt the snow. The feasibility analysis can be performed in the future using the heat pump combing geothermal and electric energy for bridge anti-icing.

When the energy piles are unable to provide enough heat during the snow events, applying salts and heating with geothermal systems could be an alternative strategy to keep the bridge deck snow free. More complicated snow melting processes need to be used in the model to consider the effect of salt on the freezing point.

In this study, Modified-DST was used to investigate effects of temperature cycles on soil-concrete interface behaviors using unsaturated clay. Different soils (sand, silt, clay) could be used with different moisture contents, relative densities, or overconsolidated ratios (OCRs). For the saturated soil, the test can be performed on higher number of temperature cycles with constant moisture contents.

Similar to Modified-DST, the Modified-TBST could be performed in different soils with different moisture contents, relative densities, or OCRs. Different expansion/contraction values can be used to simulate different temperature changes or restraints of surrounding soils.

REFERENCES

Abdelaziz, S. L., Olgun, C. G., and Martin II, J. R. 2011. "Design and Operational Considerations of Geothermal Energy Piles." *Proceedings of GeoFrontiers 2011*, Dallas, Texas, CD-ROM.

AbdelSalam, S. S., Suleiman, M. T., and Sritharan, S., 2012. "Enhanced load–transfer analysis for friction piles using a modified borehole shear test." *Geotechnical Testing Journal*, 35(6), 1–11.

Abuel-Naga, H. M., Bergado, D. T., Bouzza, A. and Ramana, G. V. 2007. "Volume change behaviour of saturated clays under drained heating conditions: experimental results and constitutive modeling." *Canadian Geotechnical Journal*, 448, 942-956.

Adam, D., and Markiewicz, R., 2009. "Energy from earth-coupled structures, foundations, tunnels and sewers." *Géotechnique*, 593, 229–236.

Akrouch, G. A., Sanchez, M., and Briaud, J. L. 2013. "Energy piles for heating and cooling purposes." *Proceedings of the 5th International Young Geotechnical Engineers' Congerence*, edited by Cui, Y.-J., Emeriault, F., Cuira, F., Ghabezloo, S., Pereira, J.-M., Reboul, M., Ravel, H., Tang, A.M. Millpress, pp. 161–164.

Alawneh, A. S. 2006. "Modeling the load-displacement curve of driven tension piles in noncohesive Soils." *Soil Mechanics and Foundation Engineering*, 43(2), 47-55.

Alsherif, N. and McCartney, J. S. 2016. "Yielding of silt at high temperature and suction magnitudes." *Geotechnical and Geological Engineering*. 342, 501-514.

Amatya, B. L., Soga, K., Bourne-Wbb, P. J., Amis, T., and Laloui, L. 2012. "Thermo-mechanical behaviour of energy piles." *Géotechnique*, 62(6), 503–519.

Amis, T. 2011. "Energy foundation in the UK." Presentation to Swiss Federal Institute of Technology Lausanne, EPFL, Switzerland. Retrieved from Internet Archive website: http://web.archive.org/web/20170217214106/http://www.gshp.org.uk/GroundSourceLive2011/TonyAmis_Piles_gsl.pdf accessed Dec 15, 2016.

Amis, T., and Bourne-Webb, P. 2008. “The effects of heating and cooling energy piles under working load at Lambeth college.” *Proceedings of the 33rd Annual and 11th International Conference on Deep Foundations*, 2008, New York, NY, USA. CD-ROM, 10 pg.

ASHRAE, 2011. “Snow melting and freeze protection.” *ASHRAE handbook—HVAC applications, SI edition*, Chapter 51. American Society of Heating, Refrigeration and Air Conditioning Engineers, Inc., Atlanta, GA.

Azizinamini, A., Power, E. H., Myers, G. F., and Ozyildirim, H. C. 2014. “Bridges for service life beyond 100 years: innovative systems, subsystems, and components.” *Strategic Highway Research Program 2, Report No. S2-R19A-RW-1*. Transportation Research Board. Washington, D. C., 2014.

Bachmann, J., van der Ploeg, R. R. 2002. “A review on recent developments in soil water retention theory: interfacial tension and temperature effects.” *Journal of Plant Nutrition and Soil Science*, 1654, 468-478.

Batini, N., Rotta Loria, A. F., Conti, P., Testi, D., Grassi, W., Laloui, L. 2015. “Energy and geotechnical behaviour of energy piles for different design solutions.” *Computers and Geotechnics*, 861, 199–213.

Batini, N., Rotta Loria, A. F., Conti, P., Testi, D., Grassi, W., Laloui, L. 2015. “Energy and geotechnical behaviour of energy piles for different design solutions.” *Computers and Geotechnics*, 861, 199–213.

Bentz, D. P. 2000. “A computer model to predict the surface temperature and time-of-wetness of concrete pavements and bridge decks.” *National Institute of standards and technology*, NISTIR 6551.

Bergman, T. L., Lavine, A. S., Incropera, F. P., and DeWitt, D. P. 2011. “Fundamentals of Heat and Mass Transfer.” 7th Edition. Hoboken, NJ: John Wiley.

Bourne-Webb, P. J., Amatya, B., Soga, K., Amis, T., Davidson, C., and Payne, P. 2009. “Energy pile test at Lambeth College, London: geotechnical and thermodynamic aspects of pile response to hat cycles.” *Géotechnique,* 59(3), pp. 237-248.

Bourne-Webb, P., 2013. “Observed response of energy geostructures.” in: Energy Geo-Structures, Laloui, L. and Di Donna, A. Ed., p. 29, *ISTE - John Wiley & Sons*, London.

Bowers Jr., G. A. and Olgun, C. G. 2015. “Experimental investigation of bridge deck deicing using energy piles.” *IFCEE 2015*, San Antonio, Texas. March 17–21, 2015.

Brandl, H. 2006. “Energy Foundations and Other Geothermal Ground Structures.” *Géotechnique*, 56(2), 81–122.

Bretz, S. E., Akbari, H., and Rosenfeld, A. H. 1988. “Practical issues for using solar-reflective materials to mitigate urban heat islands.” *Atmospheric Environment*. 32(1), 95-101, doi:10.1016/S1352-2310(97)00182-9

Brock, B. W., and Arnold, N. S. 2000. “A spreadsheet-based (Microsoft Excel) point surface energy balance model for glacier and snow melt studies.” *Earth Surface Processes and Landforms*, 25(6), 649-658, doi:10.1002/1096-9837(200006)25:6<649::AID-ESP97>3.0.CO;2-U.

Brown, D. F., and Dunn, W. E. 1998. “The surface energy budget meteorological model (SEBMET) for atmospheric boundary layer characterization,” prepared by University of Illinois, Urbana, Ill., for U.S. Army Corps. Of Engineers, Construction and Research Laboratory, Champaign, Ill.

Burghignoli, A., Desideri, A., and Miliziano, S. 1992. “Deformability of clays under non-isothermal conditions.” *Rivista Italiana di Geotecnica*, 26, 227–236.

Burghignoli, A., Desideri, A., and Miliziano, S. 2000. “A laboratory study on the thermomechanical behaviour of clayey soils.” *Canadian Geotechnical Journal*, 374, 764-780.

Campanella R. G., Mitchell J. K. 1968. “Influence of temperature variations on soil behavior.” *Journal of the Soil Mechanics and Foundations Division*, 94(3), 709-734.

Cane, D., Morrison, A. and Ireland, C. J. 1998. “Operating experiences with Commercial Ground-Source Heat Pumps-Part 2.” *ASHRAE Transactions*, 104(2), 677-86.

Cary, J. R., and Vries, D. A. 1957. “Water vapour movement in porous materials under temperature gradient.” *American Geophysical Union*, 382, 222-231.

Cary, J. W. 1965. “Water flux in moist soil: Thermal versus suction gradients.” *Soil Science*, 100, 168-175.

Cary, J. W. 1966. “Soil moisture transport due to thermal gradients: Practical aspects.” *Soil Interfaceence*, 304, 428-438.

Cekerevac, C., and Laloui, L. 2004. “Experimental study of thermal effects on the mechanical behaviour of a clay.” *International Journal for Numerical and Analytical Methods in Geomechanics*, 28(3), 209-228.

Chapman, L., and Thornes, J. E. 2005. “The influence of traffic on road surface temperatures: implications for thermal mapping studies.” *Meteorological Applications*. 12(4), 371-380, doi:10.1017/S1350482705001957.

Chapman, L., Thornes, J. E., and Bradley, A. V. 2001. “Modelling of road surface temperatures from a geographical parameter database. Part I: statistical.” *Meteorology Applications*. 4(8), 409-419, doi:10.1017/S1350482701004030.

Chapman, W. P. 1952. ‘‘Design of snow melting systems.’’ *Heat. Vent.*, April, 49, pp. 96–102.

Chiasson, A. D., Spitler, J. D., Rees, S. J., and Smith, M. D. 2000. “A model for simulating the performance of a pavement heating system as a supplemental heat rejecter with closed-loop ground-source heat pump systems.” *ASME, Journal of Solar Energy Engineering*. 122(4), 183-191, doi:10.1115/1.1330725.

City-Data. 2014. http://web.archive.org/web/20170325185055/http://www.city-data.com/bridges/bridges-Jamestown-Rhode-Island.html. Accessed March 24, 2016.

Coccia, C. J., Rosenberg, J. E., and McCartney, J. S. 2011. “Soil-structure interaction in geothermal foundations.” *Proceedings of 2011 NSF Engineering Research and Innovation Conference*, Atlanta, Georgia. CDROM.

Cress, R.G., Williams, M.W., and Sievering, H., 1995. “Dry depositional loading of nitrogen to an alpine snowpack, Niwot Ridge, Colorado.” In: Tonnessen, K.A., Williams, M.W., Trantner, M. (Eds.), Biogeochemistry of Seasonally Snow-Covered Catchments, Proceedings of an International Symposium, IAHS Publication No. 228. International Association of Hydrological Sciences, Wallingford, UK, pp. 33–40.

Cui, Y. J., Sultan, N., and Delage, P. 2000. “A thermomechanical model for saturated clays.” *Canadian Geotechnical Journal*, 373, 607-620.

DeJong, J.T., and Westgate, Z. J. 2009. “Role of initial state, material properties, and confinement condition on local and global soil-structure interface behavior.” *ASCE Journal of Geotechnical and Geoenvironmental Engineering*. 135(11), 1646–1660.

Demars, K. R., and Charles, R. D. 1982. “Soil volume changes induced by temperature cycling.” *Canadian Geotechnical Journal*, 19(2), 188-194.

Demartinecourt, J. P., and Bauer, G. E. 1983. “The modified borehole shear device.” *Geotechnical Testing Journal*, 6(1), 24–29.

Di Donna, A., Ferrari, A., and Laloui, L. 2015. “Experimental investigations of the soil–concrete interface: physical mechanisms, cyclic mobilization, and behaviour at different temperatures.” *Canadian Geotechnical Journal*, 534, 659-672.

Dingman, S.L. 1994. “Physical Hydrology.” Prentice Hall, Englewood Cliffs, N.J. 07632.

Eriksson, L. G. 1989. “Temperature effects on consolidation properties of sulphide clays.” In: *Proceedings of the 12th international conference on soil mechanics and foundation engineering*, vol 12, Rio de Janeiro, 13–18 Aug, pp 2087–2090

Eskridge, R. E., and Hunt, J. C. R. 1979. “Highway modeling—I. Prediction of velocity and turbulence fields in the wakes of vehicles.” *Journal of Applied Meteorology*, 18(4), 387-

400, doi:10.1175/1520-0450(1979)018<0387:HMPIPO>2.0.CO;2.

Eskridge, R. E., and Thomson, R. S. 1982. “Experimental and theoretical study of the wake of a block-shaped vehicle in a shear-free boundary flow.” *Atmospheric Environment*, 16, 2821–2836, doi:10.1016/0004-6981(82)90033-6.

Florides, G., and Kalogirou, S. 2007. “Ground heat exchangers – a review of systems, models and applications.” *Renewable Energy*, 32(15), 2461–78.

Fox, P. J., and Edil, T. B. 1996. “Effects of stress and temperature on secondary compression of peat.” *Can. Geotech. J.*, 33, 405-415.

Fredlund D. G., and Gan J. K. M. 1995. “The collapse mechanism of a soil subjected to one-dimensional loading and wetting.” *In Proceedings of NATO Advance Workshop on Genesis and Properties of Collapsible Soils* eds Derbyshire, E., Dijkstra, T. and Smalley, I.J. Loughborough, April 1994, pp. 173–205.

Fujimoto, A., Saida, A., and Fukuhara, T. 2012. “A new approach to modeling vehicle-induced heat and its thermal effects on road surface temperature.” *Journal of Applied Meteorology and Climatology*, 51, 1980-1993, doi:10.1175/JAMC-D-11-0156.1

Fujimoto, A., Watanabe, H., and Fukuhara, T. 2006. “Effects of tire frictional heat on snow covered surface.” *Standing international road weather conference*, 13, 117-122.

Fujimoto, A., Watanabe, H., and Fukuhara, T. 2008. “Effects of vehicle heat on road surface temperature of dry condition.” *Proc. 14th Standing Int. Road Weather Conf.*, Standing International Road Weather Commission, Prague, Czech Republic, ID05.

Gabrielsson, A., Bergdahl, U., and Moritz, L. 2000. “Thermal energy storage in soils at temperatures reaching 90 degrees C.” *J. Solar Energy Eng.–Trans. ASME*, 122(1), 3–8.

Gao, H., and Shao, M. 2015. “Effects of temperature changes on soil hydraulic properties.” *Soil Till. Res.* 153, 145–154.

Gao, J., Zhang, X., Liu, J., Li, K., and Yang, J. 2008. “Numerical and experimental assessment of thermal performance of vertical energy piles: an application.” *Applied Energy*, 85, 901–

910.

Graham, J., Tanaka, N., and Crilly, T. 2001. “Modified cam-clay modeling of temperature effects in clays.” *Canadian Geotechnical Journal*, 38(3), 608-621.

Gu, K., Tang, C., Shi, B., Hong, J., and Jin, F. 2014. “A study of the effect of temperature on the structural strength of a clayey soil using a micropenetrometer.” *Bulletin of Engineering Geology and the Environment*, 733, 747–758.

Gustavsson, T., and J. Bogren, 1991: Infrared thermography in applied road climatological studies. *Int. J. Remote Sens.*, 19(12), 1311-1328, doi:10.1080/01431169108955211.

Hall, J. W., Smith, K. L., and Littleton, P. 2009. “Texturing of concrete pavements.” *NCHRP Report 634*, Transportation Research Board, National Research Council, Washington, D.C.

Hamada, Y., Saitoh, H., Nakamura, M., Kubota, H., and Ochifuji, K. 2007. “Field performance of an energy pile system for space heating.” *Energy and Buildings*, 39(5), 517–524.

Handy, R. L. 1986. “Borehole Shear Test and Slope Stability.” *Proceeding: The ASCE Specialty Conference on In–Situ tests: Use of In–Situ Tests in Geotechnical Engineering*, Blacksburg, Virginia, pp. 161–175.

Handy, R. L., and Fox, N. S. 1967. “A soil borehole direct shear test device.” *Highway Research News, Transportation Research Record*, 27, 42–51.

Herrero, J., and Polo, M. J. 2012. “Parameterization of atmospheric longwave emissivity in a mountainous site for all sky conditions.” *Hydrol. Earth Syst. Sci.*, 16, 3139-3147, doi:10.5194/hess-16-3139-2012.

Hider, Z. E., Hibberd, S. and Baker, C. J. 1997. “Modelling particulate dispersion in the wake of a vehicle.” *Journal of Wind Engineering and Industrial Aerodynamics*, 67-68, 733-744, doi:10.1016/S0167-6105(97)00114-1.

Hossain, M. A., and Yin, J. H. 2013. “Unsaturated soil-cement interface behaviour in direct shear tests.” *Australian geomechanics journal*, 48 3, 141-154

Houston, S. L., Houston, W. N., and Williams, N. D. 1985. “Thermo-mechanical behavior of

seafloor sediments." *Journal of Geotechnical Engineering ASCE*, 111(12), 1249–1263.

Hueckel, T. and Baldi, G. 1990. "Thermoplasticity of saturated clays: experimental constitutive study." *Journal of Geotechnical Engineering*, 116(12), 1778-1796.

Hueckel, T., François, B., Laloui, L. 2009. "Explaining thermal failure in saturated clays." *Géotechnique*, 593, 197-212.

Ishikawa, N., Narita, H., and Kajiya, Y. 1999. "Contributions of heat from traffic vehicles to snow melting on roads." *Journal of the Transportation Research Board*, 1672, 28-33, doi:10.3141/1672-05

Joerger, M. D., and Martinez, F. C. 2006. "Electric heating of I-84 in Ladd Canyon, Oregon." *Final Report, SPR 304- 461*, prepared for Oregon Department of Transportation and FHWA, 2006, June.

Karademir, T. 2011. "Elevated temperature effects on interface shear behavior." Doctoral Dissertation. Georgia Institute of Technology, Atlanta, GA.

Koch, G. H., Brongers, P. H., Thompson, N. G., Virmani, Y. P., and Payer, J. H. 2002. "Corrosion costs and prevention strategies in the United States." *Report No. FHWA-RD-01-156*. Federal Highway Administration. Washington, D. C., March 2002.

Kuntiwattanakul, P., Towhata, I., Ohishi, K., and Seko, I. 1995. "Temperature effects on undrained shear characteristics of clay." *Soils and Foundation*, 35(1), 147–162.

Laffont, S., Nierhoff, G., Regniet, G., and Schmidt, G. 1999. "Verkehrsentwicklung auf Bundesfernstrassen 1998 (Development of Traffic Flow on German Federal Highways 1998)." Berichte der Bundesanstalt für Strassenwesen (BASt), No. V73, Germany.

Laguros, J. G. 1969. "Effect of temperature on some engineering properties of clay soils." *Highway Research Board Special Report*, pp. 186–193.

Laloui, L., Nuth, M., and Vulliet, L. 2006. "Experimental and Numerical Investigations of the Behavior of a Heat Exchanger Pile." *International Journal for Numerical and Analytical Methods in Geomechanics*, 308, 763-781.

Laloui., L., Di Donna, A. 2013. “Energy geostructures: innovation in underground engineering.” August 2013, Wiley-ISTE.

Leal, M., and Miller, P. L. 1972. “An analysis of the transient temperature distribution in pavement heating installations.” *ASHRAE Transactions*, 78(2), 61-66.

Lee, R. C., Sackos, J. T., Nydahl, J. E., and K. M. Pell. 1984. “Bridge heating using ground-source heat pipes.” *Transportation Research Record*, 962, 51-57.

Levinson, R., and Akbari, H. 2002. “Effects of composition and exposure on the solar reflectance of Portland cement concrete.” *Cement and Concrete Research*, 32(11), 1679-1698, doi:10.1016/S0008-8846(02)00835-9.

Liu, X., Rees, S. J., and Spitler, J. D. 2007. “Modeling snow melting on heated pavement surfaces, Part I: Model development.” *Appl. Therm. Eng.*, 27(5-6), 1115-1124, doi:10.1016/j.applthermaleng.2006.06.017.

Loveridge, F. A, Powrie, W., Amis, T., Wischy, M., and Kiauk, J. 2016. “Long term monitoring of CFA energy pile schemes in the UK.” in: Wuttke, F, Bauer, S and Sanchez, M, eds. Energy Geotechnics. 1st International Conference on Energy Geotechnics ICEGT 2016, 29-31 Aug 2016, Keil, Germany. CRC Press, pp. 585-592.

Lu, N., and Kaya, M. 2014. “A power law for elastic moduli of unsaturated soil.” *Journal of Geotechnical and Geoenvironmental Engineering*, 140(1), 46–56.

Lund, J. W. 1999. “Reconstruction of a pavement geothermal deicing system.” *Geo-Heat Center Quarterly Bulletin*, 20, 14-17.

Luo, J., Rohn, J., Bayer, M., Priess, A., Wilkmann, L., and Xiang, W. 2015. “Heating and cooling performance analysis of a ground source heat pump system in Southern Germany.” *Geothermics*, 53, 57-66.

Lutenegger, A. J., and Powell, J. J. M. 2008. “Borehole shear tests in stiff London and Gault Clay.” *Proceedings of the 3rd International Symposium on Site Characterization*, Taipei, Taiwan, April 1–4, pp. 719–723.

Lutenegger, A. J., and Tierney, K. F. 1986. “Pore Pressure Effects in Borehole Shear Testing.” *Proceeding: The ASCE Specialty Conference on In–Situ tests: Use of In–Situ Tests in Geotechnical Engineering,* Blacksburg, Virginia, pp. 752–764.

Lutenegger, A. J., Renames, B. D., and Handy, R. L. 1978. “Borehole shear test for stiff soil.” *Journal of the Geotechnical Engineering Division*, 104(11), pp. 1403–1407.

Mašín, D., and Khalili, N. 2014. “A thermo-mechanical model for variably saturated soils based on hypoplasticity.” *International Journal for Numerical and Analytical Methods in Geomechanics*, 36, 1461–1485.

McCartney, J. S., and Murphy, K. D. 2012. “Strain distributions in full–scale energy foundations.” *Deep Foundation Institute Journal*, 62, 28–38.

Mimouni, T., and Laloui, L. 2015. “Behaviour of a group of energy piles.” *Can Geotech J*. 52(12), 1913–29.

Minsk, L. D. 1999. “Heated bridge technology.” *Report on ISTEA, Publication No. FHWA-RD-99-158,* U.S. Department of Transportation, July 1999.

Misra, A., and Chen, C. H. 2004. “Analytical solution for micropile design under tension and compression.” *Geotechnical and geological engineering*, 22(2), 199-225.

Mitchell, J. K., and Soga, K. 2005. “Fundamental of Soil Behaviour.” 3rd Ed. John Wiley & Sons Inc. New Jersey.

Miyamoto, S., and Takeuchi, M. 2002. “Snow-melting and de-icing system on road using natural thermal energy sources.” *New Challenges for Winter Road Service. XIth International Winter Road Congress*. Sapporo, Japan, January 28-31, 2002.

Moene, A. F., and van Dam, J. C. 2014. “Transport in the atmosphere-vegetation-soil continuum.” Cambridge University Press.

Montagud, C., Corberan, J. M., Montero, A., and Urchueguia, J. F. 2011. “Analysis of the energy performance of a ground source heat pump system after five years of operation.” *Energy and Buildings*, 43, 3618-3626.

Morino, K. 1994. “Study on heat exchanged in soil by circulating water in a steel pile.” *Energy and Buildings,* 21(1), 65-78.

Murayama, S. 1969. “Effects of temperature on elasticity of clays.” *Highway Research Board, Special Report 103, Conference on Effects of Temperature and Heat on Engineering Behaviour of Soils*. Sponsored by The Committee on Physico-Chemical Phenomena in Soils. pp. 194-203.

Murphy, K., and McCartney, J. 2014. “Thermal Borehole Shear Device.” *Geotechnical Testing Journal*, 37(6), 1-16.

Murphy, K., and McCartney, J. 2015. “Seasonal response of energy foundations during building operation.” *Geotechnical and Geological Engineering*, 33(2), 343–356.

Nam, S. H., Song, H. W., Byun, K. J., and Maekawa, K. 2006. “Seismic analysis of underground reinforced concrete structures considering elasto-plastic interface element with thickness.” *Engineering Structures*, 28, 1122–1131.

National Research Council. 2010. “HCM 2010: highway capacity manual.” *Transportation Research Board*, Washington, D.C.

National Solar Radiation Data Base (NSRDB). 2012. http://web.archive.org/web/20170325164843/http://rredc.nrel.gov/solar/old_data/nsrdb/ (accessed Nov 23).

New York City Department of Transportation (NYC DOT). 2010. “New York City bridge traffic volumes.” 2010, May 2012.

News Item. 1998. “Heated pipes keep deck ice free.” *Civil Engineering, ASCE*, 68, 19-20.

Ng, C. W. W., and Zhou, C. 2014. “Cyclic behaviour of an unsaturated silt at various suctions and temperatures.” *Géotechnique*, 64(9), 709-720.

Ng, C. W. W., Cheng, Q., Zhou, C., Alonso, E. E. 2016. “Volume changes of an unsaturated clay during heating and cooling.” *Géotechnique Lett*., 6(3), 192–198.

Noble, C. A., and Demirel, T. 1969. “Effect of temperature on strength behavior of cohesive soil.”

Highway Research Board Special Report, pp. 204–219.

Olgun, C. G., Ozudogru, T. Y., and Arson, C. F. 2014. "Thermo-mechanical radial expansion of heat exchanger piles and possible effects on contact pressures at pile-soil interface." *Géotechnique Letters*, 4(3), 170-178.

Ooka, R., Sekine, K., Mutsumi, Y., Yoshiro, S., and SuckHo, H. 2007. "Development of a Ground Source Heat Pump System with Ground Heat Exchanger Utilizing the Cast–in Place Concrete Pile Foundations of a Building." *2007 Winter Meeting of the American Society of Heating, Refrigerating and Air-Conditioning Engineers*. Dallas, TX, United states. Jan 27–31, 2007.

Ozgener, O., and Hepbasli., A. 2005. "Experimental performance analysis of a solar assisted ground-source heat pump greenhouse heating system." *Energy and Buildings*, 37(1), 101-10.

Parmenter, B. S., and Thornes, J. E. 1986. "The use of a computer model to predict the formation of ice on road surfaces." *Transport and Road Research Laboratory Research Report*, 1, 1–19.

Pasten, C., and Santamarina J. C. 2014. "Thermally induced long-term displacement of thermoactive piles." *Journal of Geotechnicaland Geoenvironmental Engineering*, 140(5), 06014003 1-5.

Petersen, E. L., N. G., Mortensen, L. Landberg, J. Højstrup, and H. P. Frank. 1998a. "Wind power meteorology, Part I: climate and turbulence." *Wind Energy*, 1(S1):25-45, doi: 10.1002/(SICI)1099-1824(199804)1:1+<25::AID-WE4>3.0.CO;2-D.

Petersen, E. L., N. G., Mortensen, L. Landberg, J. Højstrup, and H. P. Frank. 1998b. "Wind power meteorology, Part II: siting and models." *Wind Energy*, 1(2):55-72, doi: 10.1002/(SICI)1099-1824(199812)1:2<55::AID-WE5>3.0.CO;2-R.

Plum, R. E., and Esrig, M. I. 1969. "Some temperature effects on soil compressibility and pore water pressure." *Effects of Temperature and Heat on Engineering Behavior of Soils,*

Special Report 103, Highway Res. Board, Washington, D.C., 231-242.

Pra-ai, S. 2013. "Behaviour of soil-structure interfaces subjected to a large number of cycles. Application to piles." Doctoral dissertation, Université de Grenoble, France.

Prata, A. J., 1996. "A new long-wave formula for estimating downward clear-sky radiation at the surface." *Quarterly Journal of the Royal Meteorological Society*. 122 (533), 1127-1151, doi:10.1002/qj.49712253306.

Preene, M., and Powrie, W. 2009. "Ground energy systems: from analysis to geotechnical design." *Géotechnique*, 59(3), 287–290.

Priestley M. J. N., and Thurston, S. J. 1979 "Discussion of the paper titled ''Thermal calculations for bridge design.'' by Hunt et al. *ASCE Journal of the Structural Division*. 102, 1277–1279.

Prusa, J. M., Segal, M. Temeyer, B. R., Gallus, W. A., and Takle, E. S. 2002. "Conceptual and scaling evaluation of vehicle traffic thermal effects on snow/ice-covered roads." *J. Appl. Meteor.*, 41, 1225-1240, doi:10.1175/1520-0450(2002)041<1225:CASEOV>2.0.CO;2.

Qin, Y. H., and Hiller, J. E. 2013. "Ways of formulating wind speed in heat convection significantly influencing pavement temperature prediction." *Heat and Mass Transfer*, 49(5), 745-752, doi:10.1007/s00231-013-1116-0.

Ramsey, J. W., Hewett, M. J., Kuehn, T. H., and Petersen, S. D. 1999. "Updated design guidelines for snow melting systems." *ASHRAE Transactions*, 105, 1055–1065.

Ramsey, J., Chiang, H., and Goldstein, R. 1982. "A study of the incoming long-wave atmospheric radiation from a clear sky." *Journal of Applied Meteorology*, 21, 566-578, doi:10.1175/1520-0450(1982)021<0566:ASOTIL>2.0.CO;2

Rao, K. S., Gunter, R. L., White, J. R. and Hosker, R. P. 2002. "Turbulence and dispersion modeling near highways." *Atmospheric Environment*, 36, 4337-4346, doi:10.1016/S1352-2310(02)00353-9.

Rauber, M. 1995. “Energy from road surfaces.” *Caddet Renewable Energy Newsletter*, issue 1/95, Harwell, UK, pp. 25-27.

Rees, S. J., Spitler, J. D., and Xiao, X. 2002. “Transient analysis of snow-melting system performance.” *ASHRAE Trans.*, 108, 406-423.

Romero, E., Gens, A., and Lloret, A. 2001. “Temperature effects on the hydraulic behaviour of an unsaturated clay.” *Geotechnical and Geological Engineering*, 19(3), 311–332.

Rouissi, K., Krarti, M., and McCartney, J. S. 2012. “Analysis of thermo-active foundations with U-tube heat exchangers.” *Journal of Solar Energy Engineering*, 134(2), pp. 021008-1-021008-8.

Ryu, Y., Kang, S., Moon, S. K., and Kim, J. 2008. “Evaluation of land surface radiation balance derived from Moderate Resolution Imaging Spectrometer (MODIS) over complex terrain and heterogeneous landscape on clear sky days. *Agricultural and Forest Meteorology*. 148(10), 1538-1552, 10.1016/j.agrformet.2008.05.008

Saggu, R., and Chakraborty, T. 2015. “Cyclic Thermo-Mechanical Analysis of Energy Piles in Sand.” *Geotechnical and Geological Engineering*, 33(2), 321-342.

Saix, C., Devillers, P., El Youssoufi, M. S. 2000. “Element de couplage thermomechanique dans la consolidation de sols non satures.” *Can Geotech J*, 37(2), 308–317.

Sakai, M., Toride, N. and Simunek, J. 2009. “Water and vapor movement with condensation and evaporation in a sandy column.” *Soil Science Society of America Journal*, 73, 707–717.

Sato, M., and Sekioka, M. 1979. “Geothermal snow melting at Sapporo, Japan.” *Geo-Heat Center Quarterly Bulletin*, 4(3), Klamath Falls, OR, pp. 16-18.

Schlup, U., and Schatzmann, J. 1998. “Solar energy for ice control.” *Xth PIARC International Winter Road Congress*. Lulea, Sweden. March 16 -19.

Schnurr, N. M., and Falk, M. W. 1973. “Transient analysis of snow melting systems.” *ASHRAE Transactions*, 79(2), 159-166.

Shakir, R. and Zhu, J. 2009. “Behavior of compacted clay-concrete interface.” *Frontiers of Architecture and Civil Engineering in China*, 31, 85-92.

Shang, Y., Li. S., and Li, H. 2011. “Analysis of geo-temperature recovery under intermittent operation of ground-source heat pump.” *Energy and Buildings*, 43(4), 935-943.

Sharples, S., and Charlesworth, P. S. 1998. “Full scale measurement of wind induced convective heat transfer from a roof mounted flat plate solar collector.” *Solar Energy*, 62 (2), 69-77, doi:10.1016/S0038-092X(97)00119-9

Spitler, J. D., and Ramamoorthy, M. 2000. “Bridge deck deicing using geothermal heat pumps.” *Proceedings of the Fourth International Heat Pumps in Cold Climates Conference*, Alymer, Quebec, 2000.

Stewart, M., and McCartney, J. S. 2013. “Centrifuge modeling of soil-structure Interaction in energy foundations.” *Journal of Geotechnical and Geoenvironmental Engineering*, pp. 04013044-1-04013044-11.

Suleiman, M. AbdelSalam, S., and Sritharan, S., 2011, “Improving Prediction of the Load–Displacement Response of Axially Loaded Friction Piles.” *Proceedings of Geo–Frontiers 2011, Advances in Geotechnical Engineering, ASCE*, pp. 36–45.

Suleiman, M. T., and Xiao, S. 2014. “Soil-Pile Interaction of Geothermal Deep Foundations.” *Proceedings of the 27th Central Pennsylvania Geotechnical Conference*, Hershey, PA on April 23-25, 2014.

Suleiman, M. T., Sritharan, S., and White, D. J. 2007. “Experimental and analytical investigation on lateral load response of bridge columns with deep foundations in frozen soils.” *Final Report*, National Science Foundation.

Sultan, N., Delage, P., and Cui, Y. J. 2002. “Temperature effects on the volume change behaviour of Boom clay.” *Engineering Geology*, 64(2-3), 135-145.

Suryatriyastuti, M., Mroueh, H., and Burlon, S. 2012. “Understanding the temperature-induced mechanical behaviour of energy pile foundations.” *Renewable and Sustainable Energy*

Reviews, 16(5), 3344-3354.

Tang, A. M., and Cui, Y. J. 2005. "Controlling suction by the vapour equilibrium technique at different temperatures, application in determining the water retention properties of MX80 clay." *Canadian Geotechnical Journal*, 42(1), 287-296.

Tang, A. M., Pereira, J. M., Hassen, G., and Yavari, N. 2013. "Behavior of geat-exchanger piles from physical modeling." in *Energy Geostructures: Innovation in Underground Engineering*, edited by Laloui., L and Donna, D. A. August 2013, Wiley-ISTE, pp. 79-97.

Tarnawski, V. R., Leong, W. H., Momose, T., and Hamada, Y. 2009. "Analysis of ground source heat pumps with horizontal ground heat exchangers for Northern Japan." *Renewable Energy*. 34(1), 127-34.

Tawati, A. E. 2010. "Impact of the rate of heating on the thermal consolidation of compacted silt." *Master thesis*, University of Colorado, Boulder.

Tidfors, M., and Sällfors, G., 1989. "Temperature effect on preconsolidation pressure." *Geotechnical Testing Journal*, 12(1), 93-97.

Towhata, I., Kuntiwattanakul, P., Seko, I. and Ohishi, K. 1993. "Volume change of clays induced by heating as observed in consolidation tests." Soils and Foundations. 33(4), 170-183.

Trenberth K. E., Fasullo, J. T., and Kiehl, J. 2009. "Earth's global energy budget." *Bulletin of the American Meteorological Society*, 90, 311–323, doi:10.1175/2008BAMS2634.1.

Trenberth, K. E., and Fasullo, J. T. 2012. "Tracking Earth's energy: From El Niño to global warming." *Surv. Geophys.*, 33:413–426, doi:10.1007/s10712-011-9150-2.

Trigo, I. F., Barroso, C., Viterbo, P., Freitas, S. C., and Monteiro, I.T. 2010. "Estimation of downward long-wave radiation at the surface combining remotely sensed data and NWP data." *Journal of Geophysical Research*, 115: D24118, doi:10.1029/2010JD013888.

Tsiatas, G., McEwen, E. E., and Chen, H. 2002. "Monitoring of long-term creep and temperature behavior of the Jamestown-Verrazzano Bridge." *Publication FHWA-RI-RTD-02-1*. FHWA, Rhode Island Department of Transportation.

Tsutsumi, A., Tanaka, H. 2012. "Combined effects of strain rate and temperature on consolidation behavior of clayey soils." *Soils Found.* 52 (2), 207–215.

Uchaipichat, A., and Khalili, N. 2009. "Experimental investigation of thermo-hydro-mechanical behaviour of an unsaturated silt." *Géotechnique*, 59(4), 339-353.

Unsworth, M. H., and Monteith, J. L. 1975. "Long-wave radiation at the ground I. Angular distribution of incoming radiation." *Quarterly Journal of the Royal Meteorological Society*, 101, 13-24, doi:10.1002/qj.49710142703.

Vega, A., and McCartney, J. S. 2015. "Cyclic heating effects on thermal volume change of silt." *Environmental Geotechnics*, 25, 257–268

Villar, M. V., and Lloret, A., 2004. "Influence of temperature on the hydro-mechanical behaviour of a compacted bentonite." *Applied Clay Science*. 26, 337-350.

Walton, G. N. 1981. "Passive solar extension of the building loads analysis and system thermodynamics (BLAST) program." *Technical Report*, United Stated Army Construction Engineering Research Laboratory, Champaign, IL.

Wang, B., Bouazza, A., and Haberfield, C. 2011. "Preliminary observations from laboratory scale model geothermal pile subjected to thermal-mechanical loading." *Proceedings of the GeoFrontiers 2011*, Dallas, Texas, CD-ROM.

Wang, B., Bouazza, A., Singh, R., Haberfield, C., Barry-Macaulay, D., and Baycan, S. 2014. "Posttemperature effects on shaft capacity of a full-scale geothermal energy pile." *Journal of Geotechnical and Geoenvironmental Engineering*, 141(4), 10.1061/ASCEGT.1943-5606.0001266, 04014125.

Wang, T., and Su, L. 2010. "Experimental study on water vapour migration in unsaturated loess under effect of temperature." *J. Cold Regions Eng.*, 24(3), 77–86.

Weather Underground. 2012. http://web.archive.org/web/20170406144744/https://www.wunderground.com/

Wood, C. J., Liu, H., and Riffat, S. B. 2009. "Use of energy piles in a residential building, and

effects on ground temperature and heat pump efficiency." *Géotechnique*, 59(3), 287–290.

Xiao, S., and Suleiman, M. T. 2015. "Investigation of thermo-mechanical load transfer t-z Curves behavior of soil-energy pile interface using modified borehole shear tests." *Geotechnical Special Publication*. 1658-1667.

Xiao, S., M. T. Suleiman, C. Naito, and S. Neti, 2013. "Use of geothermal deep foundations for bridge deicing." *Journal of the Transportation Research Board*, 2363, 56-65, doi:10.3141/2363-07

Xiao, S., Suleiman, M. T., and McCartney, J. S. 2014. "Shear behavior of silty soil and soil-structure interface under thermal loading." *2014 GeoCongress, Geo-Characterization and Modeling for Sustainability*. Atlanta, Georgia, February 23-26, 2014.

Xiao, S., Suleiman, M. T., Elzeiny, R., and Al-Khawaja, M. J., 2016, "Cyclic Loading Effects on Soil-Energy Pile Interaction" in Energy Geotechnics, edited by Wuttke, F., Bauer, S., and Sanchez, M., CRC Press 2016, pp. 529–534.

Xiao, S., Suleiman, M. T., Elzeiny. R., Xie, H., and Al-Khawaja, M. J., 2017a. "Soil-concrete interface properties subjected to cyclic thermal loading using direct shear test." *Geotechnical Frontiers 2017*, Orlando, Florida, March 12-15, 2017.

Xiao, S., Suleiman, M. T., Naito, C. J., and Al-Khawaja, M. J. 2017b. "Modified-thermal borehole shear test device and testing procedure to investigate the soil-structure interaction of energy piles." *Geotehcnical Testing Journal*. Accepted.

Xiao, X. 2002. "Modeling of hydronic and electric-cable snow-melting systems for pavements and bridge decks." *M.S. Thesis*, Oklahoma State University, Stillwater, OK, 2002.

Xie, P., Gu, P., and Beaudion, J. J. 1996. "Electrical Percolation Phenomena in Cement Composites Containing Conductive Fibers." Journal of Materials Science, 31. 4093-4097, doi: 10.1007/BF00352673.

Yavari, N., Tang, A. H., Pereira, J., and Hassen, G. 2016. “Effect of temperature on the shear strength of soils and the soil–structure interface.” *Canadian Geotechnical Journal*, 53(7), 1-9.

Zenewitz, J. A., 1977 “Survey of alternatives to the use of chlorides for highway deicing.” Report No. FHWA-RD-77-52.

Zhao, W., Kuhn, W. R., and Drayson, S. R. 1994. The significance of detailed structure in the boundary layer to thermal radiation at the surface in climate models.” *Geophysical Research Letter*, 21(15), 1631-1634, doi:10.1029/94GL01393.

Zhou, C., and Ng. C. W. W. 2015. “Effects of temperature and suction on the stiffness of unsaturated soil under cyclic loads,” *International Symposium on Energy Geotechnics*, Barcelona, Spain, 2-4 June 2015.

Zhou, G., and Yi, T. 2013. “Thermal load in large-scale bridges: A state-of-the-art review.” *International Journal of Distributed Sensor Networks*, 2013 (7-8), 1-17, doi:10.1155/2013/217983.

VITA

Suguang Xiao was born on April 20, 1985 in Hebi, Henan province in China. He received his Bachelor degree of Civil Engineering from Chang'an University, Xi'an, China in 2008. He obtained his Master degree of Tunnel and Underground Engineering from Tongji University, Shanghai, China in 2011. He started research towards this doctoral dissertation at Lehigh University in August 2011.